3D co-culture spheroid drug screening platform for pancreatic cancer invasion

Lam, Hoyin

Awarding institution:
King's College London

3D co-culture spheroid drug screening platform for pancreatic cancer invasion

Hoyin Lam

This thesis is submitted to fulfil the requirements for the degree of Doctor of Philosophy

University of London

2017

Division of Cancer Studies

New Hunts House, Guy's Campus

King's College London

SE1 1UL, London, UK

Declaration of Authorship

I declare the work presented in this thesis is my own, with contributions from others properly cited and acknowledged. This work was performed between September 2014 and October 2017 in the Division of Cancer Studies, King's College London.

Hoyin Lam

October 2017

Acknowledgements

For three years long, the second floor, and sometimes also the third floor of New Hunt's House (NHH) at the King's College London Guy's Campus has been my second home. It has been a great pleasure to be around, work with all the fantastic colleagues and receive the support from everyone. First of all, I would like to thank my supervisors Claire Wells, Debashis Sarker and Vicky Sanz-Moreno. Without the support and enthusiasm from you, this rather unique PhD project would not have existed.

Claire, thank you so much for your kindest support and guidance during my PhD and allowing me the freedom to be independent and shape my own project as much as I liked. Your full support and understanding has been crucial to me, and it has been a great pleasure to be part of your lab the past three years (+ a couple of rotational months). Many thanks Claire!

Debs, your support and advice from time to time as a clinical supervisor has been tremendously helpful. Thank you for being a wonderful second supervisor, showing me the work in the clinic and making time free to meet when possible, despite being inundated with work. It has been a great pleasure to have you around!

Vicky, without your never-ending enthusiasm, curiosity and drive, this PhD project would not have existed or reached the stage where it is now. Many thanks for your unconditional support as a second supervisor and providing all the valuable input to the data and the project. Your encouragement has helped me greatly in advancing my PhD and the project. Thank you!

I would also like to thank the Biomedical Research Centre at Guy's & St Thomas NHS Trust and King's College London for providing me the opportunity, funding and support to do a PhD at King's. The program was well designed and allowed me to study with students from the King's Bioscience Institute and Medical Research Council cohort along nine fantastic fellow Biomedical Research Council cohort students: Charlotte, Christina, Cinzia, Dalia, Fiona, Hersi, Jelmar, Mirella (Everlasting coffee partner) and Varsha, you all have been wonderful fellow students and friends on this journey studying towards a PhD. I also enjoyed organising the yearly

Christmas dinner for you all and hope to stay in touch with all of you. You will all do great!

Big thanks to all the lab members from the Wells group for their company, support, advice and assistance. Many thanks to the previous Wells group members: Anna, Helen, Fahim, Nicole and Nouf for their guidance during the beginning. Great thanks to all the Wells group '2.0' members: Katerina (The lab's 'Hilarious' care taker), Mario (The lab's teenager sidekick), Maddie (our 'Orange Alarm' and cake expert of the lab), Kiruthikah (Our in-house doc and Jersey potato supplier), Michaela (the real post-doc), Cristian (My best student and handyman), Lujain (The generous one), our visiting members from abroad: Ivy and Sevil. You all have made the lab a nice and cosy place over the years, and I wish you all the best of luck with everything.

Many thanks to all the members from the Sanz-Moreno lab, especially: Jose, Irene, Eva, Pahini, Gaia, Mirella and Bruce for your assistance and technical advice, you all have been very nice and helpful to me as a 'Pseudo' lab member. I would also like to acknowledge Steph, Ritu, Jonathan M, 'Jez', Yoli, James A, James MP, Fabian, Gregory, Tamara, Lizzy, Sweta and all the other members in the department for their encouragement, advice and kindness. In addition, I would like to thank my PhD committee chair John M and members Snezhka and Vicky for their time and input.

I would also like to reach out to my collaborators at ICR Chelsea: Fernando and Nicola, many thanks for all the help and contribution with the animal work. Also, many thanks to collaborators George, Zareen, John and Tony from Bart's for their support.

Finally, I am extremely grateful to my family members; My parents for their love and support throughout my life, telling me to dream big and be ambitious. My pseudo family Tjong, for their support and kindness throughout my education. My partner Alice for her unconditional love, care and 24/7 support, looking after my health and mood during difficult times. I am also very indebted to her family members for treating me as one of their own and providing me a home and family, while being away from home. Without all of you, I would not have been where I am now and all this would not have been possible.

Abstract

Pancreatic ductal adenocarcinoma (PDAC) is the 5th most common cause of death by cancer in the UK, accounting for 5% of all cancer deaths in the UK. Only 8% of the PDAC patients from all stages combined, survives for 5 years or longer. Late stage diagnosis combined with early cancer cell dissemination and poor response to current available treatments highlights the need for novel therapeutics tackling tumour growth and invasion.

Previously, it has been shown that cellular plasticity during disease progression and the tumour stroma could contribute to cancer metastasis and resistance to therapy. Furthermore, progression in genetic sub-type classification of PDAC has shown differences in patient survival and response to treatment. However, PDAC cell plasticity and morphology in the presence of matrix has not been extensively addressed nor linked with sub-types thus far. Moreover, while 3D models are increasingly applied in order to mimic in vivo conditions more closely, the majority of current screening assays do not include components of the stroma and are based mainly on cell viability. In addition, well established genetic engineered mouse models (GEMM) and patient derived xenograft (PDX) are not cost effective or widely accessible for screening purposes. Understanding the behavioural characteristics and drug responses of PDAC cells with models mimicking the in vivo microenvironment is pivotal in developing novel therapies.

To address the need for invasion models that can be used for screening, I have first investigated PDAC cell behaviour with the 2.5D model *in vitro* and selected a representative cell line for screening. Subsequently, I have developed and optimised a 3D co-culture spheroid screening platform to assess compounds for inhibition of PDAC invasion in the presence of pancreatic stellate cells. A select drug library with 99 FDA approved compounds was probed for potential drug repurposing for PDAC invasion and selected for further validation. Together these experiments will provide us novel insight into the invasive behaviour of pancreatic cancer cells and identify potential novel molecular targets against PDAC cell invasion.

List of publications

Thillai, K.*, **Lam, H**.*, Sarker, D. & Wells, C. M. Deciphering the link between PI3K and PAK: An opportunity to target key pathways in pancreatic cancer? *Oncotarget*, doi:10.18632/oncotarget.13309 (2016).

* Contributed equally to this work

Lam, H., Sarker, D. & Wells, C. In vitro models of drug screening for pancreatic cancer. Pancreatology **16**, S8, doi:10.1016/j.pan.2016.04.029 (2016).

Table of contents

Table of abbreviations

5-FU	5-fluorouracil
α-SMA	α smooth muscle actin
ADEX	Aberrantly differentiated endocrine exocrine
ADM	Acinar-to-ductal metaplasia
ANOVA	Analysis of variance
BRCA2	Breast cancer type 2 susceptibility protein
BSA	Bovine serum albumin
CAF	Cancer associated fibroblast
CDKN2A	Cyclin dependent kinase inhibitor 2A
CTCF	Corrected total cell fluorescence
CXCL12	C-x-c motif chemokine ligand 12
DAPI	4’,6-diamidino-2-phenylindole
DMEM	Dulbecco modified eagle medium
DMSO	Dimethyl sulfoxide
DNA	Deoxyribonucleic acid
ECM	Extracellular matrix
EDTA	Ethylenediaminetetraacetic acid
EGF	Epidermal growth factor
EMT	Epithelital mesenchymal transition
ERK	Extracellular signal-regulated kinase
EtOH	Ethanol
FACS	Fluorescence activated cell sorting

FBS	Fetal bovine serum
FDA	Food and drug administration
FGF	Fibroblast growth factor
FOLFIRINOX	Folinic acid, 5-fluorouracil, irinitecan and oxaliplatin
GAP	GTPase activating protein
GDP	Guanosine diphosphate
GEFP	Guanine nucleotide exchange factor
GEMM	Genetic engineered mouse model
GFP	Green fluorescent protein
GSEA	Gene set enrichment analysis
GTP	Guanosine triphosphate
HA	Hyaluronic acid
H&E	Hematoxylin and eosin
HCl	Hydrochloric acid
HDAC	Histone deacetylase
HGF	Hepatocyte growth factor
Hh	Hedgehog
HRP	Horseradish peroxidase
ICAF	Inflammatory cancer associated fibroblast
IFP	interstitial fluid pressure
IGF	Insulin-like growth factor
IL-6	Interleukin 6
IPMN	Intraductal papillary mucinous neoplasia

KMD6A	Lysine Demethylase 6A
KPC mice	KRAS $^{LSL.\ G12D/+}$; $p53^{R172H/+}$; $PdxCre^{tg/+}$ mice
KRAS	Kirsten rat sarcoma viral oncogene homolog
LAPC	Locally advanced and unresectable pancreatic cancer
LIMK1	LIM domain kinase 1
LOX	Lysyl oxidase
MCN	Mucinous cystic neoplasia
MDSC	Myeloid derived suppressor cell
MEK	Mitogen activated protein kinase kinase
MLC2	myosin-light chain 2
MLL3	Mixed-lineage leukemia protein 3
MMP	Matrix metalloproteinase
MTA	Material transfer agreement
MyCAF	myofibroblastic cancer associated fibroblast
NaCl	Sodium chloride
NaF	Sodium fluoride
Na_3VO_4	Sodium orthovanadate
NGF	Nerve growth factor
PanIN	Pancreatic intraepithelial neoplasia
PARP	Poly-adenosine diphosphate-ribose polymerase
PBS	Phosphate buffered saline
PCC	Pancreatic cancer cell
PDA	Pancreatic ductal adenocracinoma

PDAC	Pancreatic ductal adenocarcinoma
PDGF	Platelet derived growth factor
PD-L1	Programmed death-Ligand 1
PEGPH20	PEGylated recombinant human hyaluronidase 20
PI3K	Phosphatidylinositol-4,5-bisphosphate 3-kinase
PMSF	Phenylmethylsulfonyl fluoride
PSC	Pancreatic stellate cell
QM	Quasi-mesenchymal
RBM10	RNA binding motif protein 10
RFP	Red fluorescent protein
RNA	Ribonucleic acid
ROBO	Roundabout receptor
ROCK	Rho associated coiled coil containing protein kinase
RTK	Receptor tyrosine kinase
SEM	Standard error of the mean
SLIT	Slit glycoprotein
SMAD4	SMAD family member 4
TAM	tumour associated macrophages
TCCF	Total corrected cell fluoresence
TEMED	Tetramethylethylenediamine
TGFβ	Transforming Growth Factor β
TP53	Tumour antigen p53
Treg	Regulatory T-cell

TRIS	Tris (hydroxymethyl)aminomethane
uPA	urokinase type plasminogen activator
uPAR	urokinase plasminogen activator receptor
tPA	tissue type plasminogen activator
VEGF	Vascular endothelial growth factor

List of Figures

List of tables

1. Introduction

1.1. Pancreatic ductal adenocarcinoma

Pancreatic ductal adenocarcinoma (PDAC) originates from the exocrine compartment of the pancreas and is the most common form of pancreatic cancer, accounting for 95% of all pancreatic cancers (1). The term pancreatic cancer has therefore often been used for PDAC synonymously. The pancreas is an endoderm derived organ located behind the stomach in the abdominal cavity (2) (Figure 1-1). It plays an important role in nutrient metabolism and consists of an exocrine and endocrine compartment. The exocrine compartment comprises of ductal, acinar and centroacinar cells that are involved in the production of digestive enzymes and their transportation through a network of ducts into the duodenum (3). The endocrine compartment harbours the islets of Langerhans, which are small clusters of glucagon- (α-cells), insulin- (β-cells), somatostatin- (δ-cells), ghrelin (ε-cells) and pancreatic polypeptide- (PP-cells) producing cells that maintain glucose homeostasis (3). Given the exocrine compartment accounts for >90% of the pancreas, it is therefore not surprising that exocrine tumours are more common than endocrine tumours (3).

Precursor lesions of PDAC include non-invasive intraductal papillary mucinous neoplasia (IPMN), mucinous cystic neoplasia (MCN) and the most common form pancreatic intraepithelial neoplasia (PanIN) (4, 5). A series of studies have reported that acinar cells might be the origin of PDAC through KRAS driven acinar-to-ductal metaplasia (ADM) transformation into duct-like cells with stem-cell like potential which could initiate PanIN formation, and progress to PDAC (6-10). However, recent findings have also suggested that transformation of ductal cells could potentially give rise to PDAC (11-14). It might not be surprising that through trans-differentiation or transformational processes that different cells of origin of the pancreatic exocrine compartment could give rise to PDAC in distinct manners.

Pancreatic cancer commonly occurs in the head of the pancreas with 65% of the cases, in contrast to the 15% for occurrences in the body, 10% in the tail and 10% occurring in multifocal manner (15). Some pancreatic cancers can occur as primary tumours with a size of less than 2cm, which are found infiltrating into the surrounding tissues,

including lymph nodes and nerves, and are considered as locally advanced and unresectable pancreatic cancer (LAPC). Nevertheless, the majority of patients are diagnosed with metastatic disease. Pancreatic cancer spreads most commonly to the liver and the peritoneal cavity, and less commonly to the lung, bone and brain (16).

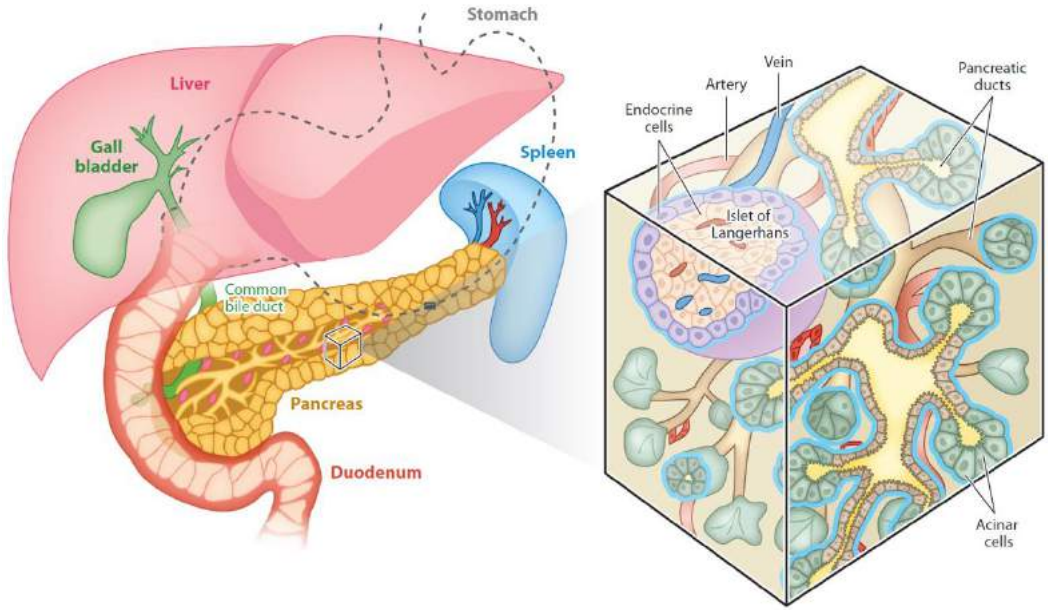

Figure 1-1. Anatomy of the pancreas.

The pancreas is located in the abdomen behind the stomach and is connected to the duodenum. The organ consists of a ductal network connecting acinar cells that secrete digestive enzymes and pancreatic fluid to the duodenum. Islet of Langerhans are found embedded within the exocrine tissue and are responsible for glucose homeostasis (Illustration from Shih et al 2013) (2).

1.1.1. Epidemiology

Pancreatic cancer is a lethal disease and is the 3rd leading cause of death by cancer in the US and 5th in the UK, with an estimated 50 000 and 10 000 new cases diagnosed every year in the USA and UK respectively (1, 17). Despite extensive research and improved surgical techniques in the past three decades, the survival rates have not improved while the death rate for pancreatic cancer has increased by 0.4% per year (1). This is mainly due to lack of biomarkers for early diagnosis, high resistance to current chemotherapy and high propensity for early metastasis (18).

The 5- year survival rate for all stages combined is only 8%, where most patients succumb to the disease in their first year of diagnosis (1). 10% of the patients are diagnosed with local disease (stages IA, IB and IIA), which are potentially curable with resection or are diagnosed borderline resectable (Table 1-1) (19). These patients have the best 5-year survival rate of 31.5%. Unresectable disease can be categorised in locally advanced and metastatic disease. About 29% of the patients are diagnosed with locally advanced pancreatic cancer (stages IIB and III) (19). In this situation, the cancer cannot be removed entirely by surgery due to its growth into or surrounding nearby major blood vessels, but has not yet spread to distant organs. These patients have an overall 5-year survival rate of 11.5%. 52% of the patients are diagnosed with metastatic disease (stage IV), which has a 5-year survival rate of less than 3% (19). The remaining 9% of the patients are either not diagnosed or were unable to be diagnosed for staging. These patients fall into the category of unknown staging and have a 5-year survival of 5.1% (19).

Table 1-1: Pancreatic cancer staging, stage description and related 5-year survival rate (20)

Stage	Stage description	5-year Survival rate
0	Pancreatic carcinoma in situ or pancreatic intraepithelial neoplasia III (PanIN III).	31.5% (19)
IA	No spread of the cancer outside the pancreas and has a diameter of 2cm or smaller.	
IB	No spread of the cancer outside the pancreas and has a diameter larger than 2cm.	
IIA	Spread of the cancer outside of pancreas, but not into major blood vessels, nerves, lymph nodes or distant sites.	
IIB	Spread of the cancer outside of pancreas and lymph nodes, but not into major blood vessels and nerves or distant sites.	11.5% (19)
III	Spread of the cancer outside of pancreas and into major blood vessels and nerves, maybe have spread to lymph nodes, but not to distant sites.	
IV	Spread of the cancer outside of pancreas to distant sites.	2.7% (19)

1.1.2. Risk factors

Pancreatic cancer is more common in older people, with people aged 75 years and older accounting for 47% of the diagnosed cases (21). Furthermore, pancreatic cancer has an equal prevalence of 50% in both men and women (21). The disease has a rare incidence before age of 40, but the risk increases by 40-fold for developing the disease at 80 years old (22). Smoking has been the most well-established environmental risk factor for pancreatic cancer. Nitrosamines found in cigarette smoke has been reported to be potent carcinogens, exposing smokers to approximately a 1.74-fold increase in risk of developing pancreatic cancer (23). Several other risk factors such as obesity, chronic pancreatitis, diabetes mellitus and familiar history were linked to increased risk (24). Furthermore, it has been reported that African-Americans have the highest incidence rate of developing pancreatic cancer across different ethnical groups, whereas Asian/Pacific Islanders and American Indian/Alaska Native have the lowest incidence rate (19).

1.1.3. Molecular genetics in PDAC progression

Genetic diversity is commonly found in pancreatic cancer, with frequent genetic mutations occurring in various genes such as *KRAS* (>90%), *CDKN2A* (95%), *TP53* (75%) and *SMAD4* (50%) (25). Furthermore, the progression from PanIN stages I, II and III to PDAC demonstrates that consecutive accumulation of these mutations results in accelerated progression of the disease (Figure 1-2) (26). Indeed, a genetic mouse model has demonstrated that expression of $KRAS^{G12D}$ alone in the progenitor cells of the pancreas will develop PDAC, but only after long latency (27). However, inactivation of tumour-suppressive genes *CDKN2A* and *TP53,* and *SMAD4* at later stages increases stepwise progression towards PDAC and metastasis (28-31). Moreover, telomere shortening has been reported in low-grade PanINs and contributes to chromosomal instability (32, 33). Subsequently, loss *BRCA2,* a tumour-suppressor gene responsible for homology directed DNA damage repair, at later stages in sporadic PDAC could further contribute towards genetic instability and become susceptible for PARP inhibitors (34, 35).

The *KRAS* gene encodes two small GTPases, KRAS4A and KRAS4B, with the latter being the more dominant transcript in the pancreas (26). Inactive GDP-bound KRAS is normally activated by RAS guanine nucleotide exchange factors (RasGEFs), which are proteins that facilitate activation of KRAS by catalysing the exchange of GDP for GTP (26). Activated GTP-bound KRAS is able to bind to downstream factors and activate the downstream signalling pathway (26). The GTP-bound KRAS is then inactivated by RasGAPS, which are proteins that catalyse the hydrolysis of the KRAS bound GTP back to GDP (26). However, a point mutation in codon G12 of the *KRAS* oncogene (found in 98% of all PDAC cases) will prevent the formation of van der Waals interactions between KRAS and RasGAPs, which in turn impairs the ability of RasGAPs to hydrolyse the GTP bound to KRAS. This results in constitutive activation of downstream signalling pathways driving proliferation, anti-apoptosis, evasion of the immune response, remodelling of the tumour microenvironment and metastasis (36).

Recent genetic sequencing and analysis efforts demonstrated that majority of the mutations (e.g. *KRAS*, *CDKN2A*, *TP53*, *SMAD4*) and additional mutations (e.g. *KDM6A, RBM10, MLL3*) found in pancreatic cancer patients can be grouped in 10 molecular mechanisms: KRAS, ROBO/SLIT Pathway, RNA processing, Cell cycle, DNA Repair, TGFBeta signalling, Notch Signalling, Wnt Signalling, Chromatin and SWi/SNF pathways (Table 1-2) (37). Furthermore, genetic studies on metastatic PDAC have found that genetic heterogeneity is not only present in the primary tumour, but also present in metastatic lesions, which might be required to successfully disseminate and colonise at distant sites (38, 39). Therefore, it is believed that multiple genetic abnormalities would accelerate PDAC progression in parallel with *KRAS* mutation.

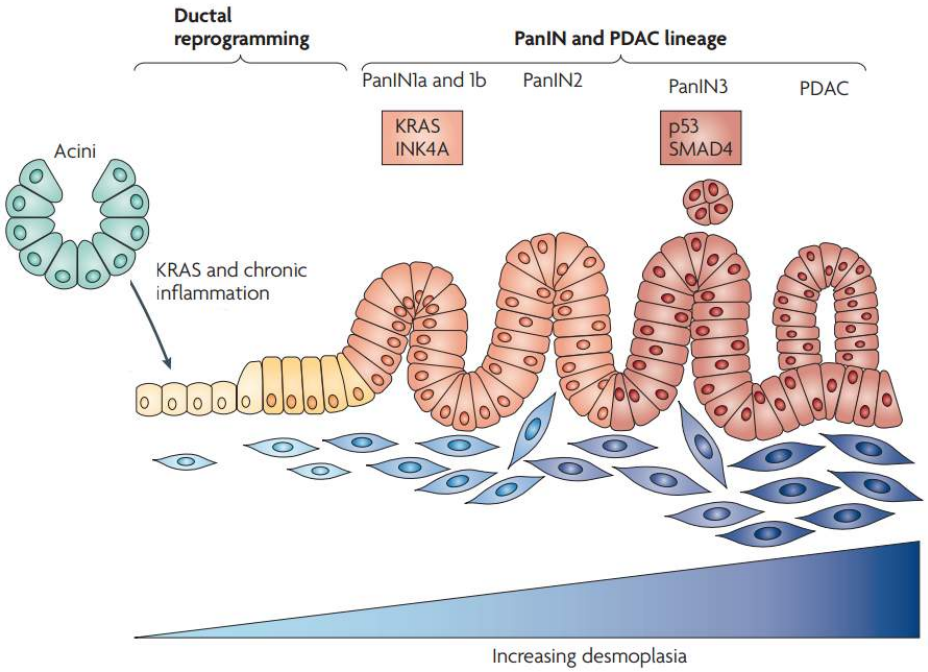

Figure 1-2. Progression of acini into PDAC through cumulative mutations in onco- and tumour-suppressive genes.
Activation of *KRAS* in acini gives rise to the development of PanIN. Inactivation of *INK4A* (CDKN2A) causes PanIN1 to progress into PanIN2. Inactivation of *p53* and *SMAD4* occurs during later stages and will accelerate the progression of PDAC formation with increased desmoplasia (Illustration adapted from J. P. Morris et al 2010) (40).

Table 1-2. Gene mutations in pancreatic cancer categorised in 10 Molecular mechanisms.

Molecular mechanism	Mutated genes
KRAS	*KRAS, MAPK4*
ROBO/SLIT pathway	*ROBO1/2, SLIT2. MYCBP2*
RNA Processing	*RBM10, SF3B1, U2AF1*
Cell Cycle	*CDKN2A, TP53, TP53BP2*
DNA Repair	*BRCA1/2, ATM, PALB2, ATF2*
TGFBeta Signalling	*SMAD3/4, TGFBR1/2, ACVR1B/2A*
Notch Signalling	*JAG1, NF2, BCORL1, FBXW7*
Wnt Signalling	*RNF43, MAPK2, TLE4*
Chromatin (histon modification)	*KDM6A, MLL2/3, SETD2*
SWI/SNF Complex (nucleosome)	*ARID1A/1B, SMARCA4, PBRM1*

1.1.4. Signalling pathways and therapeutic targets in PDAC

KRAS belongs to the Ras GTP binding protein family (41, 42). Downstream effector pathways of KRAS include PI3K-PDK1-Akt, RAF-MEK-ERK, PLCε, Tiam1-Rac and RalGDS (Figure 1-3) (41-43). Not only has it been shown that KRAS play a major role in PDAC formation, but also that Ras sustains PDAC through regulation of anabolic glucose metabolism via MAPK and Myc signalling pathways (40, 44). Recent findings have demonstrated that activation of major KRAS downstream pathways were able to phenocopy *KRAS* driven PDAC in genetic mouse models. Targeted expression of *PIK3CA*^{H1047R}, which encodes for the catalytic subunit of PI3K p110α, in the acini induced ADM, PanIN and subsequently PDAC (45). Furthermore, inhibition or deletion of proteins of the PI3K-PDK1-Akt pathway were able to suppress PDAC progression (45). Another study has demonstrated that targeted expression of activated *BRAF*^{V600E} in the pancreas was able to induce PDAC (46). Moreover, pharmacological inhibition of the MEK demonstrated anti-tumour effects in PDAC cell lines (46). These finding demonstrate an important role of KRAS and its downstream pathways in PDAC progression and possibly therapy.

Despite extensive research on KRAS inhibition, the first effective KRAS inhibitor has yet to reach the clinic. Nevertheless, a plethora of inhibitors targeting the downstream effectors of KRAS, such as Akt, MEK and BRAF, are currently being tested in clinical trials (www.clinicaltrials.gov). Furthermore, recent allosteric inhibitors against KRAS have been developed and showed promising results *in vitro* (47). However, it has been reported that differential KRAS mutations result in distinct MEK inhibitor responses, which demonstrates the complexity of targeting KRAS and its downstream effectors (48). Furthermore, targeting KRAS and its downstream pathways might establish acquired resistance as demonstrated in other cancer targets (49). Recent findings have shown that relapse occurs between 9 and 47 weeks after *KRAS* inactivation and tumour regression in genetic mouse models (50). *KRAS* re-activation was found in half of the population, while the other half demonstrated PDAC maintenance through YAP1, a protein in the hippo pathway which induces proliferation, invasion and epithelial mesenchymal transition (EMT) (50, 51). Moreover, several experiments have demonstrated the independency of K-Ras in

certain PDAC cell lines (52, 53). This demonstrates that multiple pathways might need to be targeted for effective treatment of PDAC.

Other potential pathways for targeting include growth signalling pathways, such as epidermal growth factor (EGF), fibroblast growth factor (FGF), hepatocyte growth factor (HGF), insulin-like growth factor (IGF) and transforming growth factor-β (TGF-β), and developmental signalling pathways, such as Hedgehog (Hh), Notch and Wnt. These pathways are known to be important in the development of the pancreas and have been reported to play a role in PDAC progression as well (54-56). However, more work is needed to improve these specific therapies, despite the lack of an favourable response in advanced and metastatic pancreatic cancer patients in clinical trials (See 1.1.6. current therapies).

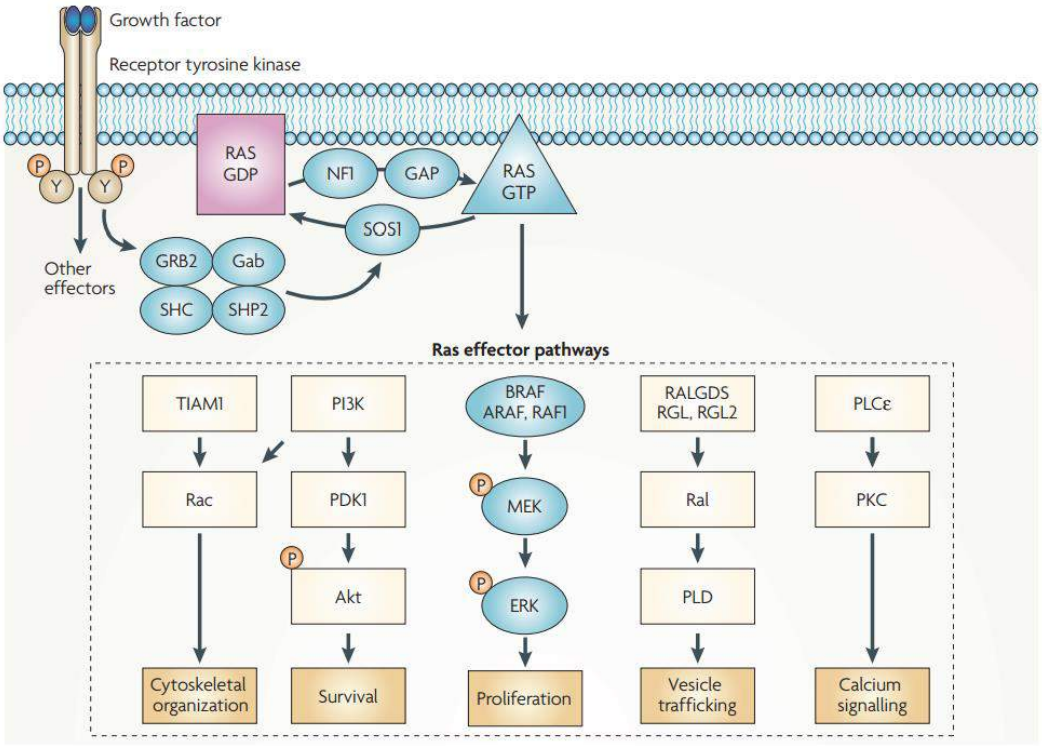

Figure 1-3. KRas downstream signalling pathways involved in cancer.
KRas is normally activated through receptor tyrosine kinases (RTKs) signalling. In most cancers KRas is found in a constitutively active state and activate downstream signalling pathways. PI3K-Pdk1-Akt and Raf-Mek-Erk have been reported to be the major downstream pathways involved in PDAC progression (Illustration from Schubbert et al 2007) (41).

1.1.5. Pancreatic cancer subtypes

The molecular and genetic alterations identified in genomic sequencing and translational studies has shown to contribute towards tumour heterogeneity in individual patients, resulting in the discovery of different sub-type classifications (37, 53, 57-59). Subtype heterogeneity has been shown to be responsible for variability in therapeutic efficacy in breast and lung cancer (60, 61). In 2011, three subtypes for PDAC have been categorised through combinatorial analysis of transcriptional profiles of primary samples from various studies and combined with mouse and human cell lines: classical, quasi-mesenchymal (QM) and exocrine-like (53). The classical subtype is associated with high expression of adhesion and epithelial genes and KRAS dependency, while the QM subtype is associated with high expression of mesenchyme associated genes and low KRAS dependency. Furthermore, exocrine-like subtype is associated with high expression of digestive enzyme genes. Each of these subtypes were correlated with difference in clinical outcome and therapeutic response (Figure 1-4).

During the course of this project, additional subtypes have been described (37, 58). Waddell et al has established four subtypes with potential clinical utility based on structural variation patterns in chromosomal structure: Stable, Locally rearranged, Scattered and Unstable (58). In contrast, Bailey et al used RNA expression profiles to investigate the transcriptional networks and defined four subtypes that were similar to Collisson's classification: Squamous (QM subtype), Pancreatic progenitor (Classical), immunogenic and aberrantly differentiated endocrine exocrine (ADEX) (Exocrine subtype) (37, 53). This finding further supports the presence of subtypes and the transcriptional differences that drives them.

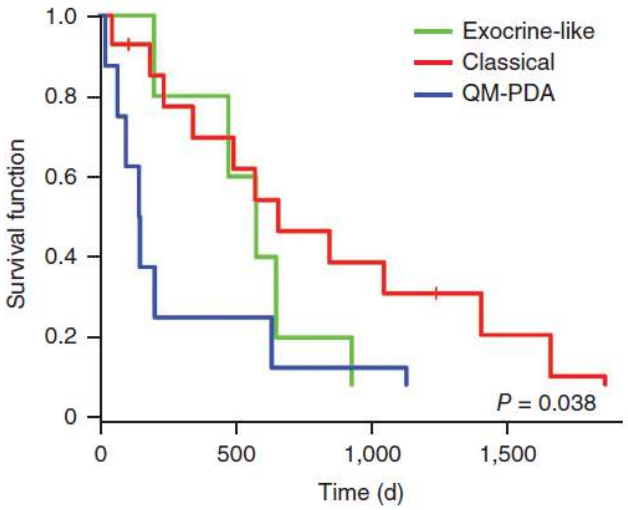

Figure 1-4. Survival of different subtypes.
Survival curves of patients divided into the three different subtypes: Classical, quasi-mesenchymal (QM-PDA) and exocrine-like. Different subtypes are linked with different clinical outcome and therapeutic response (Illustration from Collisson et al 2011) (53).

1.1.6. Current therapies

Current therapy for advanced pancreatic cancer is treatment with gemcitabine alone or in combination with other therapeutics (25). These combination chemotherapies, which include gemcitabine in combination with capecitabine or nab-paclitaxel, and the combi treatment of folinic acid (Leucovorin), 5-fluorouracil, irinotecan and oxaliplatin (FOLFIRINOX), have slightly improved the 1 year survival of advanced pancreatic cancer patients (Table 1-3) (62, 63).

Gemcitabine is a deoxycytidine analog that is incorporated into DNA and inhibits DNA replication and repair through a 'masked chain-termination' process (64). Nab-paclitaxel is an albumin-bound form of paclitaxel, and is found to inhibit cell division through blocking the depolymerisation of microtubules (65). Capecetabine is a fluoropyrimidine and is metabolised into 5-fluorouracil (5-FU) in 3 steps (66). 5-FU is an uracil analogue with a fluorine atom at the C-5 position instead of hydrogen and blocks DNA replication through inhibiting thymidylate synthase and by incorporating itself into DNA (67). Folinic acid has been shown to enhance the effects of 5-FU on thymidylate synthase (68). Irinotecan inhibits DNA topoisomerase I and oxaliplatin is a platinum based DNA damaging drug (67). However, none of the therapies are targeting specific pathways in pancreatic cancer, and display severe side effects with modest benefits.

Several attempts in targeting pathways have been successful in genetic mouse models *in vivo*, but has been translated into minimal efficacy in clinical trials. For example, Erlotinib, a small molecule inhibitor targeting the EGFR tyrosine kinase is the only approved targeted therapeutic used in combination with Gemcitabine. Nevertheless, the survival benefit only increased from 5.9 months to 6.2 months on average (69). Similarly, Cetuximab, an antibody against EGFR have been tested in clinical trials with little efficacy (69, 70). Other notable examples include combination therapy of gemcitabine with the IGFR antibody (Ganitumab), VEGF antibody (Bevacizumab) or the Smoothened (SMO) inhibitor Saridegib, all of which failed to demonstrate improved survival compared to gemcitabine alone (71-73). These

studies demonstrate the molecular complexity of PDAC and differences between therapeutic successes in genetic mouse models and clinical trials. However, majority of the clinical studies are conducted in advanced or metastatic pancreatic cancer patients and could potentially provide improved response and outcome in non-metastatic or resectable pancreatic cancer patients. Nevertheless, novel therapies targeting pancreatic cancer invasion mechanisms could benefit resectable and unresectable patients.

Recent advances in immunotherapy in other cancers such as melanoma and lung have prompted promising outcomes for pancreatic cancer patients. However, immunotherapy has not been successful in treating advanced pancreatic cancer thus far. A phase I study demonstrated that none of the 14 patients with locally advanced or metastatic pancreatic cancer patients responded to the treatment with a programmed death-ligand 1 (PD-L1) specific monoclonal antibody (74). In a phase II study, only one out of 27 locally advanced or metastatic pancreatic cancer patients responded to the treatment with Ipilimumab, an anti-CTLA-4 monoclonal antibody, in a significant delayed response (75). Nevertheless, these studies did not screen patients on microsatellite instability in their tumours, which has been associated with an increased rate of response to immunotherapy, especially in melanoma and lung cancer patients (76, 77). This suggests that immunotherapy in pancreatic cancer might not be as promising and needs further investigation. Furthermore, this also highlights the need for alternative therapies against pancreatic cancer.

Table 1-3. Therapies for pancreatic cancer and their 1-year overall survival rates.

Drug combination	1-year overall survival
Gemcitabine	20.6-22% (62, 63)
FOLFIRINOX	48.4% (62)
Nab-Paclitaxel-Gemcitabine	35% (63)
Gemcitabine-Capecitabine	24% (78)

1.2. The role of the tumour microenvironment in PDAC

The tumour microenvironment plays a crucial role in the progression of pancreatic cancer and could influence the outcome of therapeutics. The majority of the pancreatic tumour volume is made up by the tumour stroma (79). Furthermore, stromal cells and immune cells are known to have an important role in PDAC progression and therapeutic resistance (80, 81). Therefore, the key to therapeutic success may lie in understanding the interplay of various compartments in the tumour microenvironment and the tumour.

Desmoplasia, the proliferation of fibrotic tissue, is one of the hallmarks of PDAC and is characterised by a large tumour stroma that undergoes extensive remodelling with increased expression of collagen I and the loss of normal tissue architecture. Cross-talk between normal epithelial cells, invading tumour cells, fibroblasts, pancreatic stellate cells (PSC), endothelial cells, and infiltrated inflammatory cells, which are all embedded within the extracellular matrix (ECM), are found within the tumour stroma (80, 82) (Figure 1-5). The complex interplay within the stroma results in autocrine and paracrine signalling activated through secreted growth factors that sustain the tumour and promotes tumour growth and metastasis (82, 83). Furthermore, unlike the majority of tumours, there is a poor angiogenic response in PDAC. The desmoplastic reaction results in an abnormal vasculature with leaky blood vessels and capillaries that induces a hypoxic environment (79).

Researchers have tried to target the tumour microenvironment for PDAC therapy, but its increased ECM stiffness, induced hyaluronic acid (HA) content, high interstitial fluid pressure (IFP) and hypovascular nature lead to decreased delivery and efficacy of chemotherapy (84, 85). Therefore, it was thought that stromal depletion could enhance therapeutic response. However, recent reports on the depletion of PSC in the microenvironment demonstrated increased tumour progression and aggressiveness (86, 87). Alternatively, another study has demonstrated that targeting lysyl oxidase (LOX) in KPC mice can inhibit metastasis and increase the efficacy of Gemcitabine through reducing collagen cross-linking in the stroma (88). Additionally, the use of PEGPH20, a drug that degrades Hyaluronan in the tumour microenvironment of pancreatic cancer patients has demonstrated increase efficacy

when used in combination with nab-paclitaxel plus Gemcitabine versus nab-paclitaxel plus gemcitabine alone in a phase II trial (89). These studies have shown that the role of the tumour microenvironment increases the complexity of PDAC therapy, yet yield a large potential as therapeutic target. Future experiments should include stromal cells from the tumour microenvironment in order to discover potential successful therapeutics.

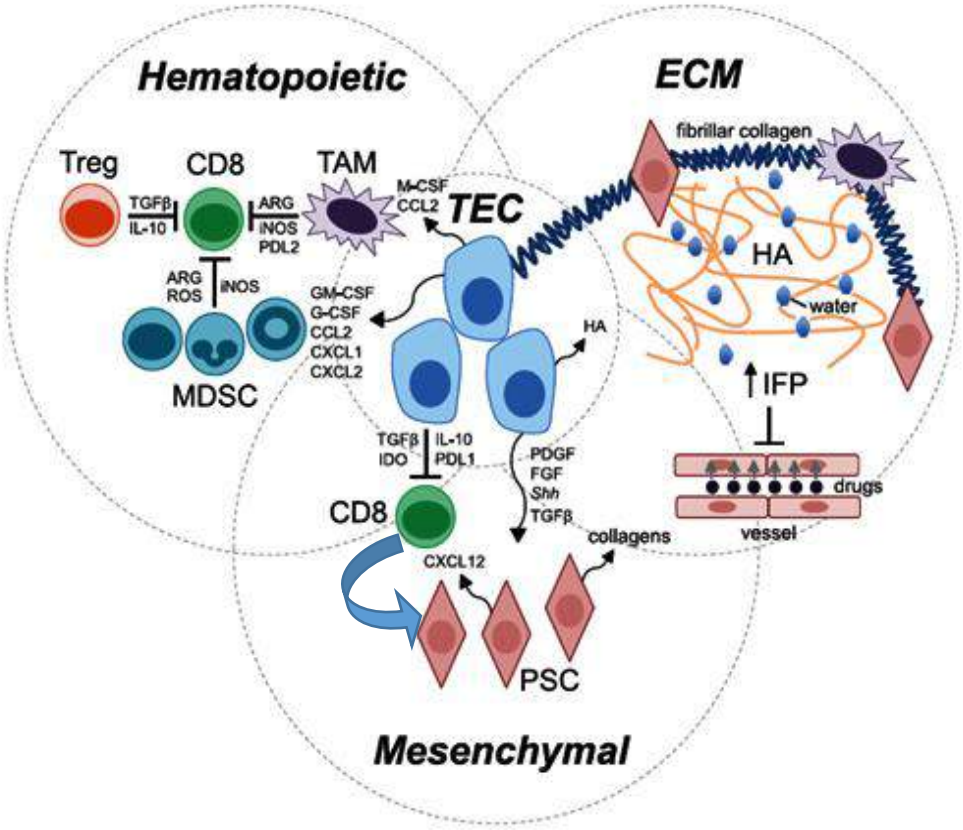

Figure 1-5. A schematic representation of complex cross-talk interactions between various components in the tumour microenvironment of PDAC.
Immunosuppressive cells (tumour associated macrophages (TAM), regulatory T cells (Tregs) and myeloid derived suppressor cells (MDSCs)) infiltrate the stroma and induces pro tumorigenic inflammation. Tumour epithelial cells (TEC) activates PSCs in the mesenchymal compartment induces production of ECM components and subsequently invasiveness in TECs. PSCs are in turn able to sustain their own activity through autocrine signalling. The ECM undergo extensive remodelling and induces HA production, IFP and stiffness, contributing to resistance to chemotherapy. (Illustration adapted from Stromnes et al 2014) (80).

1.2.1. Pancreatic stellate cells

Pancreatic stellate cells are star-shaped fibroblasts found in the periacinar space and comprises 4% of the organ in their dormant state (90). They are characterised by abundant lipid droplets in the cytoplasm and have low capability of ECM synthesis and low cell division activity (79). Furthermore, PSCs express glial fibrillary acid protein (GFAP), nestin, vimentin, desmin, N-cadherin and nerve growth factor (NGF), which distinguishes them from other fibroblasts (91).

Secreted cytokines (IL-1 and IL-6) and growth factors (FGF, PDGF, TGF-β and VEGF) by inflammatory cells and pancreatic cancer cells (PCCs) are able to activate PSCs (90, 92). Upon activation, PSCs will lose their lipid content and adopt a myofibroblastic phenotype characterised by the expression of α-smooth muscle actin (α-SMA) (93). Activated PSCs are already found in PanIN stages and are the major contributor of ECM proteins with collagens I, III and fibronectin being the major components of the fibrotic tissue (93). Through secretion of ECM proteins, growth factors ((FGF, PDGF, TGF-β1 and VEGF), inflammatory cytokines and chemokines (CXCL12 and IL-6), and proteases such as matrix metalloproteinases (MMPs), PSCs are capable of sustaining PSC activation through autocrine and paracrine signalling, as well modulating the matrix and inducing PDAC progression (80, 90, 92, 94). Co-culture of PCCs and PSCs induced proliferation of PCCs through Notch signalling *in vitro* (95). Furthermore, PSCs enhanced sphere formation abilities of pancreatic cancer cells and induced resistance to radiation therapy and Gemcitabine, implicating increased 'stemness' (characteristics of stem cells; self-renewal and pluripotency) and a cancer stem cell population in PDAC with increased drug resistance (96-98). Moreover, combined orthotopic injection of PSCs and PCCs in nude mice demonstrated increased tumour growth, desmoplasia and metastasis compared to injection of PCCs alone (99, 100).

However, studies have also reported that PSCs also act as a restrictor of tumour progression (86, 87, 101). Indeed, a recent study has demonstrated that PSCs differentiate into two types of cancer associated fibroblasts (CAFs) (102). The researchers shown that by using a novel three-dimensional co-culture platform, they were able to recapitulate *in vivo* CAF heterogeneity by demonstrating ECM deposition by activation of PSCs and promoted proliferation of pancreatic organoids.

Through characterising the organoid and PSC co-culture, the authors have identified a population of CAFs in close proximity to the epithelial organoids expressing strong αSMA, named myofibroblastic CAFs (myCAFs) (102). Another population of CAFs with high expression of IL-6 and low αSMA expression was found to be more distantly distributed from the epithelial cells away. These CAFs are termed inflammatory CAFs (iCAFs), and increase inflammatory cytokines through paracrine signalling (102). This study suggests that myCAFs could have anti-tumorigenic activity and was removed in the CAF depleting experiment selected on αSMA expression, whereas the iCAFs have pro-tumorigenic activity and were not removed in the mouse models, resulting in increased progression of the cancer (86). However, it must be noted that both iCAFs and myCAFs are mutually exclusive but reversible subtypes (Figure 1-6). Therefore, further elucidating the pro- and anti- tumorigenic impact of PSCs is crucial for therapeutic development against PDAC.

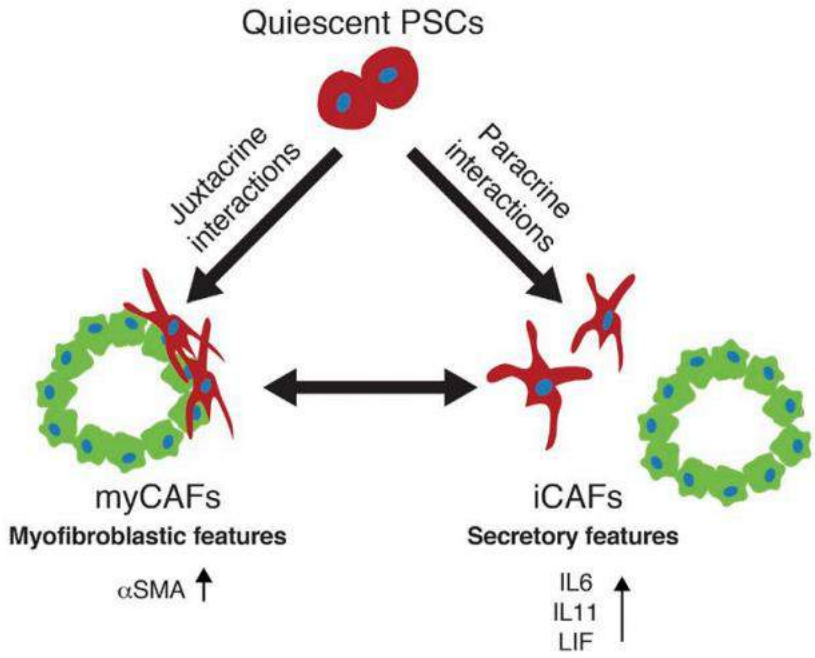

Figure 1-6. Schematic of relation between PSCs, myCAFs and iCAFs.
Upon activation, quiescent PSCs can differentiate either into myofibroblastic CAFs (myCAFs) through juxtacrine interactions or into inflammatory CAFs (iCAFs) through paracrine interactions, each with distinctive features. (Illustration from Ohlund et al 2017) (102).

1.3. Cancer metastasis

Tumour metastasis is known to be the main cause of cancer lethality (103, 104). Tumours metastasise by cancer cell dissemination, migration and invasion into surrounding stroma. Afterwards, cancer cells intravasate into the bloodstream and survive the sheer force and pressure, and then extravasate from the bloodstream to a distant site and colonize into a new metastatic lesion (105). The high propensity of PDAC dissemination has led to a poor survival rate of patients, where often metastasis has already occurred by the time of diagnosis or has been undetectable in the form of micro-metastases (25). In order to treat PDAC metastasis, it is important to understand the underlying morphological and molecular mechanisms. Several studies have already reported the regulation of pancreatic cancer migration and invasion.

1.3.1. Regulation of cellular morphology during migration and invasion

Cells are able to interconvert between various modes of cellular migration to facilitate cell migration and invasion through various barriers. Individual cell migration and invasion can be highly plastic, allowing cells to switch between an elongated/mesenchymal-like and a rounded/amoeboid-like mode of movement to effectively migrate and invade through various tissue types (105). ROCK1 and ROCK2 are serine/threonine protein kinases of the AGC kinase family and can be activated by active Rho to interact with kinases such as LIM domain kinase 1 (LIMK1) and myosin-light chain2 (MLC2), which are involved in the regulation of the cytoskeleton (106, 107). Recently, it has been shown that novel AKT inhibitors (AT13148 and CCT129245) were able to inhibit ROCK signalling and subsequently actomyosin contractility, causing impaired cellular invasion of both amoeboid and mesenchymal cells in melanoma (108). Actomyosin contractility is regulated by ROCK signalling and is necessary for maintaining cellular shape in all types of cells, but different levels determine different modes of migration (108). Activation of ROCK signalling leads to increased actomyosin contractility at the cortex through mono-phosphorylation of

MLC2 at Serine 19 (109). It has also been reported that components of the STRIPAK complex, which regulate actomyosin contractility through inhibiting dephosphorylation of pMLC2, are involved in the regulation of the mode of cellular migration and metastasis (110). Amoeboid cells have increased activation of the Rho-ROCK signalling pathway (111) together with activation of JAK1 signalling (112), whereas the mesenchymal mode of migration is characterised by an elongated morphology with actin rich protrusions through increased Rac1 GTPase activation (113). The increase in actomyosin contractility at the cortex allows amoeboid cells to migrate through formation of blebs, which are protrusive structures capable of directing migration (114). A study from the Sanz-Moreno lab has shown that MMPs are able to regulate amoeboid cancer cell migration (115). Therefore, it might be possible that MMPs secreted by PSCs induce amoeboid phenotypic migration and invasion in PDAC. Nevertheless, various studies have demonstrated that PSCs induce invasion through EMT in PDAC (97, 116, 117).

Other studies have demonstrated that mutant p53 driven spatiotemporal regulation of RhoA activity was associated with increased invasiveness of pancreatic cancer cell (118, 119). This was further supported by another study, which demonstrated that the increase in cAMP levels decreased the levels of active RhoA or RhoC and leads to the inhibition of PDAC cell motility through F-actin remodelling (120). Furthermore, focal adhesion kinase and Src has been shown in other cancers to regulates E-cadherin dependent collective cell movement in a complex three-dimensional tumour environment (121). Moreover, Src inhibitor Dasatinib has demonstrated inhibition of metastasis in pancreatic cancer mouse model (122). These findings suggest that the role of actomyosin contractility and actin remodelling should be further investigated to increase or understanding of cellular plasticity and motility in pancreatic cancer.

1.3.2. Epithelial-mesenchymal transition

EMT is a process of cellular plasticity and induces a phenotypic change from a round-epithelial to an elongated-mesenchymal phenotype during embryonic development, tissue regeneration and wound healing (123). EMT has also been shown to promote migration, invasion, cancer stemness, as well as resistance to therapy in pancreatic

cancer (124-126). PSC cells are known to secrete extra cellular factors such as TGF-β, FGF, PDGF, EGF, MMP-2, MMP-9, collagen type I and III, and hyaluronic acid to induce EMT in pancreatic cancer cells through the activation of transcription factors Zeb1, Slug, Snail and Twist (127). These transcription factors suppresses genes regulating the epithelial phenotype (126). This leads to the down-regulation of the epithelial marker E-cadherin, nuclear translocation of β-catenin, and the up-regulation of mesenchymal markers such as N-cadherin, vimentin and fibronectin in the pancreatic cancer cells. It has been reported that up-regulation of N-cadherin and vimentin in primary tumours of PDAC patients were correlated to increased invasion and metastasis (128). Furthermore, zeb1 induced EMT was shown to induce resistance to gemcitabine in pancreatic cancer cell lines (124). Moreover, depletion of Zeb1 blocked EMT and invasion in an *in vivo* mouse model (129). In addition, another study has shown that inflammation induce EMT and accelerate metastasis in an *in vivo* mouse model during early stages of pancreatic cancer progression (130). Also, EMT transcription factor Slug has been demonstrated to regulate actin bundling protein fascin during late stage PanIN and PDAC formation in a mouse model for pancreatic cancer. Fascin was able to promote the formation of filopodia and increase invasion in PDAC cells (131). Thus, EMT plays an important role in PDAC invasion and metastasis.

1.3.3. Collective cell migration

Cancer cells are able to invade individually or in a collective manner. Histopathological sections often demonstrate collective cell invasion in tumours, which are able to move in organised structures such as cell strands and luminal structures like acini and glands (132). Cells that migrate and invade collectively remain cohesive while moving, mainly due to the retained expression of cell-cell junction proteins (133). These cell-cell junction proteins include tight junction proteins, gap junctions, catenins and cadherins, which play an important role in mediating front-rear polarity, cytoskeletal synchronisation and mechanocoupling during migration (134-136). It has been suggested that MLC2 activity might have a role in guiding collective cell migration rather than driving the migration, through

modulating cell shape and cortical actomyosin dynamics (137, 138). Recently, it has also been suggested that actomyosin contractility might be important in the retrograde flow of N-cadherin based junctions from the cell front to the rear and recycled back to the front to induce movement similar to a 'treadmill' (139). In addition, another study has shown that RhoA regulates the interaction between the leading cell and the following cells, inducing a hierarchy and increased multicellular cytoskeletal contractility (140). These studies demonstrate the important role of actomyosin contractility in guiding collective cell migration and invasion. Although collective cell invasion has not been extensively investigated in PDAC, it has been shown recently in PDAC organotypics (141). It is important to identify collective cell structures with differences in actomyosin contractility, and distinguish single cell and collective cell invasion in PDAC.

1.4. Aims

The limitation of effective therapies against pancreatic cancer and pancreatic cancer invasion calls for the discovery and the development of novel therapies. Current available pancreatic cancer models that accounts for factors in the tumour microenvironment, such as the organotypic assay or *in vivo* genetic engineered mouse models, are expensive and not suitable for drug screening purposes. It was therefore hypothesised that by developing and performing a drug screen in a 3D pancreatic cancer invasion model *in vitro* would yield promising hits against the progression of invasive pancreatic cancer.

As mentioned previously, pancreatic cancer behaviour and mode of migration has previously not been investigated. Therefore, the first aim of this study is to investigate and characterise the cellular morphology and plasticity in pancreatic cancer across a panel of human PDAC cell lines. The characterisation will provide the basis for the selection of a robust, highly invasive cell line model for the drug screen platform.

In order to bridge 2D plastic culture and in vivo or clinical models, the second aim of this study is to develop a 3D in vitro model with the selected cell line model and tumour microenvironment factors to investigate pancreatic cancer invasion. Furthermore, the model will be designed and optimised for drug screening against pancreatic cancer invasion.

In the final part of this work, the aim is to identify potential novel therapeutics by performing a drug repurposing screen with the developed 3D drug screen platform against pancreatic cancer invasion. A drug library with selected FDA approved drug compounds will be screened and promising hits will be validated.

2. Methods and materials

2.1. Cell culture

Pancreatic ductal adenocarcinoma cell lines (Table 1) Capan1 (Kindly provided by Prof. H. Kocher at Barts Cancer Institute, UK), Capan2, PaTu8902 (Obtained from DSMZ, Germany), Colo-357 (Kindly provided by Prof. Michalski University Hospital Heidelberg, Germany) and SW1990 (Kindly provided by Dr. G. Sala at University of Chiety-Pescara, Italy) were cultured in RPMI (Sigma) supplemented with 10% fetal bovine serum (FBS) (Gibco) and 1mM Penicillin/streptomycin (Gbico). Panc-1 (Kindly provided by Mr. H. Kocher at Barts cancer institute, UK), PaTu8988T, PaTu8988S (Kindly provided by Dr. F. U. Weiss at Ernst Moritz Arndt Universitat Greifswald, Germany), Suit2-007 and Suit2-028 (Kindly provided by Dr. L. Castellano, Imperial College London, UK) were cultured in DMEM (Sigma) supplemented with 10% FBS and 1mM Penicillin/streptomycin. HPAC (Kindly provided by Dr. J. Hernandez Losa at Hospital Universitario Vall d'Hebron Barcelona, Spain) was cultured in DMEM/F12 (Sigma) supplemented with 10% FBS and 1mM Penicillin/streptomycin. CFPAC-1 (Kindly provided by Dr. A. Pessina at Universita degli studi di Milano, Italy) was cultured in IMDM supplemented with 10% FBS, 1mM penicillin/streptomycin. Pancreatic stellate cell line PS-1 (Kindly provided by Mr. H. Kocher at Barts cancer institute, UK) was maintained in DMEM/F12 supplemented with 10% FBS, 1mM Penicillin/streptomycin and 1ug/ml Puromycin (Sigma) as selection marker(142). All cell lines were cultured at 37°C under 5% CO_2 with regular medium replacement. All cell lines were regularly tested mycoplasma negative by DAPI staining or by using the Sigma Lookout mycoplasma PCR detection kit (MP0035) when cultured in the absence of penicillin/streptomycin for at least 4 days.

Cells were grown as attached monolayers in sterile culture flasks (T75 from TPP or T25 and T175 from Nunc) up to a confluency of ~80% prior to washing with sterile $PBS^{-/-}$ (Gibco) and were enzymatically detached with 0.5% Trypsin-EDTA (Gibco) by incubation at 37C under 5% CO_2 between 3 to 10 min. Growth medium was added to inactivate the trypsin and the cell suspension was transferred into a falcon tube for centrifugation at 200g for 5min at RT. The supernatant was then removed and cells

were resuspended with fresh growth medium into single cells for further passaging or seeding for an experiment.

Lentiviral vectors containing Lifeact-GFP and Lifeact-Mrfpruby were kindly gifted by Prof. M Parsons at King's College London. Stable expressing Patu8988T Lifeact-GFP, PaTu8902 Lifeact-GFP and PS-1 Lifeact-Mrfpruby were generated as previously(143). Briefly: Lifeact lentiviral, packaging and envelope vectors were transfected into HEK 293T cells with lipofectamine 3000 (Invitrogen). Viral particles were harvested by collecting and passing the supernatant through a 0.45µM filter (Millipore) before infecting target cells. Infected cells were passaged 5 times to clear out all the viral particles and were then FACS sorted for medium and high level GFP/Mrfpruby expression with a BD FACSARIA 3 Fusion in a sterile hood by the staff at the Guy's St. Thomas NHS Trust BRC flowcore.

2.2. Morphological characterisation on 2.5D Collagen

Morphological characterization on 2.5D collagen was conducted on a thick layer of type 1 Collagen described as previously (115). A collagen mixture containing a final concentration of 1.7mg/ml PureCol bovine collagen type I (Advanced Biomatrix) in DMEM (GIBCO) was added into a 24-wells plate (300ul per well) and left polymerizing for 2 hours at 37°C with 5% CO_2. Similarly, 100ul per well of collagen mixture was added in a 96-wells for immunofluorescence staining purposes. 2-4x10^4 cells were then seeded in triplicate onto the thick layer of collagen in growth medium, allowed to adhere for 20 hours at 37°C with 5% CO_2. Thereafter, medium was aspirated 20 hours post seeding and cells were then washed twice with PBS (Ca^{2+}/Mg^{+}) (Gibco) prior to culturing in 1% FBS containing medium to prevent cell division, as cell division increases the tendency of cells to become roundly shaped. For morphological analysis, two to three phase contrast images were taken of each cell line in a 24-wells plate per individual experiment with a Qicam (Qimaging) attached to a Nikon TS100 inverted microscope with a x10 objective at 24 and 48 hours post seeding.

Additionally, for time-lapse microscopy, 20mM HEPES was added to each well 24hrs post seeding. The plate was then wrapped with parafilm and put on a heated stage

at 37C of an Olympus IX 71 with Qicam (Qimaging) and QCapture pro software (Qimaging). The cells were recorded for 16hrs overnight.

Morphological events were analyzed by counting the number of single cell events (Individual cells, not connected to any other cells), doublet cell events (cells undergoing division or two cells connected to each other), clustered cell events (group of cells (more than 2 cells) found attached to each other, which might form colonies) and colony cell events (group of cells (more than 2 cells) found in a tightly packed colony with defined borders) in ImageJ (Figure 1a). The total number of morphological events (100%) is defined as the sum of all events per field. Single cell morphology was defined by the 'roundness' of single cells, which was determined by manually drawing around the border of individual cells and measuring the 'roundness' shape descriptor in ImageJ. Cells with a roundness index of closer to 1 were seen as amoeboid and closer to 0 were seen as mesenchymal phenotype.

2.3. Immunofluorescence

Assessment of E-cadherin and pMLC (S19) expression was carried out in cells on thick layer collagen type 1. 1-2x10^4 cells cultured on thick layer collagen in 96 wells plate were fixed for 15min at room temperature with a final concentration of 4% paraformaldehyde 48 hours post seeding. Cells were then rinsed twice with PBS (Ca^{2+}/Mg^{+}) prior to permeabilisation with 0.3% triton-x100 in blocking buffer (4% Bovine albumin serum (BSA) (VWR) in PBS (Ca^{2+}/Mg^{+})) for 20min at room temperature. Thereafter, cells were rinsed and incubated with blocking buffer for 30min at room temperature. Cells were afterwards incubated with primary antibody (Mouse anti-E-cadherin (Abcam; HECD-1) with a final dilution of 1:100 or Rabbit anti-p-MLC2 (S19) (Cell signaling; #3671) in a final volume of 30ul blocking buffer per well on top of the 100ul thick layer collagen overnight at 4°C. The next day, after five rinses with PBS (Ca^{2+}/Mg^{+}), cells were incubated with secondary antibody (Goat anti-Mouse- or Goat anti-Rat- Alexa Fluor 488nm conjugated with a final dilution of 1:500), Phalloidin-Rhodamine (Invitrogen) with a final dilution of 1:300 and DAPI (Sigma) with a final dilution of 1:10000 in a total volume of 50ul blocking buffer per well on

top of 100ul thick layer collagen protected from light for 2 hours at room temperature. Afterwards, cells were rinsed six time with PBS (Ca^{2+}/Mg^{+}) and stored in PBS (Ca^{2+}/Mg^{+}) protected from light at 4°C till image acquisition. Imaging was carried out by transferring the collagen gel upside down onto a glass-bottomed dish (MatTek) and confocal images were taken with the Zen software on a Zeiss LSM 510 Meta (Carl Zeiss) confocal microscopy with a C-apochromat x40/1.2 NA water based objective.

Dewaxed organotypic specimen sections were marked around with a deliminating wax pen (DAKO) prior to permeabilisation with 0.2% Triton X-100 in PBS for 5min at room temperature. Sections were washed twice with PBS prior to auto fluorescence quenching by incubation with freshly prepared quenching buffer (1mg/ml sodium borohydride (Sigma) in PBS) for 10 minutes at room temperature. Samples were then washed again with PBS prior to blocking with blocking buffer (5% BSA in PBS) for 30min at room temperature. Thereafter, samples were incubated with primary antibody (Rabbit anti-cytokeratin for widespectrum screening (DAKO; Z062201-2) with a dilution of 1:500 or Mouse anti-αSMA (Dako; clone 1A4) with a dilution of 1:300) in blocking buffer overnight at 4°C. The next day, samples were washed with PBS and then incubated with secondary antibody (Goat anti-Mouse-Alexa Fluor 546nm conjugated and Goat anti-Rabbit-Alexa Fluor 488nm conjugated with a final dilution of 1:200 in blocking buffer protected from light for 1 hour at room temperature. Unbound secondary antibodies were washed with PBS and samples were incubated with DAPI (1:10000 dilution in PBS) protected from light for 5min at room temperature. Samples were washed three times with PBS prior to washing in dH_2O at room temperature. A coverslip was mounted onto the samples with Fluorsave mounting medium (Calbiochem). Images were taken on an Olympus IX71inverted fluorescence microscope with Qicam (Qimaging) and QCapture pro software (Qimaging).

2.4. Dewaxing paraffin embedded sections

Paraffin embedded sections of organotypics were rehydrated as following: 2x 5min in Xylene, 2x 3min in 100% EtOH (VWR), 3min in 80% EtOH, 3min in 70% EtOH, 3min in 50% EtOH, rinse in dH_2O and afterwards in PBS. Heat assisted antigen retrieval was carried out with slides immersed in 10mM Na^+ - Citrate buffer (adjusted to pH 6 with Citric acid) and boiled for 20 min in the microwave. Water was topped up ensuring stable concentration and equal volume during boiling. Samples were left to cool down to room temperature prior to three x 1min rinses in PBS.

2.5. Spheroid formation and 3D spheroid invasion assay

Spheroids were prepared in Corning black walled 96-wells clear black round bottom ultra-low attachment spheroid microplates (Cat nr 4515). $1*10^3$ cancer cells were seeded in 200ul DMEM-F12 growth medium per well, to generate a single spheroid per well. Alternatively, 500 cancer cells and 500 PS-1 cells were mixed and seeded in 200ul DMEM/F12 growth medium per well to yield co-culture spheroids. The plate was then centrifuged at 200g for 8min at room temperature to facilitate cell spheroid formation. Cells were cultured at 37°C with 5% CO_2 for three days prior to invasion assay initiation. Images were taken with an 10x objective on an Olympus IX71inverted fluorescence microscope with Qicam (Qimaging) and QCapture pro software (Qimaging).

When spheroids are assembled on day three, 170ul medium was removed by multichannel pipetting. A collagen mixture was prepared on ice consisting of 2.0 mg/ml Corning rat tail collagen I, 1x DMEM, 10% FBS, collagen volume x 0.023 ul of 1N NaOH and topped up with sterile distilled water to the total volume. 100ul Collagen matrix was then added to each well with a multichannel pipette. Spheroids should stay at the centre bottom of the well for the best result and reproducibility. The plates were then left polymerizing at 37°C with 5% CO_2 for 2 hours. 100ul DMEM-F12 supplemented with 10% FBS and 1mM Penicillin/streptomycin was then added on top to initiate the assay. For the drug screen, DMSO (Negative control for invasion inhibition), Dasatinib (Positive control for invasion inhibition) or test compound could be added to the medium on top to initiate the assay. Phase contrast images were

taken with a Qicam (Qimaging) attached to a Nikon TS100 inverted microscope with x4x objective at 0hrs (Start) and at 96 hrs (End). Alternatively, images can be taken at 24, 48 and 72hrs for additional tracking of the spheroid invasion and growth.

2.6. Image analysis and image quantification of spheroid invasion

GFP and phase contrast images were taken of each well containing a single spheroid at the beginning of invasion (day 0) and at the end of invasion (day 4). The phase contrast and GFP fluorescence images were transformed to 8bit in ImageJ. The brightness and contrast of the GFP fluorescence was then adjusted for each image to overlay and capture the size of the spheroid and the invasive cells. Afterwards, the thresholding was applied and set to quantify the area of the GFP signal. The area of the spheroid body and invaded cells at the end of the invasion data was then normalised against the area of the spheroid at the start of the invasion to yield the relative invasion result. Statistical analysis was done by using the average of the triplicate results from each experiment and compared across three independent experiments with one way ANOVA in the case of multiple drug conditions.

2.7. Mini 3D organotypic assay

24-wells 6.5mm diameter transwells with 0.4µm pore size (Corning; #3413) were pre-coated with 300ul 40µg/ml rat tail collagen type I (Corning) for 1 hour at 37°C with 5% CO_2. A collagen/matrigel mixture was prepared at 2.0mg/ml Rat tail collagen type I with 1.5mg/ml Matrigel with reduced growth factor (Corning) in DMEM supplemented with 10% FBS on ice. Excess collagen was then removed and 120ul of the collagen/matrigel mixture was added per transwell and polymerized at 37°C with 5% CO_2 for 2 hours. A total amount of $1x10^6$ cells either consisting of cancer cells alone, pancreatic stellate cells alone or a mix of cancer cells and pancreatic stellate cells in a 1:2 ratio, were seeded in DMEM/F12 supplemented with 10% FBS and 1mM penicillin/streptomycin on top of the transwell. The bottom of the wells was filled with 650ul DMEM/F12 supplemented with 10% FBS and 1mM penicillin/streptomycin. Cells were left to attach overnight at 37°C with 5% CO_2. The next day, medium on the top was changed to serum free DMEM/F12 supplemented with 1mM penicillin/streptomycin and the bottom medium was replaced with 350ul

complete DMEM/F12 medium. Medium was changed every other day for 7 days. Transwells were then fixed with 200ul and 600ul of 10% universal formalin (Sigma) for top and bottom respectively overnight at room temperature. Transwells were then rinsed in 70% EtOH for 10min at room temperature prior to membrane cutting and gel removal, wrapped in specimen sponges into a specimen case for automated processing, paraffin embedding, sectioning (Section thickness: 5µm), and hematoxylin and eosin (H&E) staining at Barts cancer institute, London, UK.

2.8. Immunoblotting

Cells were seeded in 6-well plates and maintained as outlined above for 24 hours. Lysates were generated of 70% confluent wells by washing the cells with PBS and lysis with 100ul NP40 based lysis buffer/well (0.5% NP-40, 30mM sodium pyrophosphate, 50mM Tris-HCl pH 7.6, 150mM NaCl, 0.1mM EDTA, 50mM NaF, 1mM Na_3VO_4, 1mM PMSF, 10µg/ml leupeptin and 1µg/ml aprotinin and 1mM DTT (all Sigma)) on ice for 10min. Lysates were then scrapped, transferred to an Eppendorf tube and centrifuged at 13 000 x g for 15min at 4°C. Supernatant was then transferred to new Eppendorf tube and boiled for 3 min at 95°C in 6x laemmli buffer (Final concentration: 1x, 375mM Tris-HCl pH 6.8, 6% SDS, 48% Glycerol, 9% β-mercaptoethanol and 0.03% bromophenol blue (all Sigma)). Samples were stored at -20°C.

30ul of protein samples were resolved by SDS/PAGE on 6.5% gels (1.25ml 3M TRIS, 2.17ml 30% acrylamide, 100µl SDS, 6.48ml ddH_2O, 100µl ammonium persulphate, 10µl TEMED) and transferred onto nitrocellulose membrane by wet transfer for 1 hour at 100V on ice. Membranes were blocked with 5% skimmed milk powder (Marvel) or 5% BSA in TBST (1M TRIS pH 7.6, 5M NaCl, 1% Tween 20) for 30min at room temperature. Primary antibodies (Mouse anti-E-cadherin (Abcam HECD-1) with dilution of 1:1000, Mouse-anti-N-cadherin (BD transduction laboratories; #32) with dilution of 1:1000, Mouse anti-Vimentin (Abcam ab20346) with a dilution of 1:1000, Rabbit anti-pMLC2(T18/S19) (Cell signaling #3674) with a dilution 1:1000, Mouse anti-MLC2 (Santa Cruz SC 15370) with a dilution of 1:200 or Mouse anti-GAPDH

(Santa Cruz; SC32233) with a dilution of 1:40000) in blocking buffer were incubated overnight at 4°C on roller bench. Membranes were then washed three times with TBST and incubated with secondary antibodies (Goat-anti-Mouse-HRP conjugated or Goat-anti-Rabbit-HRP conjugated (both DAKO) with final dilution of 1:2000) in blocking buffer for 1 hour at room temperature. Afterwards, membranes were washed three times again with TBST and developed with ECL chemo luminescence kit (Thermo Scientific) and Fuji Medical X-ray Film (Fuji Film). Densitometry analysis of specific bands was carried out with ImageJ. Target protein expression levels were compared over the loading control (internal housekeeper protein) on the same membrane.

2.9. Viability assay on 2.5D collagen I matrix

Cells were seeded on 2.5D collagen I matrix prepared as described above and allowed to adhere for 20 hours at 37°C with 5% CO_2. Next day, cells were treated with different concentrations of drug compound and DMSO as negative control in growth medium. After 72hrs, alamar blue (Acros organics) is added to the medium, yielding final concentration of 44uM and left incubating for 2 hours at 37°C with 5% CO_2. Fluorescence signal of was then read with a Perkin Elmer Fusion Alpha-FP microplate reader.

2.10. Tumour xenografts and intravital *in vivo* imaging

1 x 10^6 PaTu8902 cells stably expressing Lifeact-GFP were suspended in 100 µl of PBS:Matrigel (50:50) and injected subcutaneously into the flank of 6- to 8-week CD-1 nude mice (n=3). Tumour growth was monitored and when tumours reached visible size (5–8 mm in diameter), mice were anesthetized and imaged as described (144). For intravital imaging, seven to ten different regions were imaged simultaneously for two hours for each tumour (approximately 50 µm deep on average). Mice were kept in accordance with UK regulations under project PPL80/2368.

2.11. Genetic analysis

Gene enrichment analysis was performed using GSEA (http://www.broadinstitute.org/gsea/index.jsp). Each gene in the gene set is represented in the x-axis, while the enrichment score for each gene is plotted in the y-axis. GSEA analysis does not apply a threshold to the data.

2.12. Statistical analysis

Statistical analysis was carried out on the averages of 3 or more independent experiments (n=3), using Graphpad Prism software. Student's T-test, ANOVA or Two-way ANOVA were used for parametric data when two groups, multiple groups or multiple groups with two independent factors were compared respectively. Tukey's multiple comparisons test was applied where applicable. Kruskis-Wallis test was applied for non parametric data with multiple comparisons. P value of less than 0.5 was deemed significant. Pearson correlation coefficient statistical analysis was performed for the comparison of data on linear relationship, with a positive p value deemed as having a linear correlation.

3. Morphological Characterisation and Cell Line Model Identification for the Drug Screen

3.1. Introduction

Early cancer cell dissemination and poor response to current available treatments highlight the need for novel therapeutics and targets for tackling PDAC. The majority of cancer therapies are cytostatic drugs or traditional chemotherapy, initially designed to target cell proliferation in hematopoietic cancers with high proliferation capabilities, such as Gemcitabine which is the standard of care for PDAC. Nevertheless, metastasis is the leading cause of cancer death by solid tumours such as PDAC. Around 60% of PDAC patients are presented with local invasion whereas around 30% are diagnosed with distant metastasis (145). Therefore, more focus is needed in developing novel therapies against invasion and treating metastatic disease.

Cellular migration and invasion underlie the metastatic dissemination, abilities which are defined as one of the hallmarks of cancer by Hanahan and Weinberg (146). Tumour cells are able to adopt various modes of migration, which involves changes in cell morphology, in order to overcome challenging environments during invasion. Various modes of cancer cell migration include mesenchymal and amoeboid like single-cell migration, multicellular streaming and collective cell migration (147). This ability to display heterogeneity is also known as cellular plasticity, and is normally observed during development, but has been reported to be displayed by cancer cells spontaneously and contributes towards tumour progression (113, 148, 149). Despite increased investigations into PDAC in recent years, little is known regarding cellular plasticity and the mode of migration of PDAC cells. Uncovering the cellular plasticity and the mode of migration of PDAC could lead to novel therapeutic strategies against metastatic PDAC cells.

Recent findings have demonstrated that the tumour microenvironment in PDAC contributes towards tumour growth, metastasis and resistance to therapy (150). Activated PSCs in the stroma have been demonstrated to induce EMT in pancreatic cancer cells, which is correlated with increased metastasis and drug resistance of the

tumour (116, 124, 151). Moreover, recent sub-type classification based on gene expression has identified correlations with therapeutic resistance and survival rates between classical and quasi-mesenchymal (QM) sub-types (53). Thus, given the clinical relevance, it is therefore important to take subtyping and stromal interactions into account when developing a 3D model for drug discovery *in vitro*.

Previously, it has been demonstrated that melanoma cancer cells on 2.5D thick layer collagen recapitulates their behaviour in 3D collagen environments (113). It is therefore interesting to see whether this is also the case for pancreatic cancer cells. Furthermore, investigating the expression of EMT markers such as E-cadherin, N-cadherin, Vimentin, and the presence of actomyosin contractility could provide valuable information regarding cellular plasticity, mode of migration and invasion. It has been demonstrated that E-cadherin plays a role in collective cell migration (152), while the loss of E-cadherin is often accompanied with EMT (123). In addition, it has been well documented that actomyosin contractility affects cell morphology and migration in 3D matrix (112, 113, 115, 153).

The 2.5D model allows for simple morphological analysis and identification of protein expression on collagen I matrix, but does not allow the assessment of invasiveness of the cells. 3D invasion models such as spheroid invasion assay and the organotypic assay provide the possibility to assess invasiveness, 3D cell behaviour and drug penetration. However, protein extraction and viability assays are more complicated to perform in these 3D models. Combing the use of 2.5D and the 3D models, I can characterise cellular morphology and assess cellular invasion in the presence of tumour micro environmental and genetic factors.

This chapter aims to characterize the panel of human pancreatic cancer cell lines with *in vitro* multidimensional models in order to identify a cell line model for the drug screen platform. The cell line model should be clinically relevant and highly invasive. Furthermore, I will also address cellular morphology and plasticity in pancreatic cancer as this has not been reported previously.

3.2. Results

3.2.1. Cells of quasi-mesenchymal subtype are enriched in single cell events

In order to determine a suitable cell line model, which is of QM subtype, able to form spheroids and is highly invasive *in vitro* and *in vivo,* for our drug screen against pancreatic cancer discussed in chapter 4 and 5, I first sought to characterise pancreatic cancer cell behaviour on the 2.5D collagen I assay (Figures 3-1). Cellular morphology in each individual PDAC cell line was investigated by quantifying the morphological events and analysing individual cell morphology. Morphological events were categorised as single cells, doublet cells or dividing cells, clustered cells with 3 cells or more cells, and tight defined colony cells (Figure 3-1 B). The doublet cell and cluster cell events could be seen as transition phases between single individual cells and when forming tight collective moving colony cells. Phase contrast images were taken at 24 and 48 hours and each event was counted manually in ImageJ (Figure 3-1C). Cell lines were categorised by origin (primary tumour or metastasis), differentiation status (well, moderate and poorly differentiated) and sub-type classification (Classical or Quasi-mesenchymal) (Table 3-1)(53). No significant differences were found between morphological events at 24 and 48 hours post seeding. Furthermore, no differences were found when morphological events of cell lines were compared based on origin or differentiation status (Data not shown). However, differences were observed in the percentage of single cell and colony cell events in the population when cell lines were compared based on sub-type classification (Figure 3-2A and B). QM cell lines formed significantly less colonies (average 4.7% vs 32.1%) and were more enriched in single cell (average 42.2% vs 30.1%) events compared to classical cell lines (Figure 3-2B). No significant differences were found in the doublet cell or clustered cell events, suggesting that doublet and clustered cell events could be intermediate modes between single and colony cell behaviour.

However, differences in the cluster cell event percentages indicate a possibility of an extra “subtype” than just the classical and the quasi-mesenchymal ones. The “first group” of cells such as Capan2, PaTu8988S and CFPAC1 show high tendencies of forming well defined colony cell (average of 39.55%) events with a low percentage of

Table 3-1: Differentiation state, sub-type classification, source of origin and common genetic alterations of the used PDAC cell lines.

Cell line	Differentiation state	Subtype	Source of tumour cells	KRAS	TP53	CDKN2A	SMAD4
CAPAN2	Well (154)	Classical (53)	Primary tumour (155)	12V (154)	WT (154)	WT (154)	WT (154)
CFPac1	Moderate (156)	Classical (53)	Liver metastasis (155) (cystic fibrosis patient)	12V (154)	242R (154)	WT (154)	HD (154)
Colo357	Well (157)	QM-PDA (53)	Celiac lymphnode metastasis	WT (158)	WT(158)	Meth (158)	HD(158)
HPAC	Moderate – well (154)	Classical (53)	Primary tumour (154)	12D (154)	WT (154)	112stop (154)	WT (154)
Panc1	Poor (156)	QM-PDA (53)	Primary tumour (155)	12D (154)	273H (154)	HD (154)	WT (154)
Patu8902	Moderate to Poor (159)	QM-PDA (53)	Primary tumour (159)	12V (160)	176S (160)	WT (160)	WT (160)
PaTu8988S	Well (161)	Classical (53)	Liver metastasis (155)	12V (48)	282W (162)	N.A.	N.A.
PaTu8988T	Poor (161)	QM-PDA (53)	Liver metastasis (155)	12V (48)	282W (162)	N.A.	N.A.
SW1990	Moderate - well(163, 164)	QM-PDA (53)	Spleen metastasis (163)	12D (165)	WT (165)	N.A.	N.A.

WT: Wild-type; HD: Homozygous deletion; QM-PDA: Quasi-mesenchymal-pancreatic ductal adenocarcinoma; N.A.: Not available/Not determined

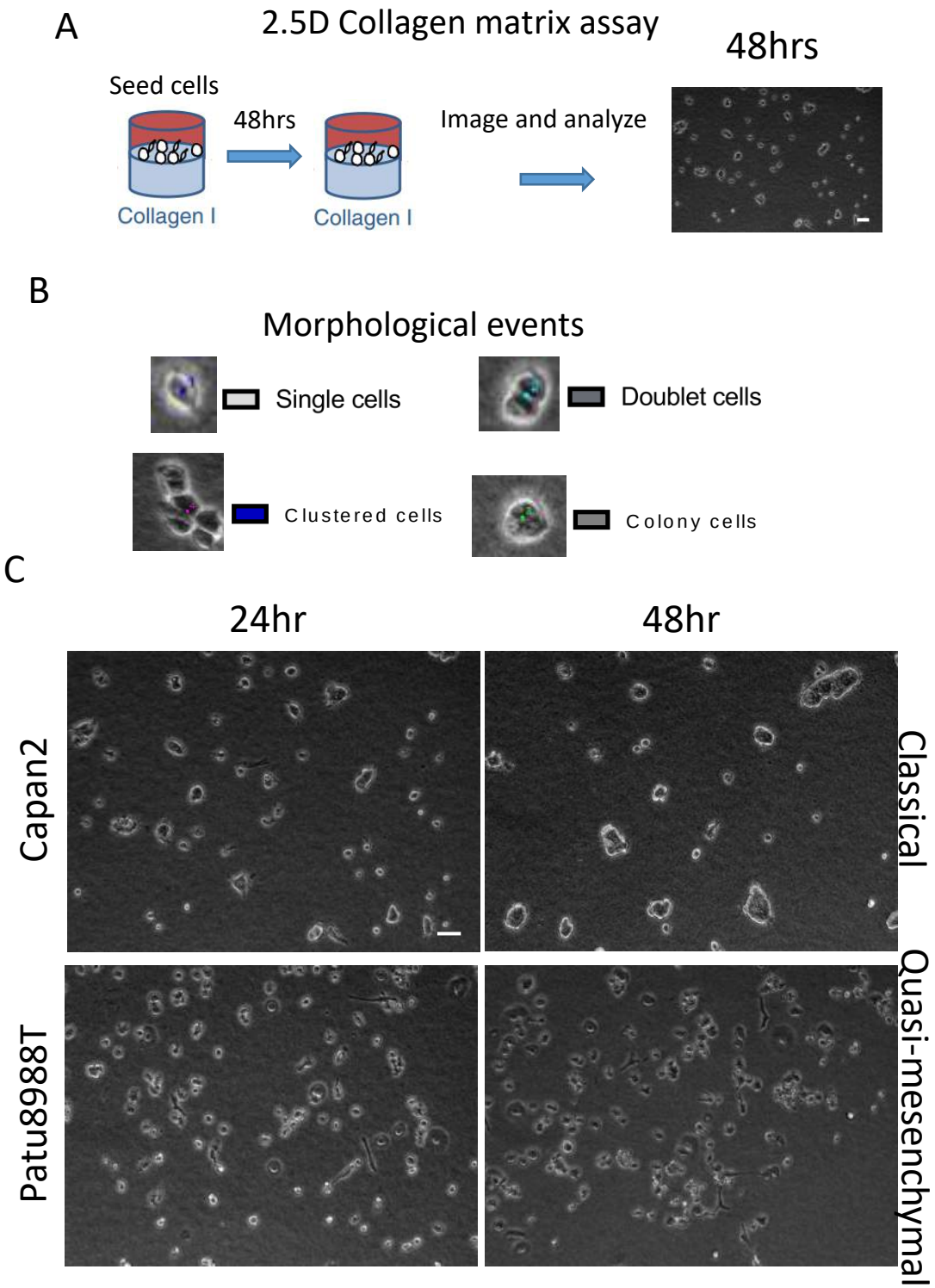

Figure 3-1. Representative phase contrast images of 2.5D morphological event characterisation of classical and quasi-mesenchymal subtype.
A) Schematic representation of the 2.5D collagen I matrix assay. B) Representative images of the morphological events: single cells, doublet cells, clustered cells and colony cells C) Phase-contrast images of Capan2 (Classical) and PaTu8988T (Quasi-mesenchymal) cells on thick layer collagen type I taken at 24hrs and 48hrs post seeding. Scale bar= 50µm.

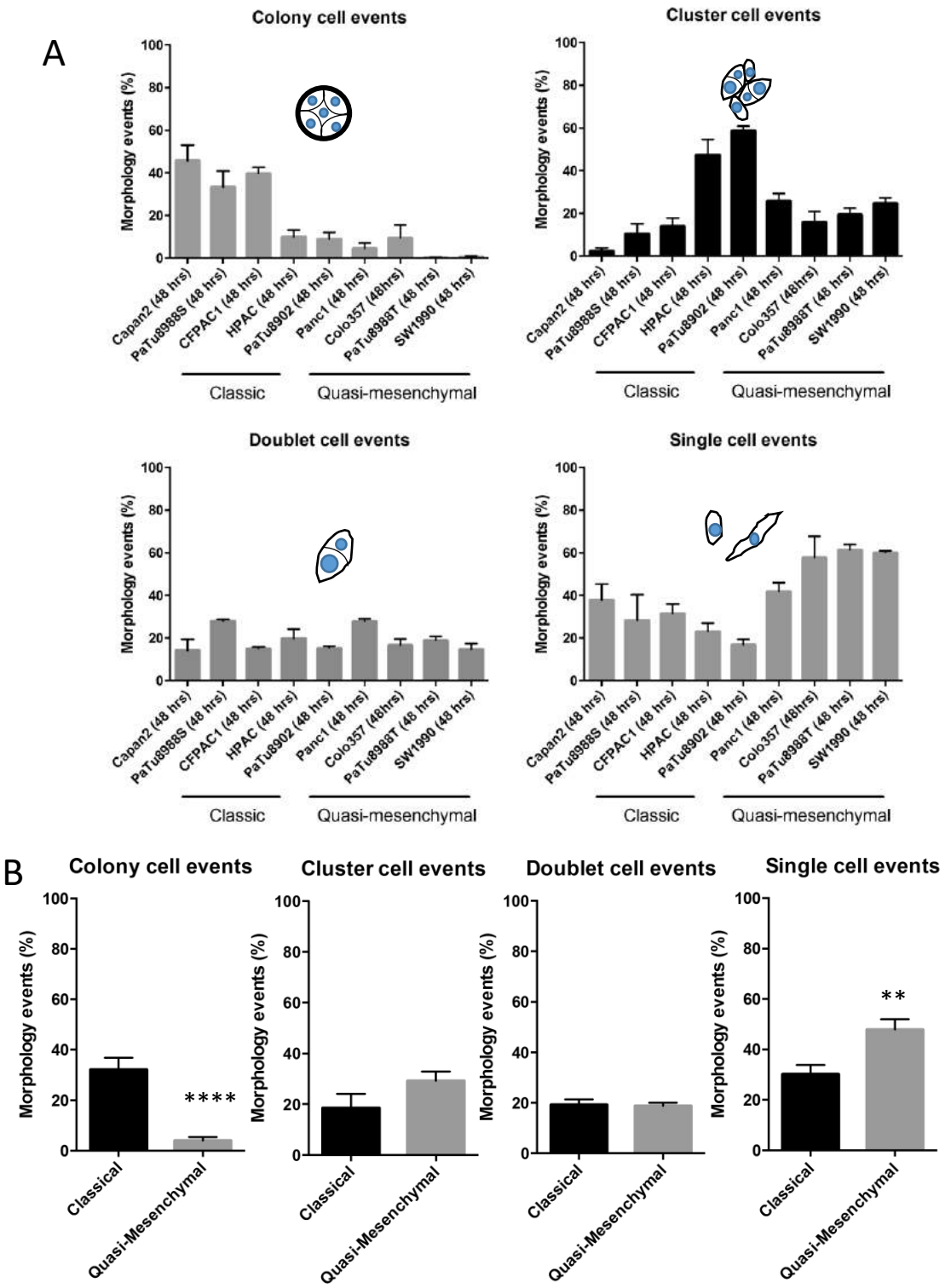

Figure 3-2. Morphological events on 2.5D bovine collagen I matrix.
A) Percentage of morphological events (Colony cell, cluster cell, doublet cell and single cell) of individual cell lines on 2.5D bovine collagen I quantified at 48hrs, grouped in classical and quasi-mesenchymal subtype. 100% is the sum of all morphological events added up. ±SEM, n=3 with 10 morphological events per field, out of 3 fields per triplicate, per individual experiment. B) Morphological events compared between classical and quasi-mesenchymal subtype. 100% is the sum of all morphological events added up. ±SEM, n=3, Student's t-test **, P<0.01, ****, P<0.001.

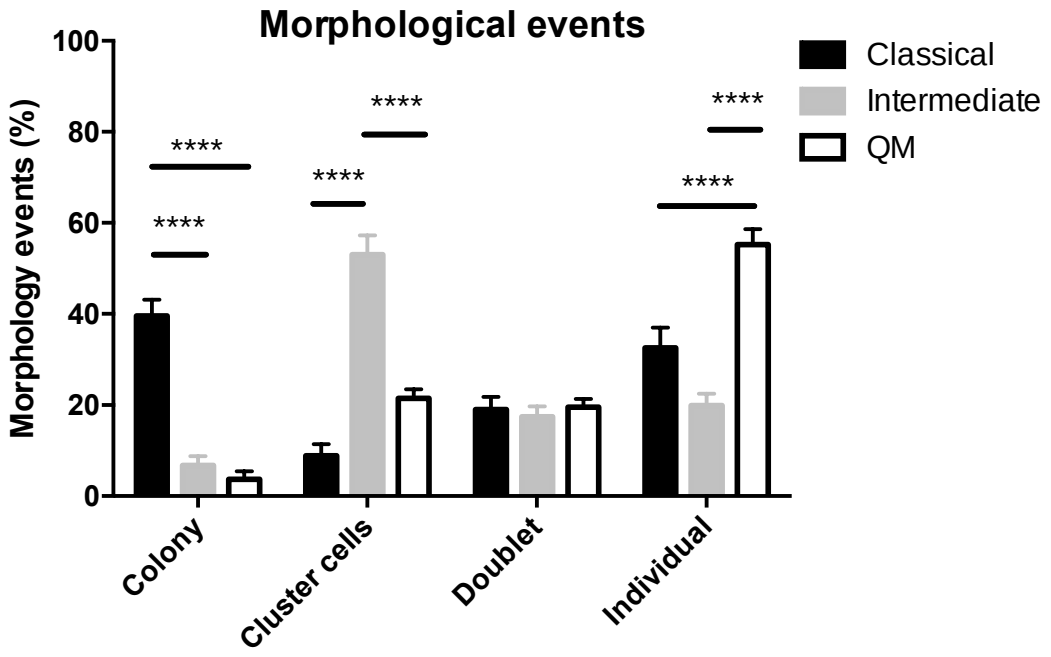

Figure 3-3. Morphological events of three different subtypes on 2.5D collagen I matrix.

Average percentage of morphological events (Colony cell, cluster cell, doublet cell and single cell) of each cell line grouped in the three groups of subtypes: Classical (Capan2, PaTu8988S and CFPAC1), "Intermediate" (HPAC and Patu8902) and QM (Panc1, Colo357, Patu8988T and SW1990). ±SEM, n=3 with 10 morphological events per field, out of 3 fields per triplicate, per individual experiment, per cell line. Two-way ANOVA with Tukey's multiple comparisons test. ****, P<0.001.

cluster cell formation (average of 8.87%) (Figure 3-3). These cells could be defined as strong Classical colony forming epithelial cells and seems to be able to organise themselves into a colony in an efficient manner. Despite HPAC and Patu8902 being categorised in two distinct subtypes, their morphological behaviours were very similar to each other. Cell lines from this Intermediate "second group" readily form clustered cells (average of 53.1%), but are not able to organise themselves efficiently into a tight collective coordinated colony cell behaviour (average of 9.5%). This may suggest that these cells are partially undergoing EMT, demonstrating a more transient interaction with neighbouring cells. The QM or "third group", consisting of Panc1, Colo357, Patu8988T and SW1990, show strong single cell behaviour (average of 55.2%), but are unlikely to form colonies (average of 3.7%). Cells from this group seem to have fully undergone EMT into a mesenchymal phenotype and are staying individual for a longer period of time or forms transient group of cluster cells.

In order to validate the findings observed on 2.5D collagen I matrix, cell lines were tracked for 16hrs on 2.5D collagen I matrix between 24 and 48 hrs with time lapse microscopy. Cells from classical cell line Capan2 readily forms mini colonies which are collectively motile and are able to fuse together into one large collective migrating colony (Movies 1). While Capan2 cells demonstrate strong epithelial cell behaviour, the "intermediate" and QM cell lines like PaTu8902 and PaTu8988T respectively, were not able to organize a cluster of cells into a collective migrating colony (Movie 2 and 3). Where PaTu8902 cells are continuously interacting with neighbouring cells by adhering and detaching transiently, switching between single, doublet and cluster cell behaviour, Patu8988T cells seem to remain individual during majority of the time course but are able to transiently form cluster cells as well. Overall, these results show that QM cell lines are less likely to stay in colonies and are found as individual cells majority of the time compared to classical cell lines. The "intermediate" group of cells resembles the QM cell behaviour more closely, revealing the ability to transiently form cluster cell events. More cell lines need to be characterised to validate the "intermediate" sub-type in combination with future efforts in subtyping based on distinct genetic expression profiles correlated with clinical relevance.

3.2.2 QM cell lines express mesenchymal markers and demonstrate high levels of contractility

The classical and the QM sub-types were originally defined based on differential gene expression (53). As the QM sub-type was correlated with upregulated expression of mesenchymal related genes, it was not surprising to observe an enrichment of individual cell behaviour in the QM sub-type cell lines. It was therefore interesting to investigate whether this phenomenon was related with the EMT process. Furthermore, it would be attractive to validate the existence of an "intermediate subtype" which I have identified previously.

Initial differences in E-cadherin expression were observed between Classical, "intermediate" and QM cell lines in the 2.5D assay with immunofluorescent staining for E-cadherin (Figure 3-4). E-cadherin expression localised at the membrane and at the junctions between neighbouring cells in colonies was observed in the Classical cell line Capan2, demonstrating the presence of stable junction in colony cells. No E-cadherin expression was observed in cluster cells or individual cells of the QM cell line PaTu8988T. Nevertheless, Junctional E-cadherin expression was observed in cluster cells of the 'intermediate' cell line PaTu8902. Furthermore, E-cadherin localisation was also found at the membrane level of single cells and in leading cells of a cluster in PaTu8902 cells. This may suggest that 'intermediate' cells such as PaTu8902 cells express E-cadherin on the cell membrane to readily form clusters. While Classical cells efficiently establish junctions with E-cadherin, QM cells may adhere and interact transiently with neighbouring cells through other types of junctional proteins. Expression of mesenchymal markers might differentiate the three subtype phenotypes further.

In order to quantify the expression markers and confirm whether 'intermediate' and QM cells are undergoing or have undergone EMT, western blot analysis was performed on selected classical and QM cell lines for the expression of epithelial protein E-cadherin, the mesenchymal protein markers N-cadherin and Vimentin (Figures 3-5 and 3-6). Furthermore, I also quantified actomyosin contractility markers pMLC2 and total MLC2 expression to investigate potential mesenchymal to amoeboid transition cells. In addition, the expression of these markers was also

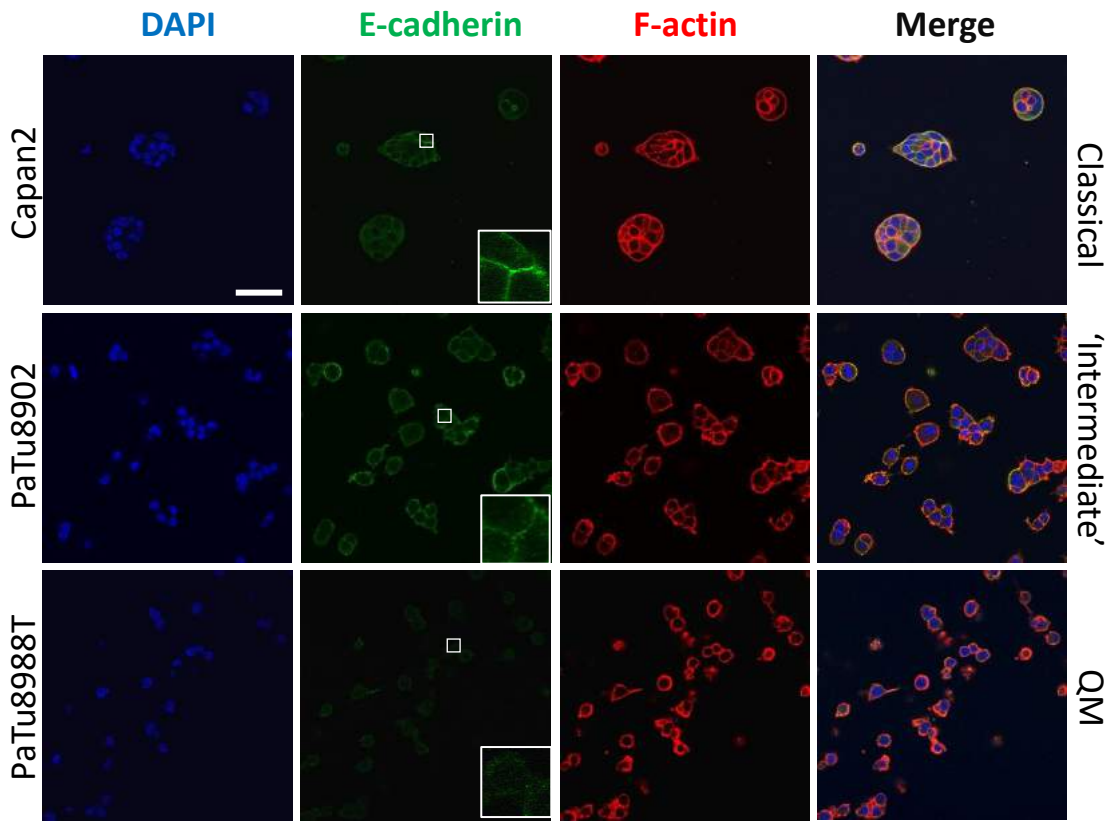

Figure 3-4. Expression and localisation of E-cadherin in classical and QM cells. Representative confocal images of Capan2, PaTu8902 and PaTu8988T cells in 2.5D assay on thick layer collagen type I for 48hrs. Staining for DAPI (Blue), E-cadherin (Green), F-actin (Red) and merged images are shown. Scale bar= 50µm.

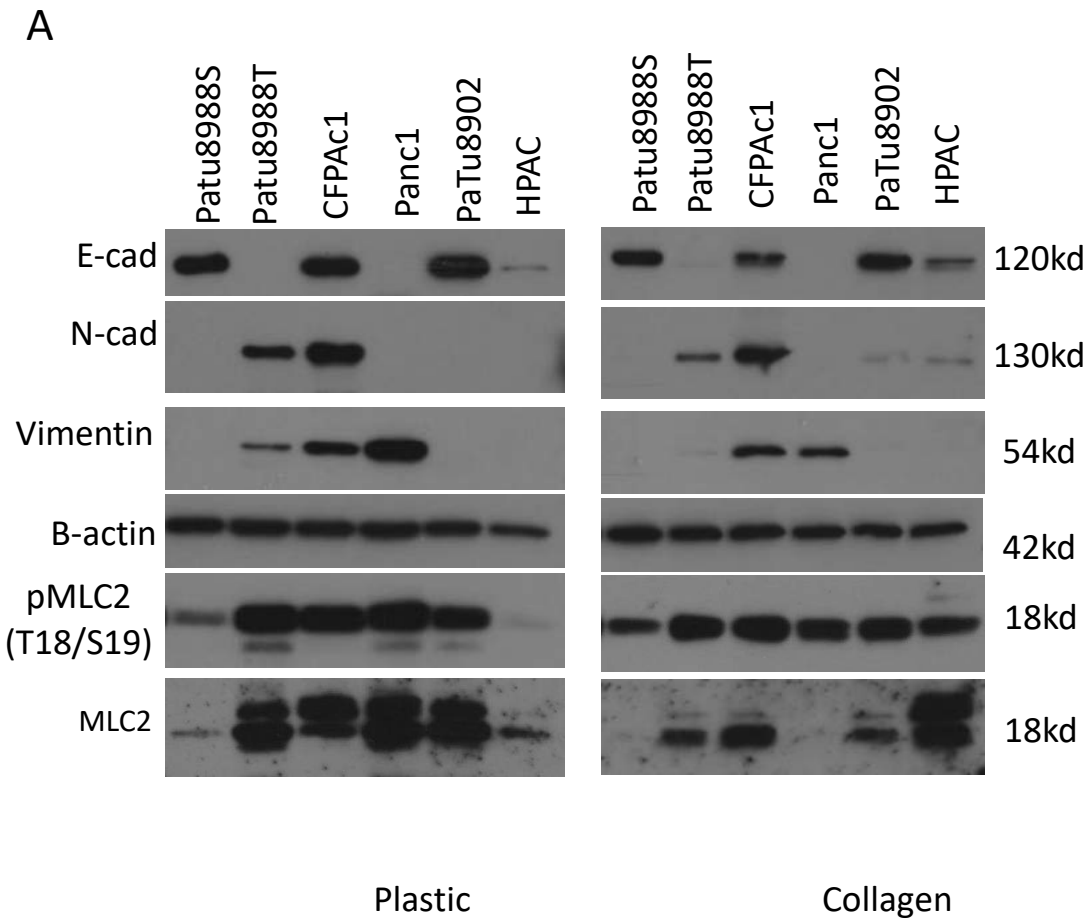

Figure 3-5. Western blot of epithelial, mesenchymal and contractility markers of cells on plastic and on 2.5D collagen I matrix.
Cells were lysed at 48hrs and blotted for E-cadherin (epithelial marker), N-cadherin and Vimentin (mesenchymal markers) and pMLC2(T18/S19) and total MLC2 (contractility marker). B-Actin was used as loading control. Blots shown are representative of three individual experiments.

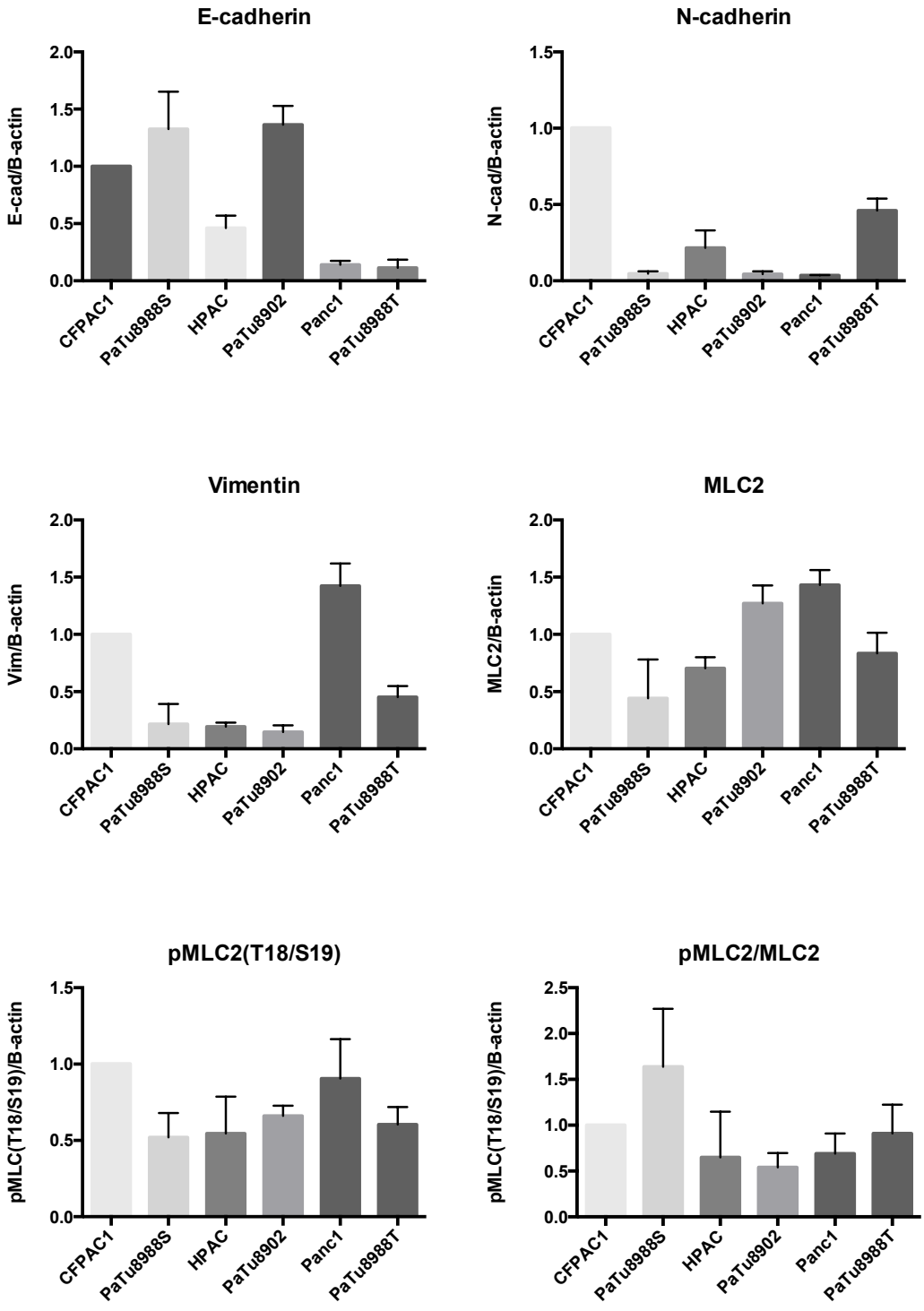

Figure 3-6. Quantification of immunoblot detection with densitometry analysis for various markers in various cell lines cultured on plastic.
Immunoblots with expression levels of E-cadherin (epithelial marker), N-cadherin and Vimentin (mesenchymal markers) and pMLC2(T18/S19) and total MLC2 (contractility marker) were quantified through the densitometry analysis with ImageJ. B-Actin was used as loading control. Data presented are average mean ±SEM of n=3.

compared between cells cultured on plastic and on 2.5D collagen I matrix. However, no significant differences were found regarding the expression of markers from cells cultured on plastic and 2.5D collagen I matrix (Figure 3-5 – 3-6). Although, E-cadherin, N-cadherin and Vimentin expression on collagen was consistent with cells cultured on plastic, detection of MLC2 and pMLC2 levels of cells cultured on collagens has been inconsistent due to technical issues. Therefore, here I focussed on the expression of these markers of cells cultured on plastic.

E-Cadherin expression was not only observed in Classical cell line such as CFPAC1 and PaTu8988S, but also in the "intermediate" cell lines HPAC and PaTu8902. QM Cells lines Patu8988T and Panc1 did not express E-cadherin, which was consistent with the findings observed with immunofluorescence staining of PaTu8988T on 2.5D assay. PaTu8988T also expressed N-cadherin whereas Panc1 did not. However, both QM cell lines expressed Vimentin, confirming their mesenchymal phenotype. Intriguingly, whereas the classical cell line CFPAC1 expressed E-cadherin, N-cadherin and Vimentin suggesting an EMT profile, 'intermediate' cell lines PaTu8902 and HPAC did not express these mesenchymal markers. These data suggest that full classical cells such as Capan2 and PaTu8988S demonstrated strong E-cadherin expression, while fully transitioned QM cells such as PaTu8988T and Panc1 expressed at least one of the mesenchymal markers such as Vimentin paired with loss of E-cadherin expression. The identification of "intermediate" cells by utilising these markers remains complex and warrants the use of additional markers to subcategorize the classical cell lines undergoing EMT and the "intermediate" cells.

Next, I also investigated the possibility of cells that have undergone MAT, especially in QM cells. High levels of double MLC2 phosphorylation (pMLC2 T18/S19) was observed in majority of the cell lines (Figure 3-5 and 3-6). HPAC and PaTu8988S showed lower levels of MLC2 phosphorylation compared to the QM cell lines and the classical EMT cell line CFPAC1. The phosphorylation levels were accompanied with a lower total MLC2 expression in both HPAC and PaTu8988S cell lines. While the QM cell lines and the EMT cell line CFPAC1 demonstrated high levels of pMLC2, the relative MLC2 phosphorylation (pMLC2/MLC2) remains similar across the cell panel, indicating similar levels of "engagement" of contractility have been present in each

individual cell line. Nevertheless, the overall contractile forces that these cells exert would be higher compared to HPAC and PaTu8988S.

In order to confirm the findings from the immunoblot analysis, a gene set enrichment analysis (GSEA) for contractile genes identified previously by Sanz-Moreno et al was conducted with QM and Classical cells in collaboration with Dr. Irene Rodriguez Hernandez from Sanz-Moreno lab (Figure 3-7) (112). Gene expression in QM cells such as Panc1, SW1990 and PaTu8988T were enriched for genes associated with actomyosin contractility, whereas classical cells like Capan2 and PaTu8988S were correlated with downregulation of these target genes. This data further supports the distinction in the contractile profile between Classical and QM cells, suggesting contractility as a biomarker for identifying QM subtype cells.

Overall, these results demonstrate that EMT and contractility markers can distinguish QM from the classical cells. Classical cells demonstrated E-cadherin expression localised to the junctions and have lower overall contractility. Furthermore, we also identified cells undergoing EMT, like the CFPAC1, through the expression of E-cadherin, N-cadherin and Vimentin, with high levels of MLC2 phosphorylation. However, GSEA data suggested that the contractile machinery is not as upregulated in CFPAC1 as in QM cells, confirming its subtype as Classical cell line. QM cells showed expression of Vimentin with or without N-Cadherin, which was also paired with high levels of MLC2 phosphorylation. Furthermore, QM cells were shown to be significantly enriched in genes associated with a contractile expression profile. Nevertheless, the expression profiles of previous suggested ‘intermediate’ cell lines were not differentiated from either the QM or the Classical expression profiles based on the markers used here. As more work is needed to confirm the existence of the “Intermediate” subtype, I therefore continued with the reported Classical and QM subtype classification only.

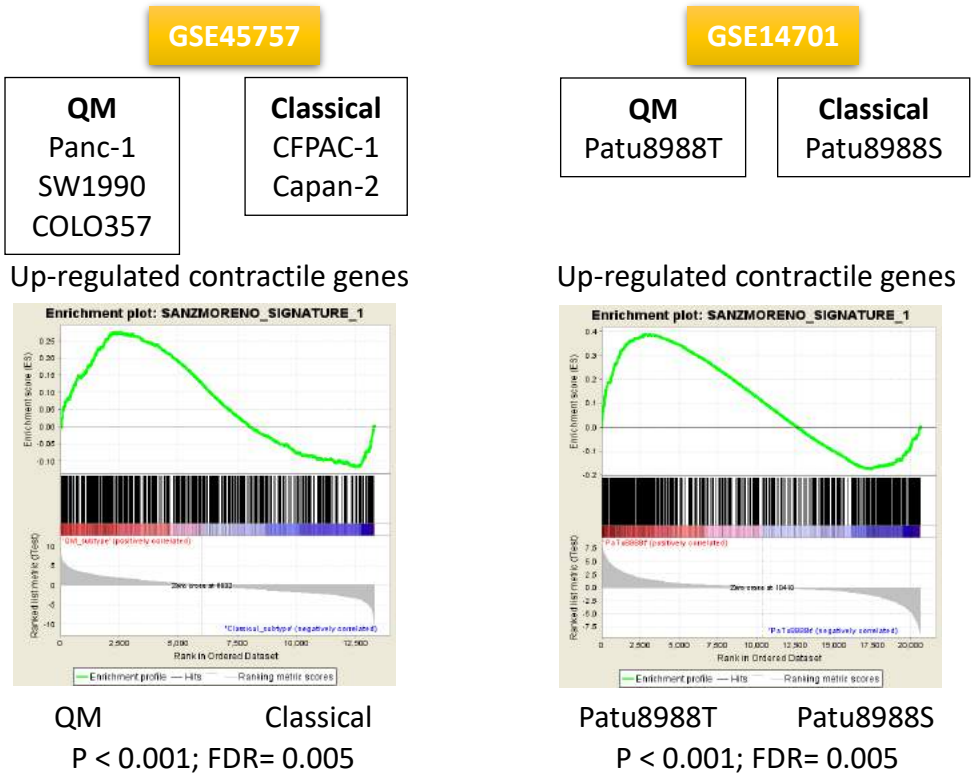

Figure 3-7 Gene set enrichment analysis of Classical and QM cells for contractile genes.

GSEA plots comparing QM and Classical cell lines based on expression of contractile genes identified by Sanz-Moreno et al with accession numbers GSM586484–GSM586501 (112). Only gene expression data of QM and Classical cell lines conducted with the same platform and in the same experiments were used. Note: data and analysis generated by Dr. Irene Rodriguez Hernandez.

3.2.3 Individual pancreatic cancer cells adopt a round morphology and demonstrate cellular plasticity

Since QM cell lines were more enriched in individual cells and demonstrated high levels of MLC2 phosphorylation in the overall cell population, it was logical to characterise the individual cells based on morphology and also to investigate whether there were differences in the individual cell population between Classical and QM cell lines. The roundness of each individual cell on 2.5D collagen was analysed with ImageJ using the roundness parameter (Figure 3-8). Cells were more elongated with roundness values closer to zero while cells were more round with values closer to 1.

A round cell morphology was adapted by majority of individual cells of all cell lines, except for SW1990, which demonstrated a mixed population distribution of round and elongated individual cells. As a consequence of these results, no differences were found when the data was either clustered based on cell line origin, differentiation status or sub-type classification (Figure 3-8B to D). These results were validated and confirmed by analysing the roundness of individual cells with F-actin immunofluorescence staining on 2.5D collagen I matrix (Data not shown), supporting the robustness of the phase contrast analysis method.

However, a subset of mesenchymal individual cells was found in certain cell lines such as the PaTu8988T and the SW1990 (Figure 3-8). It was therefore interesting to assess whether certain pancreatic cancer cells exhibit cellular plasticity. Time-lapse microscopy revealed that certain PaTu8988T, SW1990 and CFPAC1 cells in the population were able to switch between round and elongated cells on the 2.5D collagen I matrix (Figure 3-9A and Movie 4 to 6), demonstrating cellular plasticity. Although Capan2 and PaTu8902 cells mainly adopted a round morphology (Figure 3-8), time lapse movies showed the presence of plasticity in single cells, which seemed to be very transient and adopted a round morphology majority of the time (Figure 3-9B and Movie 7 and 8). These results demonstrate that individual pancreatic cancer cells are mostly round and exhibit cellular plasticity, able to transiently switch between a round and an elongated state.

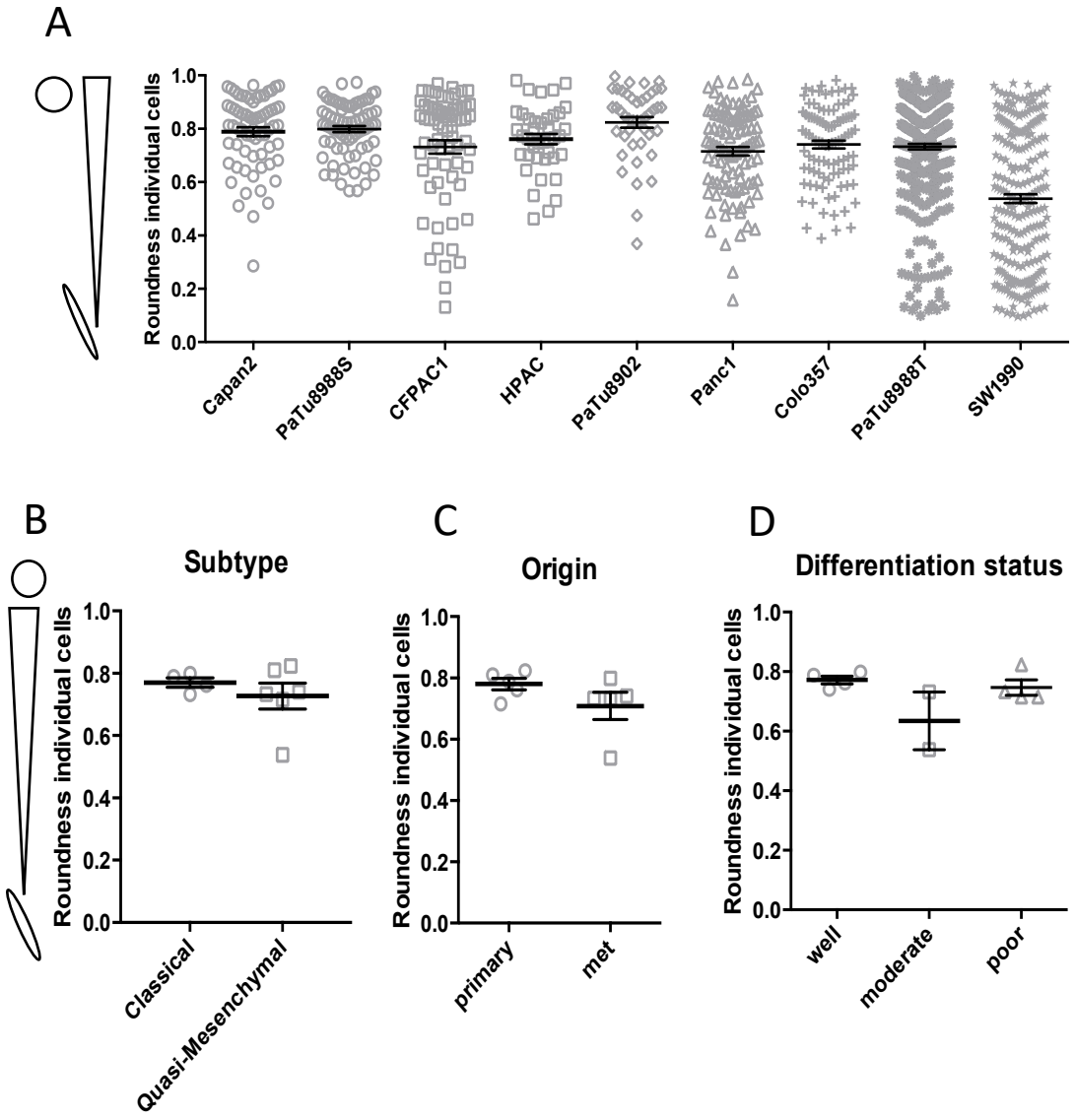

Figure 3-8. Single cell morphology on 2.5D bovine collagen I matrix.
A) Roundness of individual cells were measured with ImageJ at 48hrs post seeding, with an index of 1 being round and 0 being elongated. Data presented are the mean ± S.E.M of 3 independent experiments, with each individual data point representing an individual cell. All individual cells in duplicate fields were analysed per experiment. B) Comparison of Individual cell roundness by subtype: classical and quasi-mesenchymal subtype cells, C) by cell origin: primary and metastasis derived cell lines, and D) by differentiation status: well, moderate or poorly differentiated. Data presented are the means of each cell line across 3 independent experiments ± S.E.M.

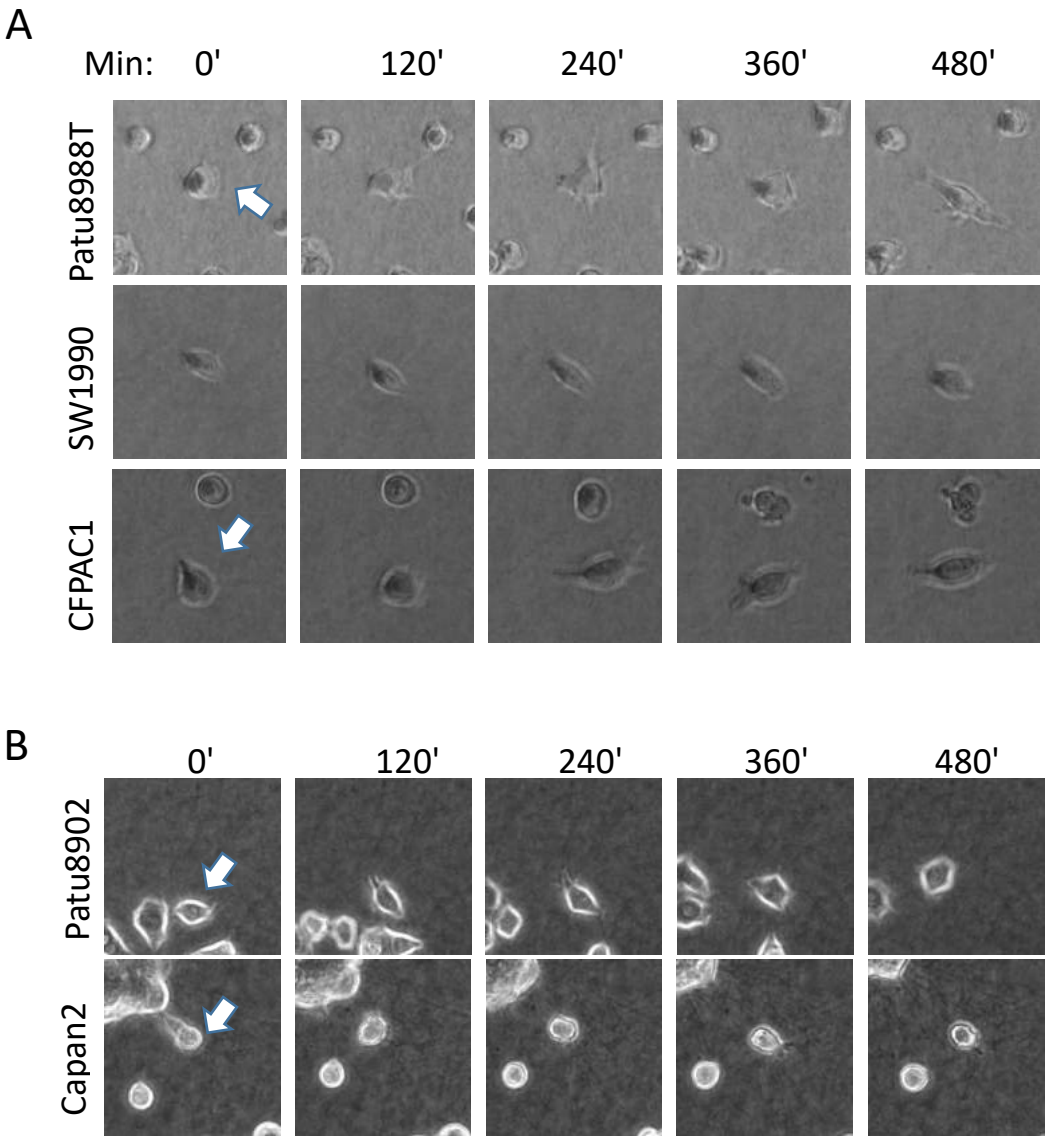

Figure 3-9. Cellular plasticity of pancreatic cancer cells on 2.5D collagen I matrix
A) Time lapse movie of individual PaTu8988T, SW1990 and CFPAC1 cells with frames taken at 0, 120, 240, 360 and 480 minutes. B) Time lapse movie of individual Patu8902 and Capan2 cells with frames taken at 0, 120, 240, 360 and 480 minutes. White arrow indicating the individual cells demonstrating cellular plasticity.

3.2.4 Individual pancreatic cancer cells are contractile and are able to bleb

As majority of the individual pancreatic cancer cells were round by morphology, it was noteworthy to see if there were differences between them. Beside round epithelial cells there are also round amoeboid cells. Previously I have demonstrated that the QM cells had higher contractility compared to classical cells, through immunoblot detection of MLC2 phosphorylation in whole cell lysates and gene set enrichment analysis for contractile genes (Figures 3-5 to 3-7). This approach did not distinguish the contractility of single cells and cluster or colony cells. Therefore, we utilised immunofluorescence staining and confocal imaging of individual cells on 2.5D collagen I to identify pMLC2 levels and bleb formation (Figure 3-10A). pMLC2 levels of individual cells were quantified by ImageJ using the corrected total cell fluorescence (CTCF or total corrected cell fluorescence (TCCF)) method (Figure 3-10B) (166). Phosphorylation of MLC2 was present in all individual cells, with varying intensities. PaTu8902 showed the highest average intensity of pMLC2, whereas Panc1 had the lowest average intensity of pMLC2. However, no significant differences were found when we compared Classical individual cells against QM individual cells (Figure 3-10C).

To further identify which cell lines individually undergone MAT and became amoeboid, I investigated the formation of blebs in the individual cells (Figure 3-11A). All cell lines were able to form blebbing cells, except for PaTu8902. Patu8988T had the highest proportion of blebbing cells among its single cell population. We then compared the ability of bleb formation in single cells between Classical and QM cells (Figure 3-11B). The data suggests that single cells of QM subtype have a higher tendency to form blebs, however this was not significant, due to large variances in the QM population.

Although QM cells and CFPAC1 demonstrated high levels of contractility, this was not reflected back in the individual cell population. Nevertheless, all cells demonstrated contractility while only Patu8902 did not utilise blebs, despite having the highest intensity for MLC2 phosphorylation, suggestion an alternative high contractility movement. Indeed, when investigating the PaTu8902 morphology further, the formation of pseudopods by the cell line has been identified, while maintaining cell

contractility (figure 3-11C). Furthermore, this alternative subtype of the amoeboid phenotype was observed in majority (85%) of the round PaTu8902 individual cell population, suggesting that this is the preferred mode for PaTu8902. Future single cell analysis could further distinguish these populations.

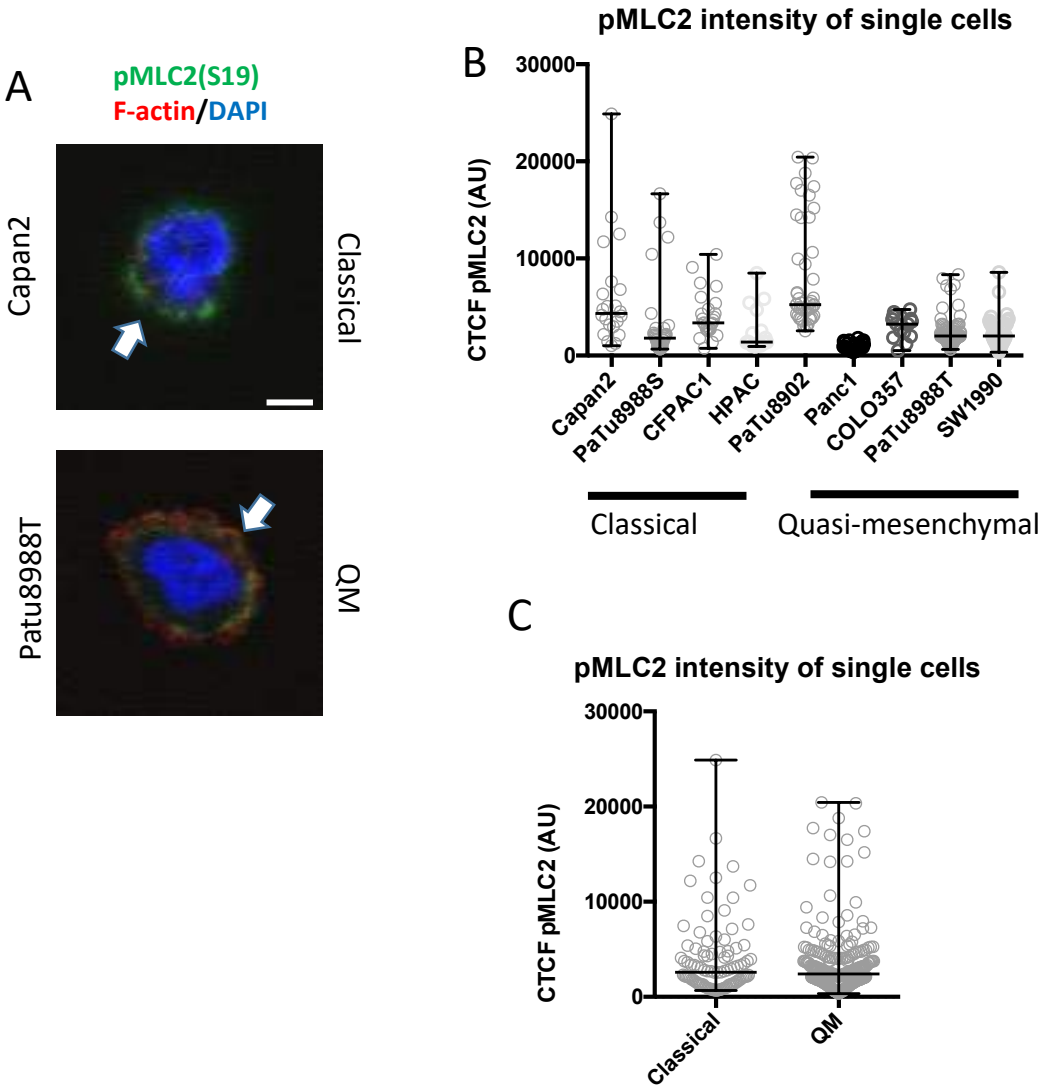

Figure 3-10. Contractility levels of individual cells on 2.5D collagen I matrix.
A) Representative Immunofluorescence images of Individual cells from classical (Capan2) and quasi-mesenchymal (PaTu8988T) subtype with bleb formation on Collagen I matrix. Localisation of F-actin (red), nucleus (blue) and pMLC2 (S19) (Green) were visualised by immunofluorescence staining. Scale bar= 5uM. B) Quantification of pMLC2 (S19) fluorescent intensity of individual cells of each cell line with ImageJ. Data presented are the Median with range of 3 independent experiments with individual dots representing single cell data. All individual cells in 5 fields were analysed per experiment. C) Quantification of pMLC2 (S19) fluorescent intensity of classical (Capan2, PaTu8988S, CFPAC1, HPAC) and quasi-mesenchymal (Panc1, Colo357, PaTu8988T, SW1990) subtype grouped together. Data presented are the Median with range of 3 independent experiments with individual dots representing single cell data of cell lines from each experiment. No statistical significance was found with the Mann-Witney test between the two subtype groups.

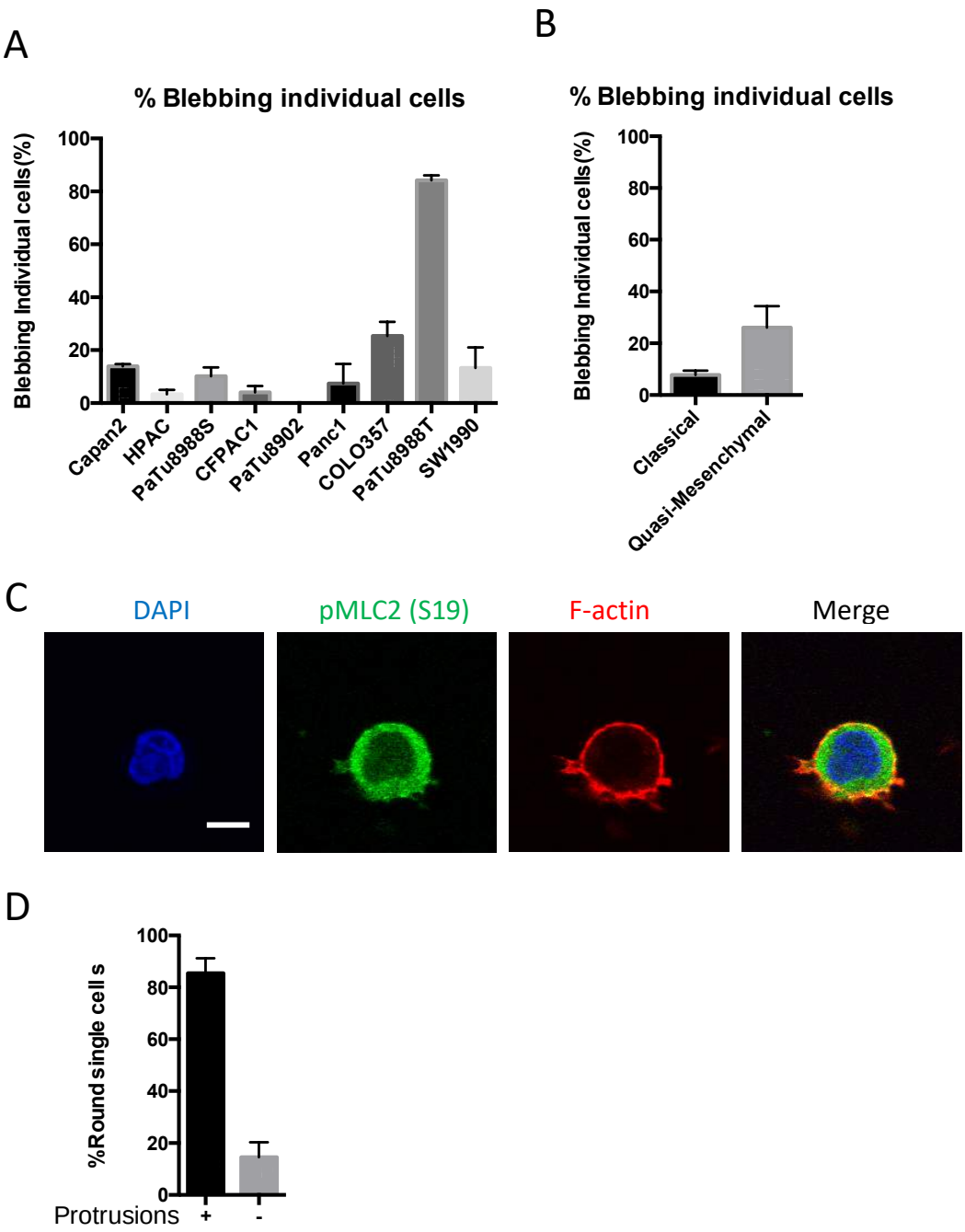

Figure 3-11. Individual cells with bleb or pseudopod formation on 2.5D Collagen I matrix.

A) Percentage blebbing cells in the individual cell population of cell lines after 48hrs on 2.5D collagen I matrix. Data presented are the average mean ±SEM of n=3 B) Percentage individual blebbing cells of classical (Capan2, PaTu8988S, CFPAC1, HPAC) and quasi-mesenchymal (Panc1, Colo357, PaTu8988T, SW1990) subtype. Data presented are the average mean ±SEM of n=3. C) Representative Immunofluorescence image of PaTu8902 round individual cell with pseudopods. Staining for DAPI (Blue), pMLC2 (S19) (Green), F-actin (Red) and merged images are shown. Scale bar= 10uM D) Percentage of round individual PaTu8902 cells forming pseudopods. Data presented are the average mean ±SEM of n=3. All individual cells in 5 fields were analysed per experiment.

3.2.5 QM cells readily form co-culture spheroids more likely over classical cells

To further characterise the cell lines and to validate a cell line model suitable for the drug screen against pancreatic cancer, I conducted functional assays to determine their invasiveness and ability to form compact spheroids. Cells were co-cultured with pancreatic stellate cells PS-1 in a round bottom ultra-low attachment spheroid formation plate to assess their anchorage independent growth and spheroid formation (Figure 3-12) (142). The formed spheroids were defined as spheroids when the spheroids did not easily fall apart after gentle resuspension. Classical cell lines HPAC and PaTu8988S were able to form a single co-culture spheroid over a time course of 3 days, while Capan2 and CFPAC1 were unable to form a single spheroid and instead showed the formation small clumps which expanded over the time (Figure 3-12A). All the assessed QM cell lines were able to form a single co-culture spheroid with PS-1 except for SW1990, which demonstrated similar clump formation behaviour as Capan2 and CFPAC1 (Figure 3-12B). It was also observed that certain cells are better in forming perfectly round tight spheres such as HPAC, PaTu8988S, PaTu8902, Clo357 and Panc1 compared to the spheroid like structure of Patu8988T. Nevertheless, QM cells seem to more likely form spheroids (4 out of 5 cell lines; 80%) compared to Classical cells (2 out of 4 cell lines; 50%) (Figure 3-12C), which reflects their aggressiveness and correlates with poorer prognosis in the clinic. More cell lines can be investigated in the future to validate this result.

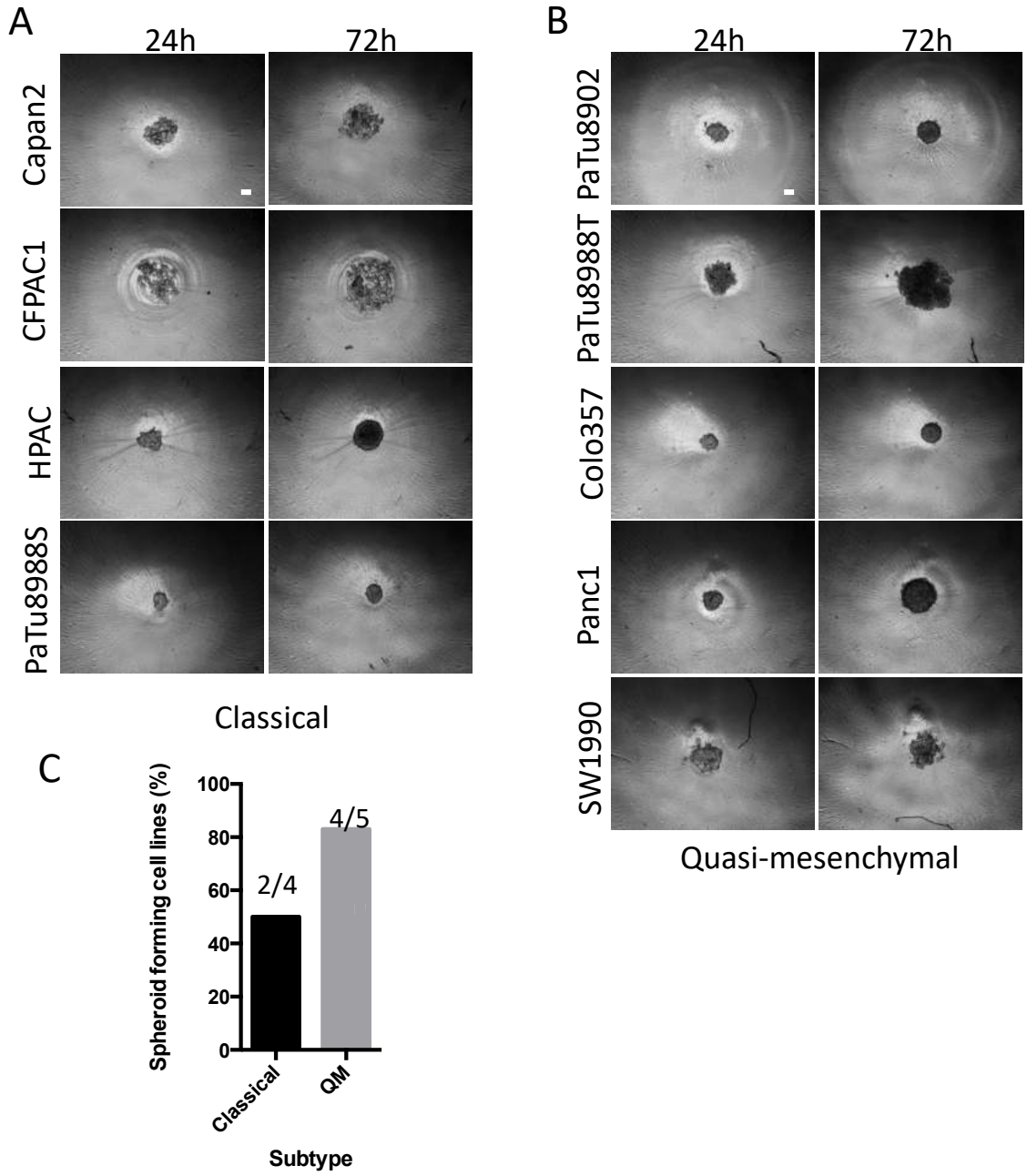

Figure 3-12. Spheroid formation ability of classical and quasi-mesenchymal subtype cells.

A) Spheroid formation of classical cell lines Capan2, CFPAC1 (non-spheroid), HPAC and PaTu8988S (Spheroid), and B) quasi-mesenchymal cell lines PaTu8902, PaTu8988T, Colo357, Panc1 (Spheroid) and SW1990 (non-spheroid) with PS-1 are shown at 24hrs and 72hrs. Scale bar = 100µm. C) The percentage of spheroid formation ability of cells from classical (4 cell lines) and quasi-mesenchymal (5 cell lines) subtypes after 72hrs. n=3.

3.2.6 QM cells are more invasive in the spheroid invasion assay

As QM cells were more likely to form co-culture spheroids with PS-1 stellate cells, it was of importance to confirm whether these cells are more aggressive by invasiveness in 3D matrix. I investigated the invasiveness of the co-culture spheroids in 3D collagen I matrix by using growth medium with 10% FBS as chemoattractant (Figure 3-13 and 3-14). Classical cell line PaTu8988S showed a collective invasion after 4 days, but no dissemination of invading individual cells (Figure 3-13A). QM cell lines PaTu8902 and PaTu8988T showed high invasion of disseminated single cells. PaTu8902 disseminated as single cells, whereas PaTu8988T invaded in round and mesenchymal cells as characterised previously in the 2.5D assay (Figure 3-8B).

The average invaded distance per quadrant and the average spheroid body diameter was then quantified in ImageJ as invasion and invasive growth parameters (Figure 3-14). QM cells PaTu8902 (886.9 µm) and PaTu8988T (780.6 µm) showed high invasion, compared to the other cell lines. Moreover, when I compared the ability of QM cell lines to Classical cell lines in 3D invasion, QM cells was shown to be significantly more invasive starting from day 3 (Figure 3-14B). In addition, I have also conducted a qualitative assessment of the spheroid invasive behaviours, categorised in single cell invasion, collective colony invasion and collective cell invasion (Table 2). Single cell invasive behaviour seems to affect the invasive distance positively, while having high collective invasive behaviour seems to decrease the invasive distance.

Nevertheless, the highest invasive cell lines where not the highest spheroid growers, demonstrating lower relative invasive growth of the spheroidal body (Figure 3-14A). Panc1 was shown to be the cell line with the highest relative invasive growth, while this did not correlate with the invasion observed earlier. Furthermore, when QM cells were compared against Classical cells, no significant increases in relative spheroidal growth were found (Figure 3-14B). These data suggest that QM cells are more invasive compared to Classical cells and this is not correlated with or affected by the relative spheroid growth observed for the cell lines. Furthermore, PaTu8902 shown to be the most aggressive and invasive cell line of QM subtype among all the tested cell lines, demonstrating single cell and collective invasion, and could therefore be a potential candidate as the representative cell line model for the drug screen.

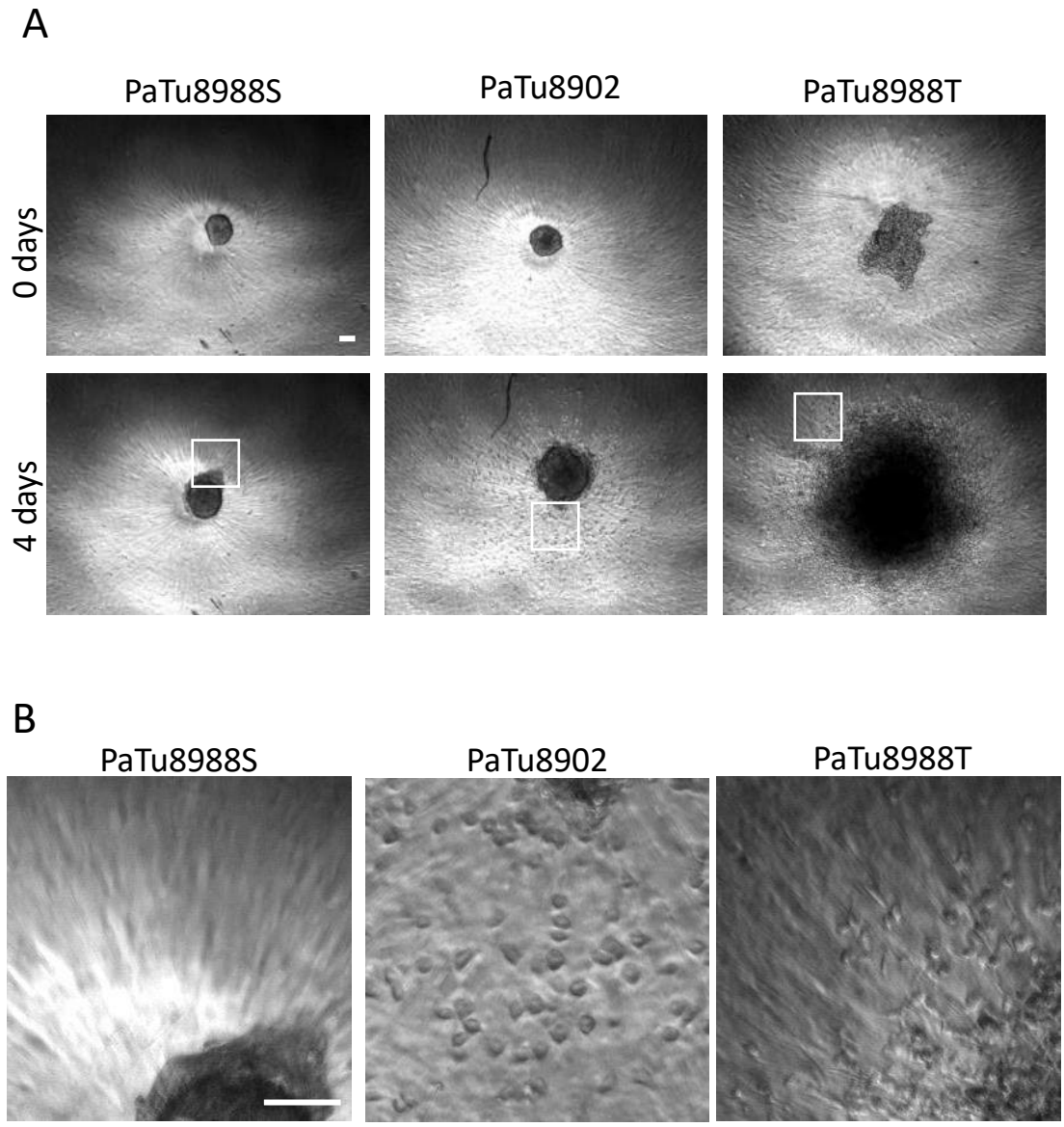

Figure 3-13. invasion of Spheroids in 3D rat tail collagen I matrix.
A) Representative phase contrast images of PaTu8988S, PaTu8902 and PaTu8988T co-culture spheroid invasion at 0 and 4 days in 3D collagen I matrix. Scale bar= 100µm.
B) Enlargement of insert of invasion day 4. Scale bar= 100µm.

A

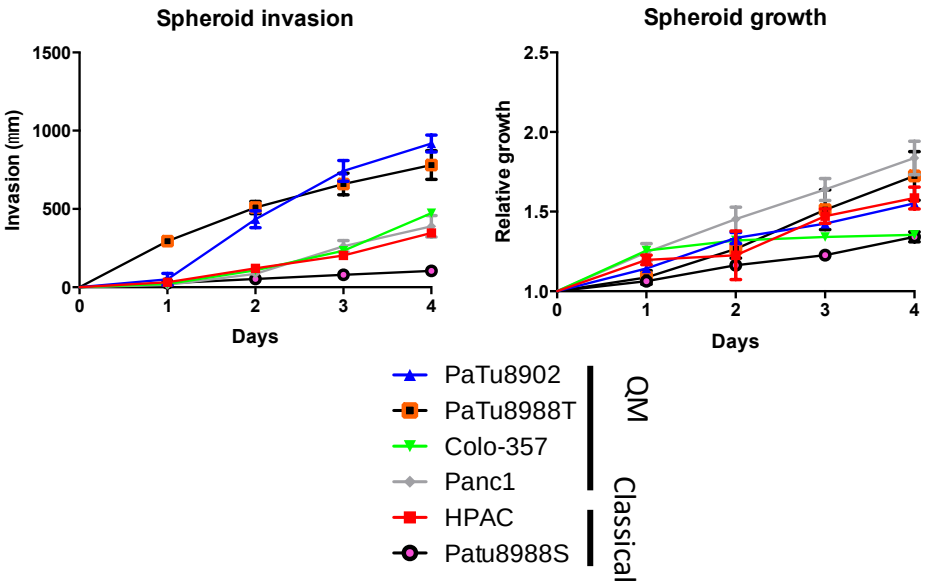

B

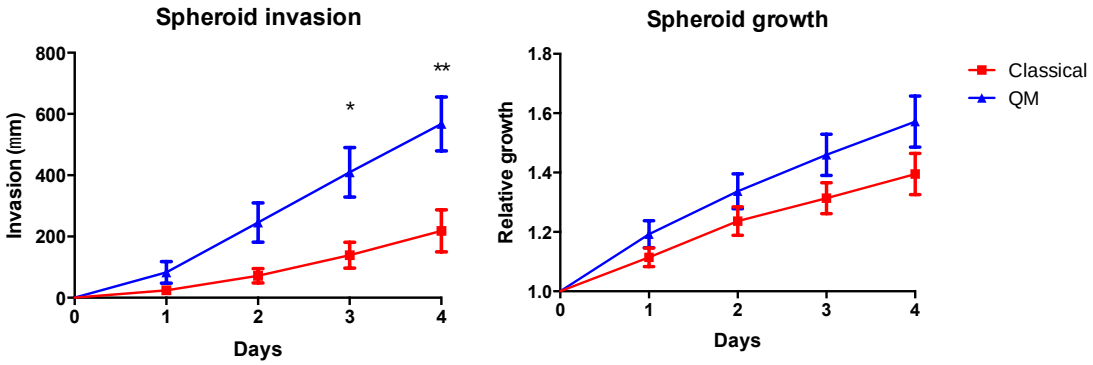

Figure 3-14. Spheroid growth and invasion in 3D rat tail collagen I matrix.

A) Quantification of average invaded distance per quadrant in µm and the relative spheroidal growth measured by the average size of the diameter of the spheroid body of the individual cell lines. B) Quantification of average distance invaded of furthest cells per quarter per triplicate in an individual experiment. Two Way ANOVA with Tukey's post hoc test was used for statistical significance. **, P<0.01. Data presented are the mean ± S.E.M, N=3.

Table 5 Quantitative and qualitative data of cells in the spheroid invasion assay

Cell line	sub-type	Origin	Single cell invasion	Collective colony invasion	Collective invasion	Retains spheroid body	Morphology d0	Average total distance invasion in µm	Invasiveness
HPAC	Classical	Primary	+	+	++	Yes	Sphere	371.1	Low
Patu8988S	Classical	Metastasis	-	-	+	Yes	Sphere	65.0	Low
Patu8902	QM	Primary	++++	-	+	Yes	Sphere	886.9	High
Patu8988T	QM	Metastasis	++++	-	+	Yes/No	Spheroid	780.6	High
Panc1	QM	Primary	++	-	++	Yes	Sphere	338.3	Low
Colo-357	QM	Metastasis	+	-	+++	Yes	Sphere	264.2	Low

- Not present, + Present, ++ Mainly Present, +++ Highly Present, ++++ Abundantly present
Single cell invasion: Single cells disseminate from the spheroid body
Collective colony invasion: Colonies/groups of cells disseminate from spheroid body
Collective invasion: Non-disseminated collective invasion from the spheroid body

3.2.7 Validation of PaTu8902 invasive behaviour in other models

In order to investigate whether PaTu8902 would be the ideal representative cell line model for the drug screen, I validated the findings of PaTu8902 from the 2.5D assay and the spheroid invasion assay with an alternative approach. The PaTu8902 cell line was tested in the 3D mini organotypic assay, a miniature version of the conventional organotypic assay (141, 167) (Figure 3-15). PaTu8902 cells were able to form an organised epithelial layer with luminal structures present in the absence of PS-1 stellate cells (Figure 3-15A and B). Furthermore, no single cell and collective cell invasion were observed. However, when PS-1 was introduced in a 2:1 ratio between PS-1 and PaTu8902 cells, an increase in the thickness of the epithelial layer was observed, suggesting a form of invasive growth. The PaTu8902 cells also seemed to be larger than when they were cultured without PS-1 cells. In addition, majority of the PaTu8902 cells seemed to adopt a round morphology and even invaded into the matrix as single cells too (Figure 3-15A; white arrows). PS-1 cells were found to form a layer in between the matrix and the epithelial layer, with several PS-1 cells invading into the matrix as well (Figure 3-15A and B). These findings demonstrated that PaTu8902 cells in the 3D mini organotypic assay recapitulated the round morphology observed in the 2.5D assay. Furthermore, their invasiveness was also confirmed in the form of collective invasion and single cell invasion when co-cultured with PS-1, which was initially observed in the 3D spheroid invasion assay.

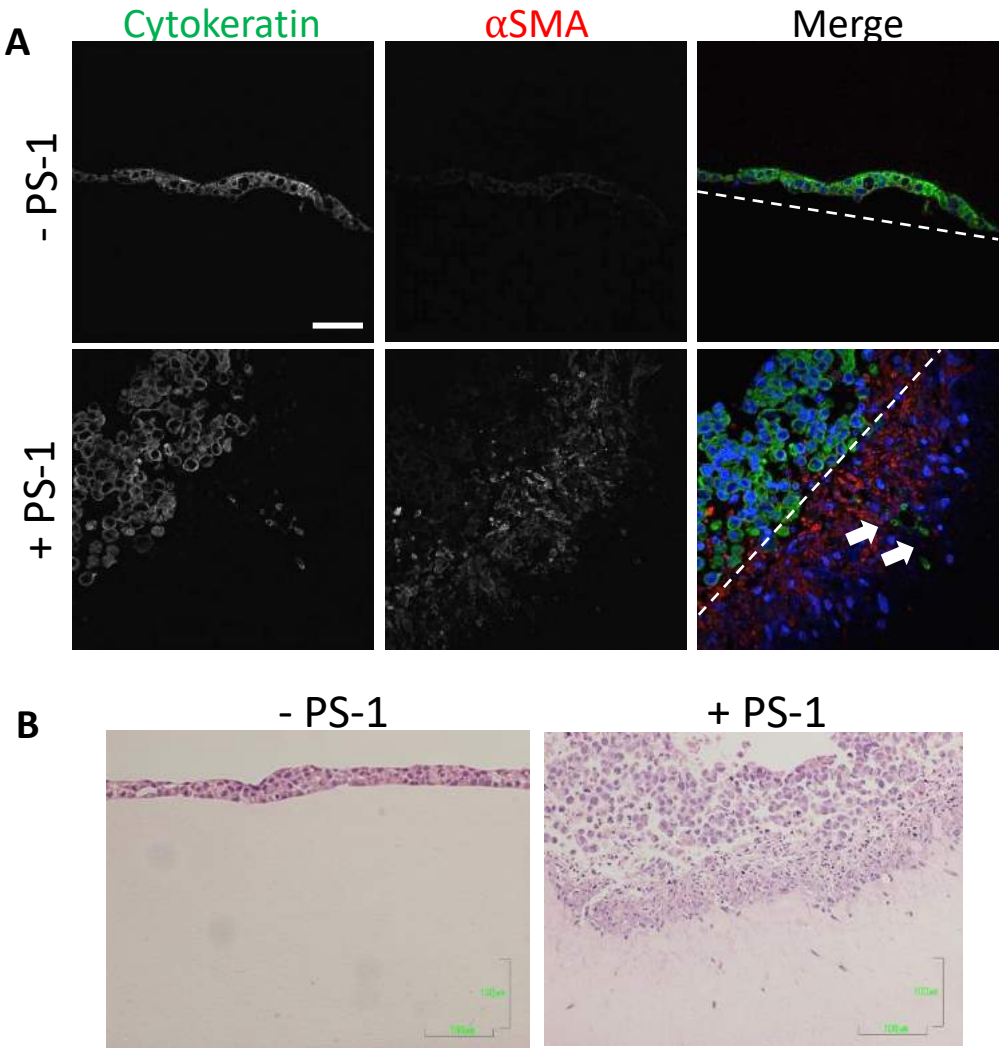

Figure 3-15. Invasion of PaTu8902 in the presence of PS-1 in the organotypic assay. A) Confocal images of organotyic assays with PaTu8902 cells (Stained with Cytokeratin in Green) in the presence and absence of PS-1 stromal cells (Stained with α-Smooth muscle actin in Red) after 7 days. Dashed line indicates the matrix surface and arrows indicate invading Patu8902 cancer cells. Scale bar = 50µm B) Hematoxylin and Eosin staining of organotypic assays in the presence and absence of PS-1 stromal cells after 7 days. Scale bar = 100µm

3.3. Discussion

In this chapter, the human pancreatic cancer cell lines were characterised in order to understand pancreatic cancer better and identify a representative cell line in co-culture with PS-1 stellate cells to perform the drug screen on. Little has been reported regarding the cellular morphology, plasticity, contractility and the preferred mode of migration of pancreatic cancer cells, especially in 2.5D or 3D matrix. Furthermore, the reported genetic subtypes by Collisson et al have not previously been correlated with any morphological or phenotypical characteristics *in vitro* in pancreatic cancer. Nevertheless, the use of molecular subtyping as survival and therapeutic response predictors has recently been further validated in pancreatic cancer (168, 169). A recent study on metabolic clustering utilising the subtype classification by Collisson et al was able to demonstrate metabolic differences between the two subtypes (169). QM cells were associated with a glycolytic metabolic subtype, while Classical cells were associated with a lipogenic metabolic subtype, suggesting functional relevance between genetic subtypes and distinct responses to targeted inhibitors.

Two other subtype classification papers have been published since the start of my study, supporting the existence and classification of these subtypes (37, 59). The QM subtype identified by Collisson et al 2011 has been reported to correspond with the basal subtype identified by Moffitt et al, and the squamous subtype identified by Bailey et al, (37, 59). Furthermore, both reported that the basal and the squamous subtype were correlated with a poor survival compared to the other subtypes identified in their respective studies. In this study, the QM subtype was shown to be enriched for single cell behaviour and reduced colony formation ability, which was correlated with the expression of mesenchymal markers and increased invasive capabilities compared to the Classical subtype. These findings were consistent with studies of the basal subtype in breast and bladder cancer, which have been reported to be more aggressive, demonstrating increased invasive behaviour and adopted an EMT or mesenchymal phenotype, expressing vimentin and losing E-cadherin expression (170, 171). Moreover, several independent studies have demonstrated

the expression of Vimentin and loss of E-cadherin in QM cells such as Panc1 and PaTu8988T, further supporting their mesenchymal profile (172, 173).

Despite the presence of distinctive molecular subtypes, here I report that the general individual pancreatic cancer cell demonstrates cellular plasticity, being able to switch between a round and an elongated morphology. Strikingly, cellular plasticity in pancreatic cancer has previously mainly been reported in the acinar cells, allowing these cells to transdifferentiate, lose polarity and break away from the acinus during inflammation, injury and tumour development (7). These acinar cells have been identified as one of the origins of pancreatic cancer and readily undergo transformation upon Sox9 expression and mutant Kras signalling through PI3K-PD1 pathway, indicating the important role of cellular plasticity in PDAC progression (8, 45). Furthermore, a recent study has shown that loss of Smarcb1, a chromatin remodelling factor, activates myc in Kras independent cancer cells to undergo EMT transformation into a more aggressive and metastatic mesenchymal phenotype (174). In addition, it has also been shown that the cellular plasticity in pancreatic cancer cells from genetic engineered mouse models (GEMM) is regulated by the EMT transcription factor Zeb1 (129). Moreover, another study has shown that E-cadherin positive and E-cadherin negative pancreatic cancer cells could both give rise to tumours *in vivo*, demonstrating plasticity between the epithelial and the mesenchymal states of the cancer cells (130). These findings are in line with our data *in vitro*, demonstrating the existence of cellular plasticity in pancreatic cancer and is more prominent in QM subtype cells. This ability reflects the acinar to ductal metaplasia plasticity process through EMT and indicates an aggressive phenotype of cells that is able to switch morphology for survival and migration.

The EMT- MET process is an example of cellular plasticity. It has been well established that EMT and mesenchymal cells are correlated with an elongated mesenchymal morphology, while epithelial or amoeboid cells are adopting a round morphology (175, 176). Here, I have found that individual cells of all pancreatic cancer cell lines adapted a round morphology on 2.5D collagen I matrix majority of the time, disregarding the subtype. Intriguingly, this finding is consistent with a recently published study where the morphology of single cells from primary pancreatic cancer

patients on 2D and 3D substrates were analysed and found to be mainly circular (177). However, they also showed that cancer cells derived from the primary tumour site were more heterogeneous compared to cancer cells derived from a metastatic site in the liver. While my results demonstrated a slight trend towards a mixed population in the cell lines of metastatic origin, these differences were deemed insignificant. This might not be very surprising as the authors have identified a heterogeneity in mainly round structures, with a few rare elongated morphologies, which is consistent with my findings (177).

The amoeboid mode of movement is characterised by a round morphology with high contractility (176). Two subtypes of amoeboid movement have been characterised (178, 179). One of the subtypes is characterised by rounded cell migration with bleb formation for a pushing movement and lack of adhesion. The other subtype is characterised by a slightly more elongated round cell migration with low substrate interaction through the formation of actin- rich filopodia/pseudopodia at the leading edge. The amoeboid mode of invasion has been identified to be primarily present at the invasive front of primary melanoma and breast cancers, and is enriched in melanoma metastases (180-182). As majority of individual pancreatic cancer cells exerted a round morphology, I investigated whether individual pancreatic cancer cells were utilising this high contractile strategy for migration and invasion. Thus far, no one has demonstrated the ability of pancreatic cancer to adopt an amoeboid morphology. A recent intravital study in the KPC mice has demonstrated the presence of only mesenchymal mode of migration in the pancreatic tumour (183). Interestingly, my data demonstrated the presence of mainly round individual cells on the 2.5D assay, with a subset of mesenchymal cells. Furthermore, individual cell dissemination of both round and elongated cells was observed in the 3D spheroid invasion assays of PaTu8902 and PaTu8988T, supporting the presence of round invading cells beside the reported mesenchymal morphology in the literature. Despite similar pMLC2 levels were observed in individual Classical and QM cells, QM subtype cells showed a higher trend of bleb formation in single cells. Furthermore, the pMLC2 levels were higher in QM and EMT cell lines in total cell lysates by western blot analysis, suggesting a more contractile blebbing amoeboid phenotype in the QM

cells. It has been reported that an increase of cellular contractility in pancreatic cancers, marked by increased pMLC2 levels through elevated activity of the JAK-STAT3 signalling cascade, has been correlated with poor survival, increased aggressiveness and increased invasion (184). The authors also suggested that the QM subtype was correlated with this increased contractile phenotype. Indeed, the GSEA data confirmed the enrichment in gene expression of contractile genes in QM cells compared to Classical cells. Nevertheless, future gene expression analysis should be conducted with genes extracted from cells cultured on Collagen I matrix to further support the morphological and phenotypical findings on 2.5D collagen I matrix. These findings are in line with my findings, correlating increased cellular contractility with increased aggressiveness, and suggesting the presence of amoeboid mode of migration and invasion in pancreatic cancer.

Cellular contractility has also been implicated in spheroid formation (185, 186). Here I have shown that QM cells were better at forming spheroids compared to the Classical cells. A study in ovarian cancer has shown that mesenchymal cells and cell contractility were factors which positively correlated with successful spheroid formation and invasiveness in 3D collagen I (187). Furthermore, they have also demonstrated that E-cadherin and N-cadherin expression did not predict the likeliness of spheroid formation. These findings are in line with my observations in this study, demonstrating that QM cells form better spheroids compared to the E-cadherin expressing Classical cells.

However, another study has shown that inhibition of actomyosin contractility through ROCK inhibitor Y-27632 and blebbistatin (myosin II inhibitor) increased spheroid formation and upregulated CD44 in colon cancer cells (188). These $CD44^{high}$ cells were correlated with increased spheroid formation ability, increased cancer stem cell markers and increased glycolytic activity. Interestingly, CD44 has been shown to be a receptor for MMP9 and positively regulates actomyosin contractility in amoeboid melanoma cells through stimulation of ROCK signalling (115). Yet, ROCK inhibition by Y-27632 demonstrated increased spheroid formation abilities in ovarian cancers and glioblastomas, but upregulated other stem cell markers such as Sox2 instead of CD44 (189, 190).

Nevertheless, recently developed ROCK inhibitors such as GSK269962a or AT13148 has been shown to be more potent in inhibiting ROCK activity compared to Y-27632, suggesting that ROCK inhibition by Y-27632 is only partial (108). AT13148 and GSK269962a was able to completely inhibit cell contractility and migration. Partial inhibition of ROCK allows cells to switch from an amoeboid phenotype to a mesenchymal phenotype during migration and has been shown to be insufficient to inhibit cellular contractility and proliferation (113, 191). The partial inhibition of ROCK activity by Y-27632 may improve spheroid formation by increasing cell adhesion as reported previously in trabecular meshwork cells (192). Further studies with potent ROCK inhibitors, myosin II inhibitor blebbistatin and knockdown constructs in pancreatic cancer will further elucidate the mechanism and role of actomyosin contractility in spheroid formation.

Overall, this chapter demonstrates that PaTu8902 could be a suitable cell line for the drug screen as it is a QM cell line, which has been correlated with poor patient survival (53). The spheroid invasion assay has identified two high invading QM cell lines: PaTu8902 and PaTu8988T. Both cell lines have been reported to be invasive (159, 193). Although both QM cell lines demonstrated cellular plasticity, high invasiveness and robust single cell dissemination, the PaTu8902 cell demonstrated a more robust co-culture spheroid formation with PS-1 stellate cells compared to the PaTu8988T cell line. Strikingly, PaTu8902 demonstrated a round morphology in individual cells with high pMLC2 levels, but without bleb formation, unlike the PaTu8988T. However, PaTu8902 has shown to generate pseudopodial structures while maintaining a round morphology (Figure 3-9B), which could be classified as amoeboid with pseudopodia/diplopodia mode of migration (179). The invasiveness and effective cross talk ability with stromal cells has been validated in the organotypic assay for Patu8902, increasing its validity by confirming its aggressive phenotype. Moreover, PaTu8902 is the only QM cell line reported by Collisson et al to be resistant to gemcitabine (53). This would also take into account the drug resistance characteristics observed in pancreatic cancers for the drug screen. These findings overall suggest that PaTu8902 would be the choice of cell line model for the drug screen with PaTu8988T as a potential back up cell line for validation.

3.4. Future work

This work demonstrated how genetic subtypes are morphologically and phenotypically different. It was interesting to observe another sub category, the "intermediate" class, during classification by morphology. Additional cell lines could potentially uncover more sophisticated subtype classification that is not only based on genetic expression, but also on morphological and phenotypical assessment. Also, the current subtyping studies are conducted on cells grown on plastic. Future genetic studies should be carried out on cells grown on 2.5D assay or in 3D collagen to validate these findings. Taking this further with primary cells from pancreatic patients could provide us a better understanding of the molecular and phenotypical relations and predict survival and treatment response more accurately.

Genetic expression data does not directly translate into changes on protein levels due to post translational modification. Therefore, increased investigation in EMT markers (e.g. Zeb1 and Twist1), mesenchymal markers (e.g. αSMA), integrins (e.g. β1), and other cell-cell adhesion molecules could shed new light into the molecular classification and correlate this with cellular plasticity and the original set of genes used for the genetic expression analysis by Collisson et al (53).

Exciting observations have been made with cellular contractility in the investigated cell lines. It would be important to confirm the enrichment of contractile genes for all the studied QM cells cultured on Collagen I compared to Classical cells. Future work with ROCK inhibitors, Blebbistatin and myosin light chain knock down experiments would further pin down the differences in the contractility mechanisms between Classical and QM cells. Furthermore, confirming the JAK-STAT3 signalling activity might provide further information regarding the contractile machinery and the intensity between classical and QM cells. Moreover, the differences in collective cell contractility needs to be taken into account, especially when investigating the effects on spheroid formation. In addition, it is important to identify whether there is a link in pancreatic cancer between ROCK activity, spheroid formation and the upregulation of cancer stem cell markers/enrichment of cancer stem cells as found in colorectal, ovarian and glioblastoma cancers.

To further bridge genetic analysis with functional outcome, it would be of interest to investigate the common genes regulated in the QM cells that are responsible for contractility and the invasive behaviour in 3D for targeted drug discovery. In addition, secreted factors could be screened for MMPs and other ECM degrading enzymes. Here I have used a surrogate marker for cellular proliferation by measuring the spheroid body expansion. However, it would be very interesting to test and optimise the proliferation and cell death in spheroids in 3D to confirm these findings.

Also, as mentioned previously, pancreatic stellate cells have been reported to play an important role in the progression of the disease. I have demonstrated that PS-1 increased the aggressive phenotype of PaTu8902 in the organotypic assay. It is therefore exciting to dissect the effects of PS-1 further by generating conditioned medium with and without being in co-culture with cancer cells and investigate the effects of the secreted factors in the morphology and invasion studies.

The ultimate validation for PaTu8902 cells would be recapitulating all the in vitro findings with an *in vivo* mouse xenograft model and confirm these morphological and phenotypical findings in patient tissue sample. A drug screen study targeting specific markers of Classical or QM subtype cells could be potentially of interest for the advancements towards personalised medicine for pancreatic patients.

4. Development of a 3D spheroid invasion drug screening assay

4.1. Introduction

In the previous chapter, I have identified a QM cell line model that is robust in spheroid formation and is highly invasive to be used for the drug screen. In order to avoid advancement of local invasion or progression to metastatic state of the disease, it is important to not only inhibit the invasion of cancer cells, but also be able to target and kill local invasive cells and cells that are disseminating systemically. By identifying potential migrastatic drugs and combine them with the standard of care; Gemcitabine, a cytostatic drug, invasive cancer cells could potentially be targeted and killed (194). As mentioned previously, the tumour microenvironment has been implicated in tumour initiation, growth and invasion (195, 196). Including the tumour microenvironment compartments into the drug screen platform could potentially increase the clinical relevance of the drugs and may provide novel therapeutic strategies against pancreatic cancer.

Several methods have been developed to investigate the effects of the tumour microenvironment components on pancreatic cancer progression. Co-cultures of cancer cells with stromal cells or conditioned medium derived from stromal cells *in vitro* was one of the earlier models used to study the effects of stromal cells on pancreatic cancer progression (197, 198). However, transcriptomic studies in various cancers, including pancreatic cancer, have demonstrated altered expression of proliferation, cell survival or drug resistance related genes when cancer cells were cultured as 3D spheroids compared to the conventional 2D plastic culture (199-202). Furthermore, the simplicity of 2D culture limits the experimental possibilities and lacks the ability to investigate cellular invasion. Moreover, other 3D culture methods such as organotypics and the recently developed organoids have demonstrated to recapitulate *in vivo* observations more closely (203, 204). In addition, organoids are able to retain the primary phenotype and genetic expression profile for longer periods in culture and readily adapts structures resembling the original cancer when transplanted orthotopically in vivo (204-206). A 3D approach would therefore be

more desirable for studying the contributions of the tumour microenvironment on tumour progression over 2D methods.

Although genetic engineered mouse models (GEMMs) and patient derived xenografts (PDXs) are well established models to study the disease progression and the role of the tumour microenvironment *in vivo*/*ex vivo*, not every laboratory has access to mouse facilities and patient materials (203, 207-209). Furthermore, despite their power in late stage pre-clinical drug development and personalised medicine, these models are often unsuitable for high throughput drug screening due to the relative high cost, long experimental duration, the need of many mice and the lack of uniform tumour development and progression. Hence, 3D models are more favourable as a screening alternative due to their close resemblance of *in vivo* behaviour, high reproducibility, relative low cost, high adaptability and experimental feasibility, and scalability for high throughput drug screening (206, 210, 211). By utilising 3D models to bridge the gap between 2D and *in vivo* GEMM or PDX models for early phase drug discovery, it would be possible to perform high throughput drug screening in the presence of tumour microenvironmental components.

While the organoids and organotypic assays are more novel compared to the older spheroid assay, the spheroid assay is yet more straight forward, time and cost effective. Organoids require the use of primary cells either from mouse or human patients in order to form long lasting self-renewing organoids with differentiation potential (204). The organotypic assay requires the need of tissue processing in order to examine the outcome (167). Recent 3D spheroid drug screening models have been readily adapted to investigate proliferation, cell survival and cell invasion (212-214). Furthermore, co-culture systems have also been implemented in 3D spheroid cultures. A 3D pancreatic cancer co-culture spheroid model with fibroblasts has been shown to increase cell survival compared to 2D co-culture systems, demonstrating the significance of the 3D architecture (215). Therefore, the spheroid assay could be a good model to perform a drug screen while including stromal cells and extracellular matrix found in the tumour microenvironment in pancreatic cancer.

It has been reported that activated pancreatic stellate cells (PSCs) in the tumour microenvironment are supporting proliferation, survival, invasion, metabolism and

drug resistance of the cancer (102, 141, 216, 217). PSCs would be an important factor to be included in drug screens. Strikingly, no drug screens have been performed on pancreatic cancer in the presence of stellate cells thus far. Furthermore, as majority of the drug screens performed on pancreatic cancers were mainly based on cell survival or cell proliferation, no study has been reported on drug screening against pancreatic cancer invasion with pancreatic stellate cells in 3D models (206, 218, 219).

Pancreatic cancer is characterised by desmoplasia, with dense extra cellular matrix deposition, majority consisting of Collagen I fibres (220). An increase in collagen expression has been associated with increased metastasis and poor prognosis. Using Collagen I as the extra cellular matrix in the assay would increase the clinical relevance of the model. Another widely used matrix is Matrigel, produced by from Engelbreth-Holm-Swarm mouse sarcoma cells. It is widely used to mimic the basement membrane matrix in vivo and has shown to play an important role in the invasion of pancreatic cancer cells (221, 222). Moreover, pancreatic organoid cultures rely on Matrigel to propagate and retain its *in vivo* characteristics, demonstrating the important role of the matrix on supporting pancreatic cancer progression (205). Both matrices will therefore be tested.

The co-culture spheroid invasion assay that I have used in chapter 3 demonstrated robust observations and would be a good base for the drug screening platform. The aim in this chapter is to further optimise the co-culture spheroid invasion assay with cell line models identified in the previous chapter, and develop it into a drug screening platform. The drug screen assay should be straightforward with little handling steps, which would increase reproducibility and reduce time and complexity of the screen. Furthermore, cellular morphology and phenotype in the spheroid invasion assay will be validated *in vivo* through intravital imaging of mouse xenografts. Moreover, performance of positive and negative controls will be validated against the standard of care in the drug screen assay. The analysis step should be quick and robust, preferably automated in order to allow high throughput drug screening. This drug screen platform could be used as a tool to identify novel migrastatics and cryostatics by assessing invasion and growth of the 3D co-culture spheroid in the

early phase of drug discovery studies. Promising hits should be further validated with alternative 3D in vitro models or with GEMM/PDX *in vivo*.

4.2. Results

4.2.1. Defining the optimal spheroid formation conditions of Patu8988T and PaTu8902

In the previous chapter, I have conducted co-culture spheroid invasion assays with the preferred cell line models PaTu8902 and PaTu8988T in the presence of PS-1 cells (Figure 3-13). Previously, the hanging drop method was tested on the lid of petri dishes (data not shown). However, this was not optimal for drug screening as spheroids had to be transferred into wells. Hence, spheroids were generated in 96 wells ultra-low attachment U-bottom plates, containing one spheroid per well. PaTu8902 demonstrated good and robust tight spheroid formation, whereas PaTu8988T demonstrated a less compacted spheroid formation. In order to confirm the most optimal spheroid formation conditions for PaTu8988T, different total cell numbers (1k, 2k &5k), spheroid formation duration and addition of methylcellulose were assessed in the Patu8988T cell line (Figure 4-1). Different total cell numbers did not contribute to a tighter spheroid formation in PaTu8988T, but only increased the spheroid size (5k cells spheroids data not shown). Similarly, increasing the duration of spheroid formation in the wells also did not contribute to a tighter spheroid, while it increased the size of the spheroid. The spheroid structure was already assembled around day 3 and did not change overtime, while the size would increase when incubated longer.

Next, 0.32% methylcellulose was added as a crowding agent to the cultures to improve spheroid formation. However, methylcellulose did not aid the PaTu8988T in forming tighter spheroids. Moreover, doubling the total cell number or increasing the spheroid formation duration in the presence of methylcellulose did not affect the compactness and shape of the spheroids. These results suggest that spheroid formation ability of Patu8988T is not affected by cell numbers, time or external interaction with the crowding agent or treated well surface.

As methylcellulose did not make a significant difference in the spheroid formation of Patu8988T, and it would make it more difficult to remove from the well during medium removal and matrix addition, it was left out from the spheroid formation

protocol. As PaTu8988T and PaTu8902 spheroids grown with or without PS-1 started to form the spheroid body on day 2 and have formed a stable spheroid from day 3 onwards, it was decided that the spheroid formation duration should be no longer than 3 days (Figure 4-2). By controlling the spheroid formation duration, the size could be controlled to avoid the diameter to surpass 500 µm, where the development of necrotic areas in the centre of the spheroid occurs and could cause variability in the drug screen (223, 224). At day 3 the PaTu8988T spheroid has an average diameter of 400µm, while the diameter of the PaTu8902 spheroids measure around 200µm.

It is interesting to note that the PS-1 cells did not improve or hinder the spheroid formation of PaTu8988T or PaTu8902 cells (Figure 4-2). Overall, PaTu8902 has shown to be the first choice of cell line model due to its robust and tight spheroid formation over PaTu8988T at day 3 of spheroid formation. Therefore, PaTu8988T would be used as a back-up cell line potentially as validation cell line.

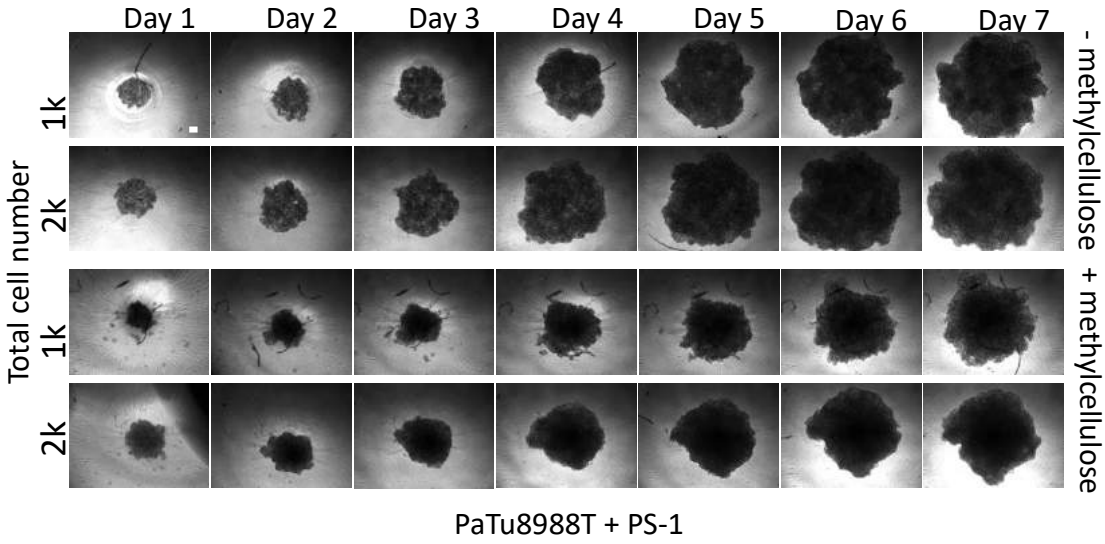

Figure 4-1. PaTu8988T and PS-1 co-culture spheroid formation optimisation.
Phase contrast images of co-culture spheroid formation of Patu8988T + PS-1 (1:1 ratio) with a total cell number of 1000 or 2000 cells per well, over the course of 7 days in the presence or absence of 0.32% methylcellulose. Scale bar= 100µm. Data shown is representative over 3 individual experiments.

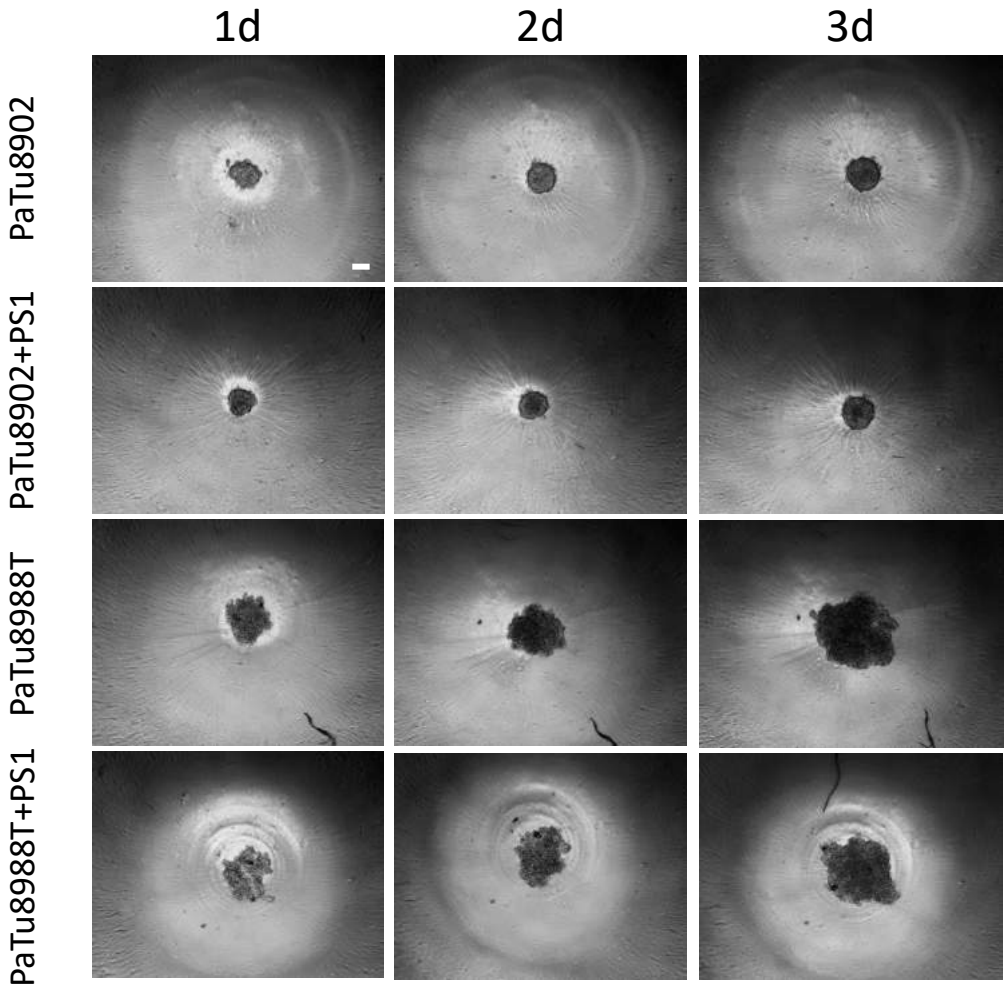

Figure 4-2. Spheroid formation of PaTu8902 and PaTu8988T with and without PS-1. Phase contrast images of PaTu8902 and PaTu8988T spheroids in the presence or absence of PS-1 stellate cells over 3 days. Scale bar= 100µm. Data shown is representative over 3 individual experiments.

4.2.2. Defining the optimal invasion conditions

After defining the spheroid formation conditions, the invasion conditions were optimised. In order to find the most suitable extracellular matrix for the invasion assay, medium was replaced with either rat tail collagen I or a growth factor reduced Matrigel matrix for the PaTu8902 + PS-1 co-culture spheroids. Initial efforts caused centrifugation necessary after matrix addition, to keep the spheroids in the middle of the well. However, this could affect the spheroids and the polymerisation step and the protocol was adapted to avoid centrifugation by simply gentle pipetting. The spheroids in collagen I retained their shape after matrix polymerisation, whereas the spheroids in matrigel started to deform after polymerisation of the Matrigel (Figure 4-3). This deformation caused by the Matrigel would increase variability in the starting point of the spheroid and would not be suitable for the drug screen. Therefore, collagen I would be the more suitable invasion matrix.

Next, the invasion duration of PaTu8902 and PaTu8988T co-culture spheroids with PS-1 were assessed in collagen I matrix with DMEM/F12 medium + 10% FBS as chemoattractant (Figure 4-4 & 4-5). PaTu8902 co-culture spheroids showed single cell dissemination from day 2 onwards. By day 4 and 5 the cells have invaded to the periphery of the well. Furthermore, collective invasion and growth of the spheroid body has been observed. The PaTu8902 has a good invasion window between day two and day 4. Taking an ending time point shorter than day 4 would reduce the invasion window and sensitivity for invasion inhibition. Conversely, having an ending time point over 4 days would reduce the invasiveness as many cells have reached the side and top of the well.

The PaTu8988T spheroids showed invasion 1 day earlier compared to the PaTu8902 spheroids, starting 1 day after invasion initiation in collagen I. Similar to PaTu8902, the PaTu8988T invasion peaks at day 4, with cells at day 5 reaching the rim and the top of the well. However, the spheroid body expansion is much larger compared to the PaTu8902, which could make it more complicated to get accurate measurements for invasion. Nevertheless, the invasion in both spheroid models should ideally be assessed up to 4 days after invasion initiation. Reducing the cell numbers could be a

potential method to increase the invasion duration when long term drug responses or drug treatments are of relevance.

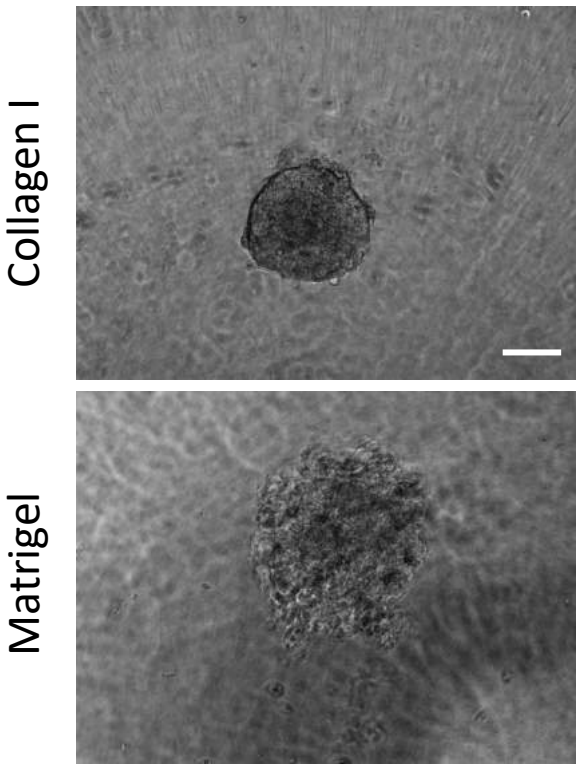

Figure 4-3. PaTu8902 + PS-1 co-culture spheroid structure in different extracellular matrix.
Phase contrast images of PaTu8902 and PS-1 co-culture spheroids in polymerised rat tail collagen I and growth factor reduced Matrigel at spheroid formation day 3 (Invasion time point d0). Scale bar= 100µm. Data shown is representative over 3 individual experiments.

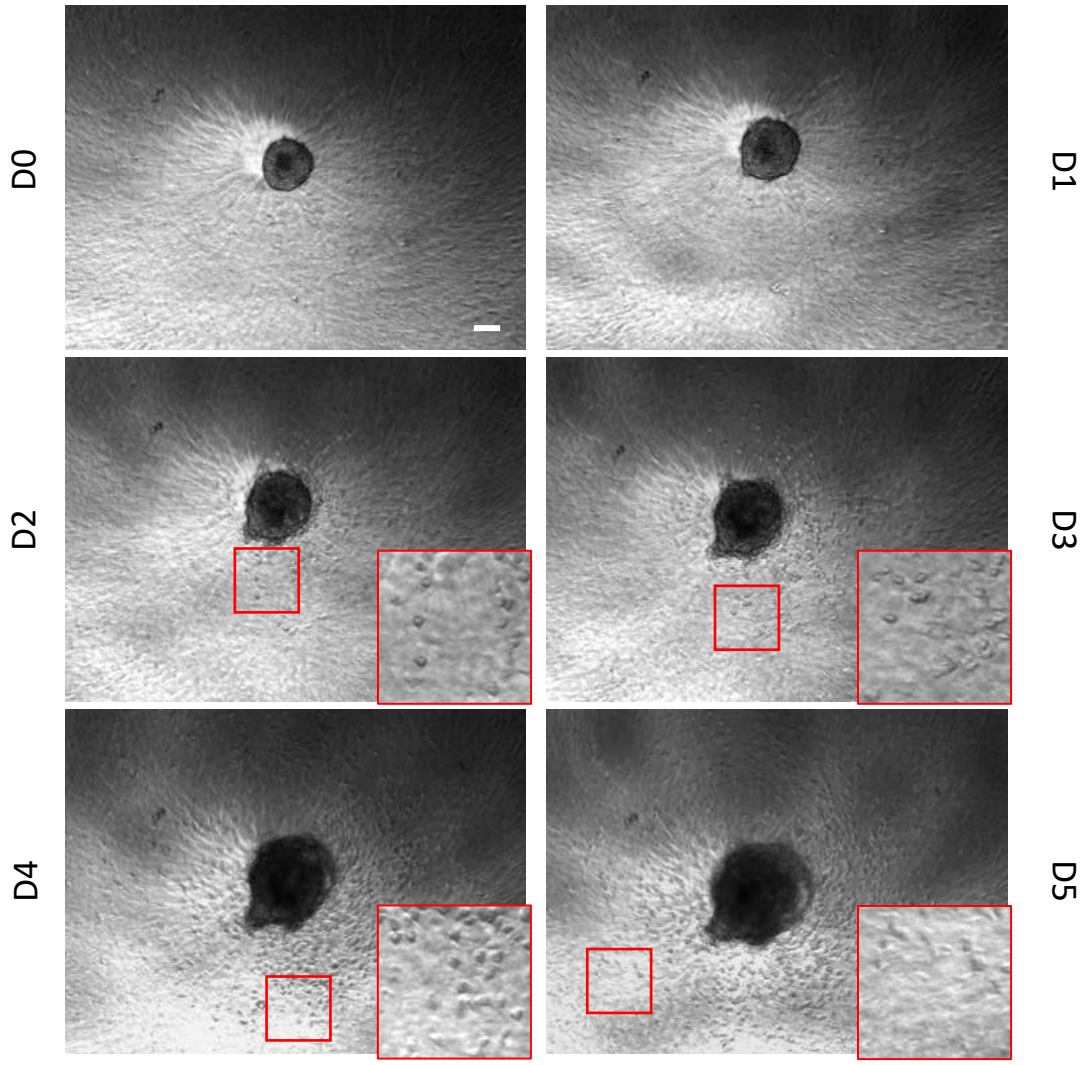

Figure 4-4. Invasion of PaTu8902+PS1 co-culture spheroid in collagen I.
Phase contrast images of PaTu8902 and PS-1 co-culture spheroid invasion in collagen I over 5 days. Scale bar= 100µm.

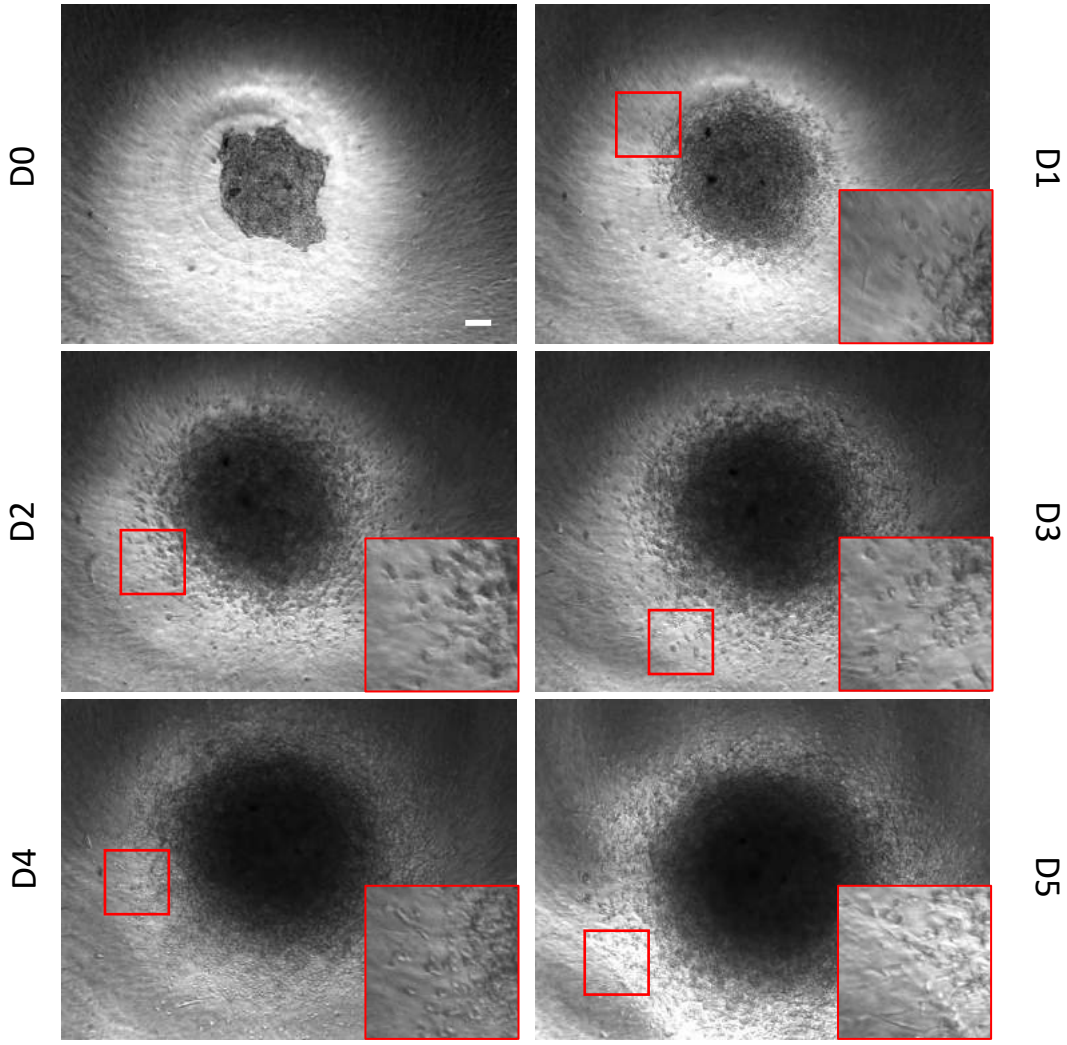

Figure 4-5. Invasion of PaTu8902+PS1 co-culture spheroid in collagen I.
Phase contrast images of PaTu8988T and PS-1 co-culture spheroids in collagen I over 5 days. Scale bar= 100µm. Insert shows close up of marked area of invasion.

4.2.3. Visualisation of PaTu8902 and PS-1 cells through fluorescent labelling

As the optimal formation and invasion conditions have been identified, it was important to elucidate the best method to identify and analyse the different cellular compartments in the spheroid. In order to facilitate analysis and the identification of the PaTu8902 and the PS-1 cells in the well, fluorescent tagging was applied. PaTu8902 and PS-1 cells were stably transduced with Lifeact-GFP (PaTu8902-GFP) and Lifeact-mrfpruby (PS-1-mrfpruby) respectively (Figure 4-6). The localisation of each compartment was visible upon spheroid formation. As the PS-1-mrfpruby cells were observed to be located inside the spheroid in clusters, the spheroid shape and invasive behaviours remained identical post transduction, demonstrating single cell dissemination of the PaTu8902-GFP cells. Similar observations have been made for the fluorescent labelled PaTu8988T spheroids (data not shown). Intriguingly, the PS-1-mrfpruby cells mainly stayed in the centre of the spheroid and only a rare few cells were observed invading (See Figure 4-6 insert).

With the fluorescent labelled cells, it was important to validate the localisation and the behaviour of the spheroids when different PaTu8902-GFP:PS-1-mrfpruby ratios were applied with the same total cell number of 1000 cells per well (Figure 4-7). Spheroid size or shape did not alter upon changes in ratios of Patu8902-GFP and PS-1-mrfpruby cells. As the PS-1-mrfpruby compartment in the centre of the spheroids increases with the increased amount of PS-1-mrfpruby ratio, the invasion remained largely similar between the different ratios. In order to keep sufficient cancer cells in the model, the 1:1 ratio was adapted for simplicity yet recapitulating similar phenotype as the 1:2 ratio with more PS-1-mrfpruby cells.

While it was tempting to test adding the PS-1-mrfpruby cells in the collagen to mimic the *in vivo* conditions more closely, I contemplated that it might result in large variability in a screen setting due to difficulties in generating an equal homogenous collagen I mixture with cells. Furthermore, different levels of contraction of the matrix caused by the PS-1 cells would also add to screen and outcome variability. Thus, the co-culture spheroids were initially generated by co-culturing both cell types in the ultra-low attachment U-bottom wells. This method has resulted in the localisation of PS-1-mrfpruby cells in the centre. In order to test whether it was

possible to have the PS-1-mrfpruby cells localised on the outer side of the spheroid, the PS-1-mrfpruby cells were added a day after the spheroid was generated. Ps-1-mrfpruby cells were still found localised in clusters inside the spheroid rather than localised on the outer side of the spheroid on day 3 of spheroid formation ((Figure 4-8). This result suggests that PS-1-mrfpruby cells are likely to actively migrate into the centre of the spheroid rather than staying in the spheroid periphery.

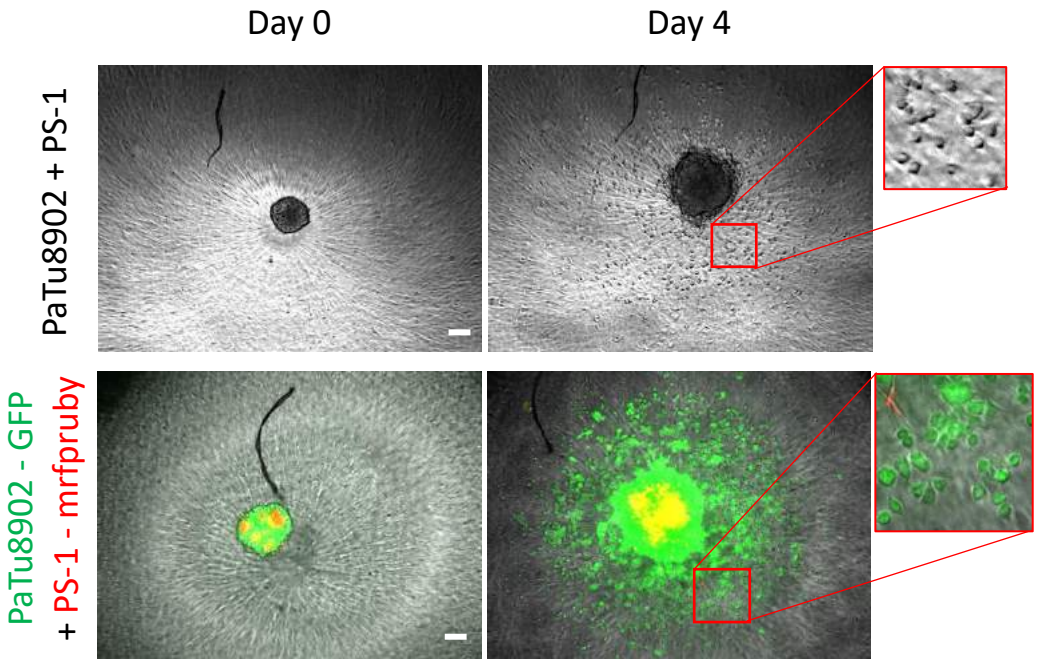

Figure 4-6. Invasion of standard and fluorescent labelled PaTu8902/PS-1 co-culture spheroids.
Phase contrast and merged images of phase contrast and fluorescent PaTu8902-GFP (Green) and PS-1-mrfpruby (Red) images, at the start of the invasion (day 0) and the end of invasion (day 4). Scale bar= 100µm.

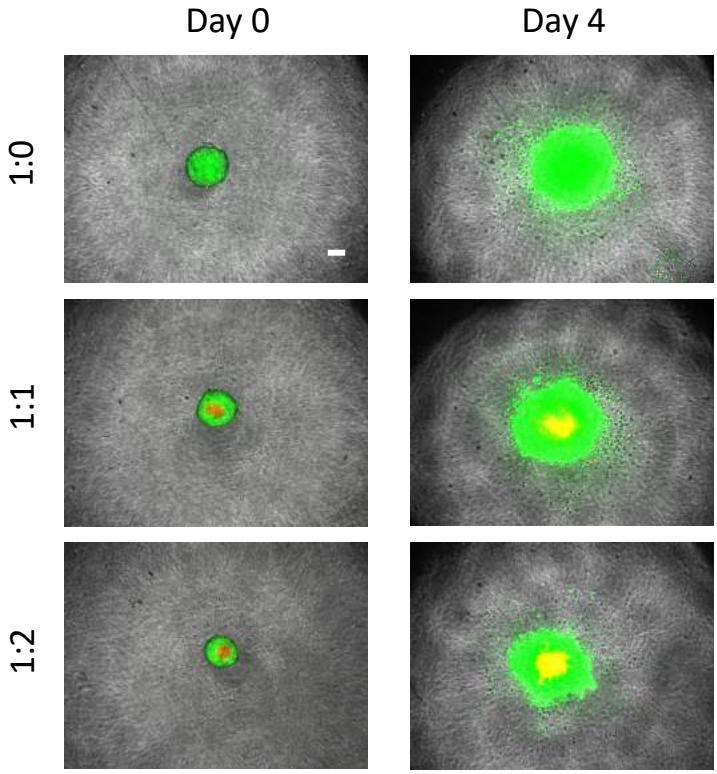

Figure 4-7. Spheroid formation and invasion of different PaTu8902-GFP and PS-1-mrfpruby ratios.
Merged phase contrast and fluorescent images of PaTu8902-GFP (Green) and PS-1 mrfpruby (Red), in a monoculture spheroid (1:0) or in co-culture spheroid with different ratios of PaTu8902:PS-1 (1:1 and 1:2) at the beginning (day 0) and the end of invasion (day 4). Scale bar= 100µm.

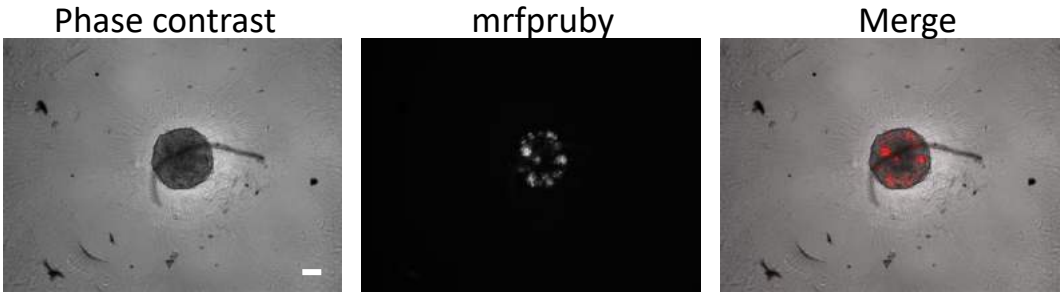

Figure 4-8. PS-1 mrfpruby localisation in alternative spheroid generation method. Phase contrast, fluorescence and the merge images of PS-1 mrfpruby cells and PaTu8902 co-culture spheroids on day 3 of spheroid formation. PS-1 mrfpruby were added a day after spheroid formation was initiatied with PaTu8902-GFP only. Scale bar= Scale bar= 100µm.

4.2.4. *In vivo* validation of PaTu8902 spheroid invasion characteristics

The 3D spheroid model suitable for drug screening has now been established. While all the conditions have been optimised, it is important to demonstrate that the model is clinically relevant and resembles *in vivo* characteristics. To further validate the *in vitro* findings of the PaTu8902-GFP cell line model *in vivo*, I collaborated with Dr. Fernando Calvo and Dr. Nicola Ferrari at the ICR to image the cells *in vivo* in a mouse xenograft. The PaTu8902-GFP cells were injected subcutaneously into a nude mouse and intravital imaging was performed 20 days' post injection. PaTu8902-GFP cells were forming small clusters/tumour bodies over time, similarly to the spheroid formation *in vitro*. Furthermore, the PaTu8902-GFP cells disseminated and invaded away as round and elongated single cells at the invasive front, whereas little migration was observed in the tumour body (centre of the tumours) (Figure 4-9). These results demonstrate that the PaTu8902 has the ability to form spheroid like tumours and invade in single cells *in vivo*, in a similar manner as shown in vitro with the spheroid assay. Future work is needed to quantify and confirm the numbers of round and elongated invading cells.

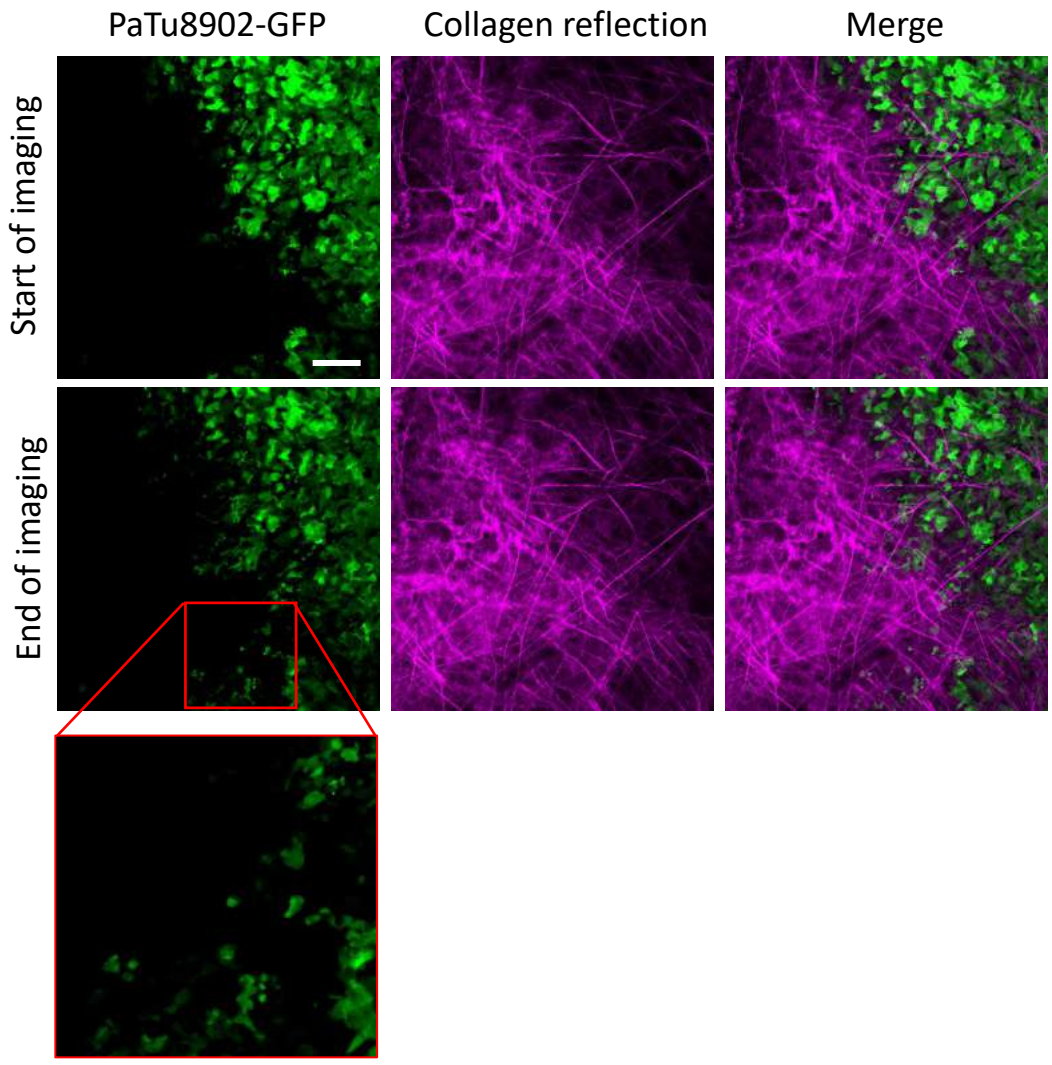

Figure 4-9. Invading PaTu8902-GFP cells in a nude mouse xenograft.
Intravital imaging of PaTu8902-GFP cells (Green) and collagen (Magenta) at day 20 post subcutaneous injection. Insert demonstrate the invasion of round and elongated single disseminated cells. Scale bar= 100µM

4.2.5. Semi- automated analysis for invasion quantification

The fluorescent labelling has allowed the localisation of both cell types. Furthermore, the fluorescent signal could aid the quantification analysis of the invasion. To quantify the invasion in a more automated manner rather than measuring the distance of each invaded or the average furthest invaded cell per quadrant, the fluorescent signal was used to quantify the measurement by utilising a threshold (Figure 3-13 and 3-14). Fluorescent images were collected from the microscope and the images were processed in ImageJ. By using the fluorescent signal, the overall invasion area can be measured as a surrogate quantification for the invaded distance. The more invasion there is, the larger the area of the fluorescent signal is going to be. The area of the fluorescent signal is measured in ImageJ with the threshold setting to mask the fluorescent signal at the start and at the end of the invasion (Figure 4-10). The measured area at the end of the invasion is then divided by the measured area at the start of the invasion to yield a relative invaded area. This is to account for any differences in the starting area. Once drug treatment is administered, the relative invaded area of the treated spheroids will be divided by the relative invaded area of the control treated spheroids to yield the relative inhibited area of invasion.

It is important to note that this approach only allows values of >0, as there will always be a starting point signal of the non-invaded spheroid. Therefore, if 100% inhibition of invasion occurs or when the cells of the spheroid has undergone apoptosis, the relative value will still be >0. One could use a relative value of 1 for the treated spheroid area in the equation to obtain the final relative invasion value where 100% invasion inhibition has occurred without any growth of the spheroid itself, as an indication. Furthermore, this surrogate approach allows for sensitivity of the inhibition of the invasion only, or rather the reduction of measured invasion area, and will be not sensitive to identify invasion inducing compounds accurately. This is due to the saturation of the invasion of the cells and the expansion of the large GFP signal from the spheroid body. Images at an earlier time point or the spheroid invasion assay executed with a less invasive cell line could increase the sensitivity for invasion inducing compounds with these methods.

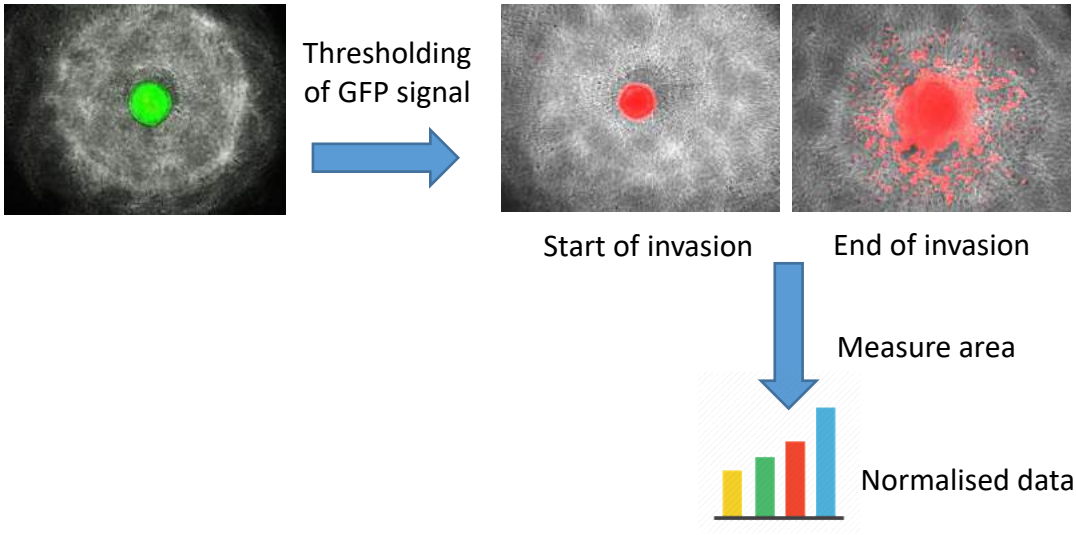

$$Relative\ invasion = \frac{drug\ area\ t_{end}}{drug\ area\ t_{start}} \div \frac{DMSO\ area\ t_{end}}{DMSO\ area\ t_{start}}$$

Figure 4-10. Semi-automated image analysis for measuring the invasion area.
A threshold on the fluorescent signal is applied to the fluorescent images taken on the microscope and the area was measured in ImageJ. This is applied at the start and at the end of the invasion. The measured area is then normalised and the relative invasion was calculated comparing the treated spheroids against the control spheroids by using the formula as shown. t_{end}= time point at end of invasion, t_{start}= time point at start of invasion.

4.2.6. Positive and negative controls for the spheroid invasion assay

With the semi-automated quantification in place and having the formula to compare treated and control treated spheroid invasion, it was important to find and validate both positive and negative controls. DMSO was used as a negative control, whereas Dasatinib was tested to be as a positive control. Both compounds were compared with the standard of care: Gemcitabine (Figure 4-11). DMSO did not affect cell invasion in the co-culture spheroids and can be used as a negative control (Figure 4-11B). As most 3D drug screens without matrix use a drug concentration between 1µM and 50µM, 10µM was used as a starting point by taking into account the penetration difficulties from the matrix and the 3D spheroidal structure (224, 225). Spheroids treated with 10µM Gemcitabine showed a decrease of invasion with a relative invasion of 0.52. However, total inhibition of invasion was not observed as there were still several invading single cells and collective invasion of the spheroid body present. Next, Dasatinib was used to test inhibition of invasion, as it has been shown previously in mice and *in vitro* to block metastasis and invasion (122). 10 µM Dasatinib demonstrated total inhibition of invasion (relative invasion: 0.34), without any single cell dissemination or collective invasion from the spheroid body. Nevertheless, spheroid growth was still observed at this concentration. These results demonstrate that good drug penetration of the matrix was achieved and that Dasatinib and DSMO can be used as positive and negative controls for the spheroid invasion assay.

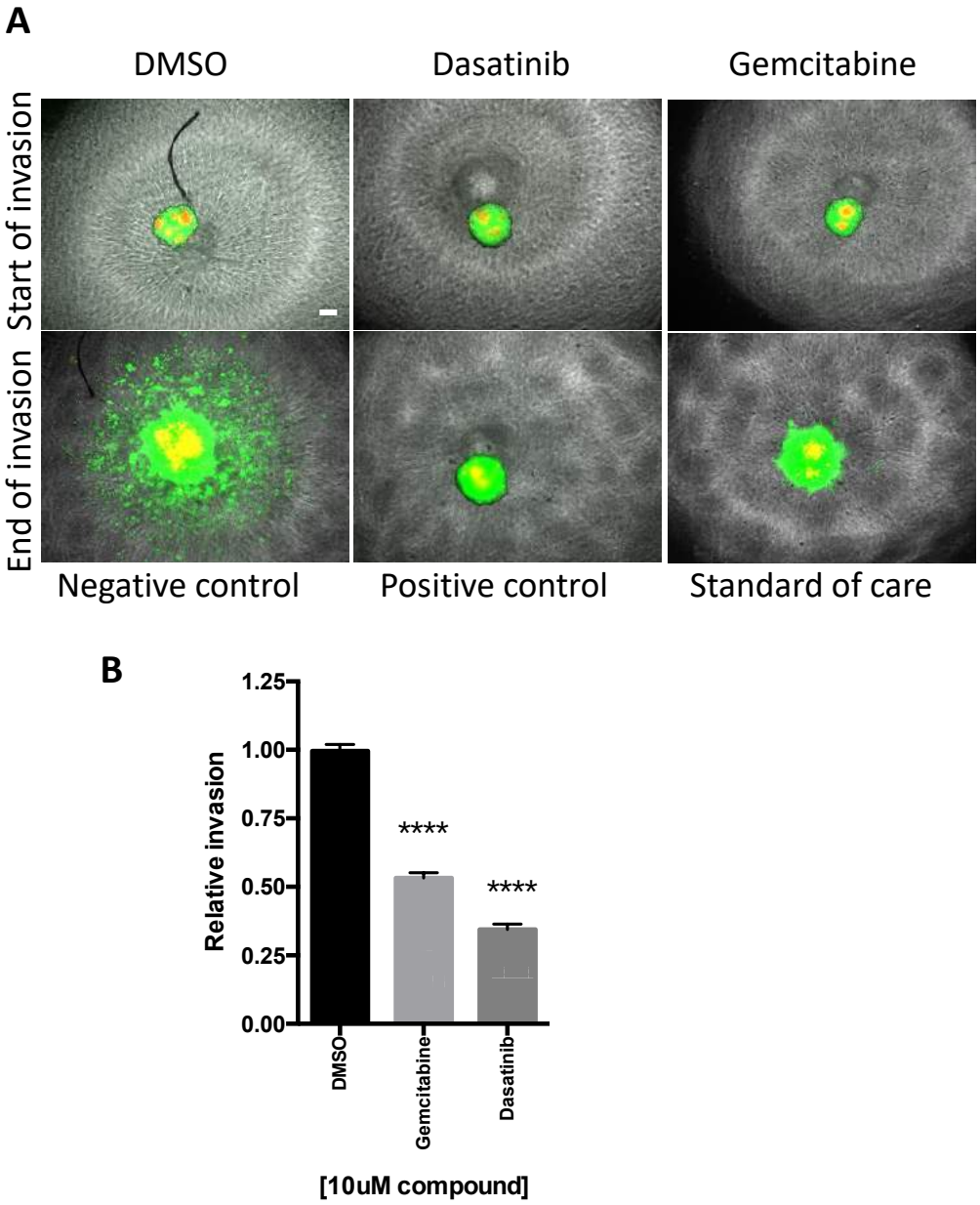

Figure 4-11. Spheroid invasion with controls and Gemcitabine.
A) Merged images of PaTu8902-GFP and PS-1 mrfpruby co-culture spheroid invasion in the presence of negative control; DMSO, positive control; 10µM Dasatinib and standard of care; Gemcitabine at the start and the end of invasion (96hrs). Scale bar= 100µm. B) Relative invasion quantified for spheroids treated with DMSO, 10µM Gemcitabine or Dasatinib. ±SEM, n=3. One-way ANOVA with Tukey's multiple comparisons test. ****, P<0.001.

4.3. Discussion

Current available 3D pancreatic cancer drug testing models are based on spheroids generated from pancreatic cancer cell lines (213, 226). However, these models do not utilise stromal cells or extra cellular matrix. Only one study has demonstrated the use of fibroblasts with pancreatic cancer cells to form co-culture spheroids, but these fibroblasts (MRC5) were not pancreas specific (215). Moreover, these pancreatic cancer spheroid screens have cell proliferation or cytotoxicity as read out and does not investigate the invasive behaviours of pancreatic cancer cells. The co-culture spheroid invasion assay developed in this chapter is the first spheroid invasion assay optimised for pancreatic cancer modelling by introducing the PS-1 stellate cells into the culture. Here the aim was to further develop and optimise the platform to enable drug screening in a robust and simple manner for novel therapeutics against invasive pancreatic cancer cells.

Several methods have been reported to generate spheroids from cancer cells. Hanging drop, ultra-low attachment coated u-bottom wells or the use of crowding agents such as methylcellulose were popular approaches for spheroid formation (212, 213, 224). Hanging drop method would not be suitable for invasion screening due to the extra handling step of transferring spheroids. Methylcellulose was previously used to facilitate spheroid formation in pancreatic cancer (213). However, the authors have also reported that in certain cell lines such as MiaPaCa2 and ASPC1, methylcellulose addition did not facilitate compact spheroid formation. This finding is similar to the results in PaTu8988T, where the crowding agent did not improve the spheroid formation, suggesting that cell intrinsic factors such as contractility and cellular adhesion in PaTu8988T does not support the formation tight spheres. Generating spheroids in the ultra-low attachment coated u-bottom wells allows for single spheroid formation without the addition of any reagents. Furthermore, there is no need for spheroid handling when initiating the invasion assay compared to the other methods, making this method the most suitable for drug screening in invading spheroids.

Strikingly, the localisation of PS-1 stellate cells in the co-culture spheroids is in the centre of the spheroid, despite the efforts of adding the stellate cells after a day of

spheroid formation to enhance homogeneous peripheral localisation. This is similar to what has been reported when cancer cells are co-cultured with stromal cells to form spheroids (215, 227, 228). Although, not every co-culture spheroid reported had fibroblasts in the centre. A study demonstrated a knock-out of *Ext1* enzyme, which impaired invasion in fibroblasts and resulted in fibroblasts sitting on the outside of the spheroids (228). Whether the orientation of the co-culture spheroids is dependent on the invasiveness of the stromal cells remain unclear. Nevertheless, the orientation did not affect the invasion of cells in this study, but could potentially contribute to increased survival through reciprocal signalling (94).

It has been shown that organoids, which are normally grown in Matrigel, did not demonstrate invasion in Matrigel (229, 230). Only if they were transferred into collagen I matrix, invasion was observed. Interestingly, when PaTu8902 + PS-1 co-culture spheroids were embedded in Matrigel, the spheroid structure started to change. Difference in stiffness, density and matrix signalling could cause the change in shape, which could be a result of increased spreading, invasion or proliferation (231). Pure matrigel stock (8mg/ml) has a higher density and smaller pores compared to collagen I, which is usually used at concentrations around 1-2mg/ml (232). Nevertheless, invasion of PaTu8902 and PaTu8988T into the matrix containing collagen I has been published previously (193, 233).

The *in vitro* spheroid formation and invasion resembled the findings *in vivo*, where cells invaded as single cells from tumour clusters towards the dense and rich collagen fibered area. It has been demonstrated that pancreatic cancer cells and cancer associated fibroblasts are able to remodel the surrounding extra cellular matrix and increase invasion through ROCK activity (234, 235). Furthermore, it has also been reported that patients with an increase in thick collagen I fibers in their tumours had a lower overall survival (184). Moreover, collagen I has been shown to increase motility and invasion of pancreatic cancer cells by inducing EMT through upregulation of Snail (236). It will be of future interest to include pancreatic stellate cells in the *in vivo* studies to identify their contribution and effect on the invasion of PaTu8902 cells. In addition, confirming findings of the role of actomyosin contractility

and ROCK activity in the invasion and remodelling of the extra cellular matrix in PaTu8902 would further validate our system and increase its clinical relevance.

Recent findings of pancreatic stellate cells contributing to the invasion of pancreatic cancer cells reveal an important role for these stromal cells in the progression of the disease. In this study, only the cancer cells have been investigated and quantified with the developed analysis method. Due to the randomly nested PS-1 cells in the spheroid at the starting point of each invasion assay, it is difficult to have a robust and stable performing assay to investigate the PS-1 cells in this manner. It has been reported that stellate cells are able to contribute to the invasion of pancreatic cancer cells through FGFR signalling for example, and can be inhibited by the use of PD173074 (141). Future studies with FGFR inhibitor PD173074 in the co-culture spheroids would be of interest to investigate and validate contributions of PS-1 cells towards PaTu8902 cancer cell invasion.

Another challenge remains regarding viability and cytotoxicity end point measurements in the invasion assay. While cell viability was being tested in various methods, I was not able to obtain a robust method for a stable and accurate read out of the in matrix embedded spheroid's viability through reagents such as MTT, Alamar blue, cell titer glo and cell titer glo 3D. Due to the presence of the extra cellular matrix, reagents do not easily penetrate the matrix and the 3D spheroid architecture homogeneously. Degrading the collagen with collagenase combined with cell titer glo 3D or flow cytometry analysis of disseminated cells could provide a solution to the penetration issue of the currently available reagents. Future efforts in realizing this could increase the attractiveness of this 3D drug screening platform for high through put high content drug discovery. Overall, the 3D co-culture spheroid is a one plate assay for invasion and growth analysis, without needing to transfer spheroids over (Figure 4-12). Furthermore, the assay is designed to be adopted for automated high throughput drug screening.

Gemcitabine and Dasatinib have demonstrated to penetrate the 3D matrix and the spheroid, resulting in partial or full inhibition of invasion respectively at the dose of 10µM. However, the reported IC50 value for Gemcitabine in PaTu8902 cells on 2D plastic by the sanger institute is several times lower than the concentration we have

used here in the 3D spheroid invasion assay (0.29µM vs 10µM) (www.cancerrxgene.org). Conversely, Collisson et al have reported a much higher IC50 value for Gemcitabine for PaTu8902 (~100 µM) cultured in 2D with similar viability reagent (cell titer glo) and treatment duration (53). Nevertheless, the concentration used in the 3D spheroid invasion assays falls into this range and has demonstrated to inhibit invasion partially, with viable cells that have invaded. Future dose calculations should be made to compare the clinical dose with the used dose in this setting. Also, dose response curves could be generated against viability of the cells in 3D.

Dasatinib has been demonstrated to inhibit invasion in vitro through src-inhibition and inhibited the development of metastasis in a genetic mouse model with KRAS and P53 mutations targeted in the pancreas (122). Similar findings were demonstrated with close to 100% invasion inhibition at 10µM in the 3D spheroid invasion model, whereas the authors have demonstrated an average of 60% inhibition of invasion in a transwell invasion model at a concentration of 100nM (122). However, Dasatinib seemed to have modest effect on cell viability in the 3D spheroid invasion assay as the spheroid still expanded despite inhibited invasion. Other studies demonstrated nanomolar to micromolar range IC50 values of Dasatinib on pancreatic cancer viability in 2D (122, 165). Nevertheless, the modest effect on proliferation by Dasatinib did not increase overall survival in pancreatic cancer or metastatic disease when used in combination with gemcitabine or alone respectively, probably due to primary tumour development and burden (237, 238). Further investigation is needed to confirm the lack of viability inhibition by Dasatinib in 3D spheroid invasion assay. Other combination therapy of Gemcitabine with Dasatinib or other compounds can be tested with the 3D spheroid model in the future.

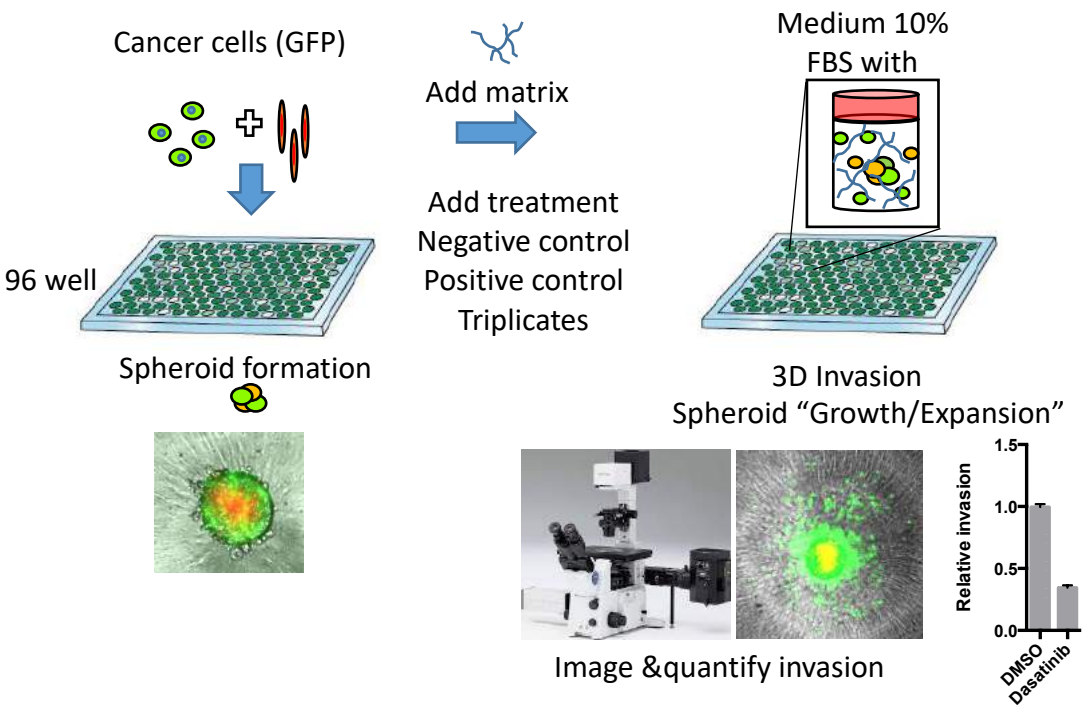

Figure 4-12. Schematic overview of the 3D co-culture spheroid invasion platform. Cancer cells PaTu8902-GFP and stromal cells PS-1-mrfpruby are seeded into a 96 wells U-bottom plate treated with ultra-low attachment coating. Spheroid formation occurs over 3 days and growth medium is exchanged for collagen I matrix. After polymerisation, growth medium containing 10% FBS is added on top of the matrix and treatments can be added into the medium. Fluorescence microscopy is used to acquire the images of spheroid invasion and semi-automated invasion quantification in ImageJ is applied to measure the invasion inhibition.

4.4. Future work

This chapter was dedicated to developing a 3D assay platform for drug screening against invasion and cytotoxicity. While the assay has been optimised for drug discovery against invasion, the growth, cytotoxicity and the contribution of PS-1 stellate cells read outs need more optimisation. Invasion conditions could be improved to increase the invasion of PS-1 cells to allow for screening stellate cell invasion inhibiting drugs. Furthermore, the analysis has to be tested with the ImageJ quantification method and might need modification to increase its sensitivity. Several live tracker dyes for cell death and hypoxia are available with a far-red fluorescent dye, which could be used to measure the changes in total cells per well. Moreover, collagenase could provide a good alternative to isolate the cells and prepare the samples for FACS/flow cytometry analysis. This allows the quantification of cell death and proliferation of the pancreatic cancer cells and the stellate cells. However, this method might reduce the high throughput capacity. Optimising the platform for high throughput or automated imaging and analysis machines would significantly increase the speed and the screening capacity. Validation with mono-culture spheroids or 2.5D collagen assays could provide valuable information in the meantime.

Alternatively, incorporation of other extra cellular matrix proteins could improve the validity and clinical relevance further. For example, Collagen IV and Hyaluronic acid have been shown to increase proliferation and invasion of pancreatic cancer (239, 240). Future works with added stromal compartments such as endothelial cells or immune cells could mimic the *in vivo* behaviour and characteristics of pancreatic cancer even more closely, which could potentially increase its clinical relevance even further.

Also, further validation of the *in vivo* model could provide us more insight into the contributions of PS-1 stellate cells by introducing them into the PaTu8902 and potentially also the PaTu8988T xenografts. Also, quantification of cell shape and collagen fibre thickness would provide valuable information regarding the invasion characteristics of the PaTu8902 and PaTu8988T cells. Moreover, future drug dose

response studies and clinical dose conversion could provide more insight into concentration translation from 2D to 3D in vitro, *in vivo* models and clinic.

5. Results III: Drug repositioning screening in pancreatic cancer

5.1 Introduction

Until now, rarely any drug screens have been performed on pancreatic cancer, mainly due to the lack of a good understanding of the disease and a model, which translates into *in vivo* and the clinic. Recent efforts have led to the development of several *in vitro* models mimicking the disease more accurately (206, 226). In order to bridge the gap between a single compartment model and complex *in vivo* models, I have developed a multi-compartmental model consisting of cancer cells, stromal cells and 3D matrix as described in the previous chapter.

High throughput drug screening of novel compounds is costly and time consuming to follow up and still might not yield clinical efficacy. Drug repurposing or drug repositioning is an alternative on-target or off-target approach to drug discovery by identifying different drugs acting on a known target or by investigating the novel mechanism of a known drug through (241, 242). The major advantage of drug repurposing is that the pharmacokinetic, pharmacodynamics and toxicity profiles or most of the drugs are already known due to previously conducted preclinical and phase I studies (241). Therefore, these drugs can be launched into phase II and III more readily and thus save time and costs. The application of non-cancer drugs for cancer therapy has been based on the exploitation of the off-target effects in addition to their principal activity. If sufficient potency is observed with the off-target effect, the drug could be tested in patients faster (243). Furthermore, as common molecular pathways or targets can give rise to different diseases, drugs targeting these common mechanisms or targets could be applied for different diseases. This approach has led to the repurposing of drugs for cancer treatment such as thalidomide (244), celecoxib (245), methotrexate (246).

Nevertheless, one of the criteria of drug repurposing is that the drug needs to have a valid mechanism of action applicable for the type of cancer to access their efficacy in the human body. Furthermore, cancer treatments with unknown side effects of repurposed drugs will need validation with new clinical studies (247). Moreover, several drugs such as digitoxin and doxycycline, demonstrated significant toxicity and

unwanted drug-drug interactions (248, 249). Also, different route of administration, dosing or drug formulation pose different toxicity profiles and efficacy that need further investigation (241). Therefore, it is important to assess the biological activity, the selectivity of the drug and pharmacological parameters of a potential repurposed drug prior to selection for further clinical investigation, to avoid failure in later stages.

In order to accelerate the development of therapeutics against pancreatic cancer and the translation from bench to bedside, I have utilised an FDA approved library for drug repurposing screening in my 3D spheroid invasion assay. The aim of this chapter is to define the drug library, to perform the screen in the 3D spheroid invasion assay and to validate the screen results acquired by semi-automated analysis with manual scoring. Furthermore, top 5 hits will be taken forward for validation on the 2.5D Collagen I assay. The validated hits could then be taken forward for further validation *in vivo*.

5.2 Results

5.2.1 Drug library assembly for drug repurposing screen

Prior to performing the drug screen, I had to assemble a drug screen library containing FDA approved drugs for drug repurposing. Enzo Life science had the smallest FDA approved drug library available consisting of 800 drugs compared to libraries with 1000+ compounds provided by other companies. The lack of having an automated workflow in line restricted the number of compounds that I would be able to screen through the 3D spheroid invasion assay. Performing a high throughput drug screen was in this stage physically not possible given the time frame. Therefore, the drug library had to be narrowed down to a feasible size.

Starting with 800 FDA approved drug compounds, I have first filtered out the duplicate compounds which where categorised in the same indication (e.g. Anti-Inflammatory, anti-viral), as these usually have similar targets or mechanism of action (Figure 5-1). These duplicates were filtered by age as older compounds are usually less specific compared to newer compounds, which would make it harder to determine or validate the mechanism of action if the compound was found promising. This also accounts for drugs that have multiple targets, to be excluded in this filtering stage. However, some of the anti-neoplastics were kept in the library as potential controls, while duplicate kinase inhibitors were excluded from the library to allow space for unknown anti-neoplastic compounds. These filtering steps narrowed down the drug library to 99 compounds, making it feasible for the semi high throughput screening. Subsequently, 10 in-house compounds, either of specific interest (e.g. Rock inhibitors) or compounds obtained from pharma through an MTA were included in the final drug library, yielding 109 drug compounds to be tested.

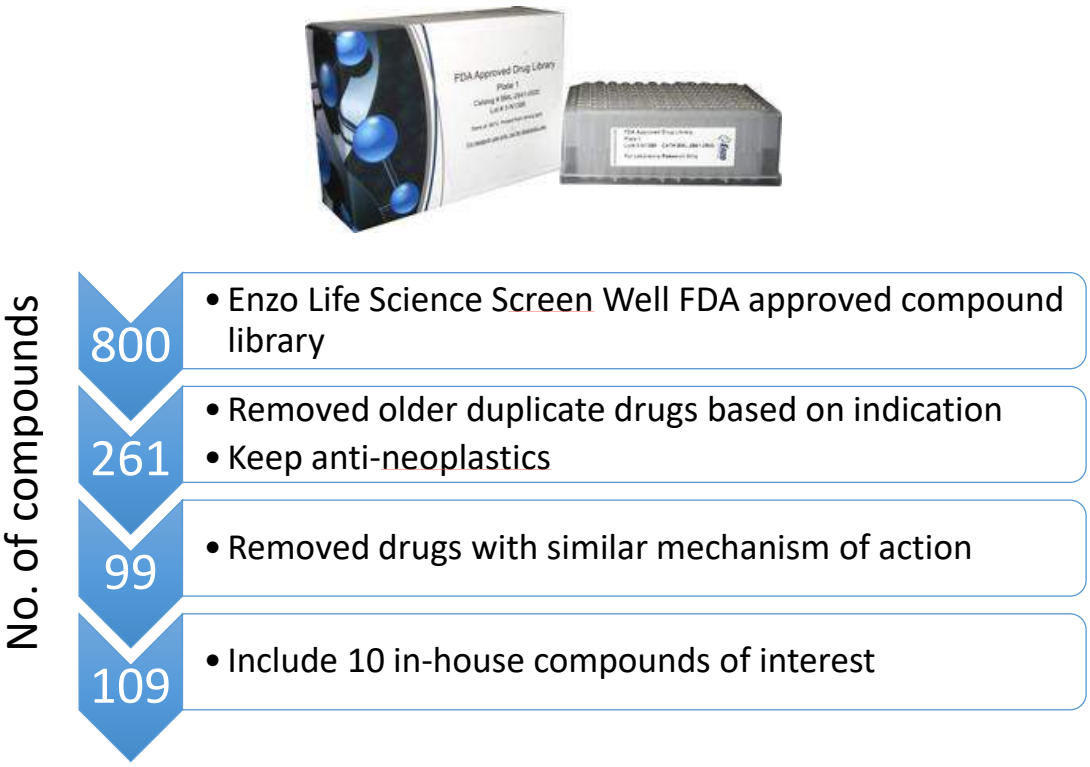

Figure 5-1. Drug compound library selection process
Schematic representation of drug screen library compound selection. 800 compounds from Enzo Life Science Screen Well FDA Approved compound library were first filtered down by excluding older compounds with the same drug indication and keeping the anti-neoplastic compounds yielding 261 compounds. Drugs with similar mechanism of action were then excluded and 10 in-house compounds of interest were added contributing to a final drug library of 109 compounds.

5.2.2 3D spheroid invasion assay drug screen

As defined in chapter 4.2.6, 10µM was used as screening concentration throughout the screen in order to overcome the difficulties of matrix and 3D structure penetration, to generate compounds with medium to strong invasion inhibition effects for follow up studies. In order to save time and cost, drug screens are often conducted in triplicates to screen out promising compounds for further validation. The same approach was adopted for this screening experiment due to time and cost restrictions. Each 96 wells screening plate contained triplicates of either DMSO and Dasatinib as negative and positive controls for invasion inhibition respectively. Gemcitabine was also included into every plate as an extra internal control and a less strong positive control. This provides space for 27 compounds to be screened per plate. In order to carry out the screen for all the drugs, 5 plates were used in total to complete the screen. To determine the effectiveness of the newly developed assay for drug screening and to confirm the quality of the results obtained from each screening plate, a Z'-factor was calculated (250). The Z'-factor was calculated for all plates based on Dasatinib as positive control and DSMO as negative control, resulting in an average Z'-factor of 0.55 across all the screening plates; proving to be an excellent assay when the Z'-factor lies between 1 and 0.5 (250). Only one plate did not demonstrate an acceptable Z'-factor and was therefore discarded and repeated.

Screen results were normalised to DMSO to obtain the relative invasion value to allow for cross plate comparison (Appendix 1: List of drugs). The semi-automated quantification method will, in most cases, not reach a value of 0 due to the presence of a GFP signal from the spheroid even in the presence of invasion inhibition. The exception would be where the drug has eradicated all the cells, which would be unlikely. Indeed, the screen results demonstrated a range of responses and values above 0, ranging from total inhibition of invasion similar as Dasatinib (e.g. Tranexamic acid, Nebivolol) to increased invasion (e.g. valsartan, caffeine) (Figure 5-2, 5-3, 5-6 & Appendix: List of drugs). Furthermore, several compounds have shown to yield a lower relative inhibition value than the positive control Dasatinib (e.g. GSK2126458, Doxorubicin, Digoxin), suggesting that these compounds are inhibiting the growth of the spheroid or affect the viability of the spheroid (Figure 5-3 and 5-5).

As there is not direct growth and viability read out from the 3D spheroid invasion screen, further investigation is needed to determine the effects of these compounds on cell growth and viability. Overall, the screen has identified several compounds with a stronger inhibition of invasion effect compared to gemcitabine and compounds which may affect viability of these invasive cells in 3D.

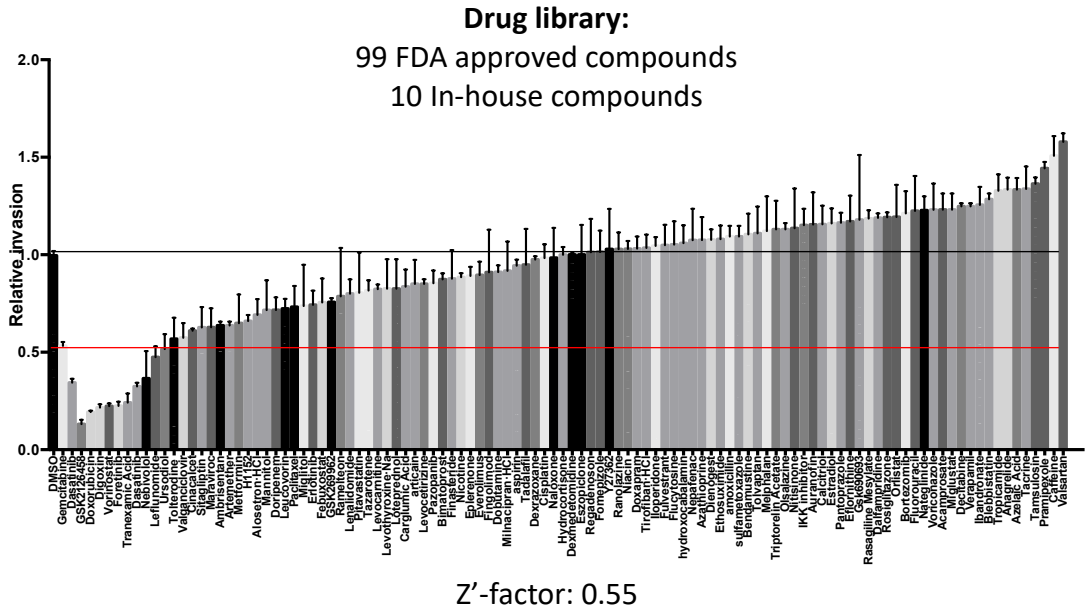

Figure 5-2. Drug repositioning screening including in-house compounds
Drug screen results ranked hits from invasion inhibition to increased invasion. DMSO used as negative control, Dasatinib used as positive control and Gemcitabine as standard of care comparison. Data shown of average relative invasion triplicates ± S.E.M. Black line indicates relative invasion of 1 and red line indicates relative invasion of Gemcitabine.

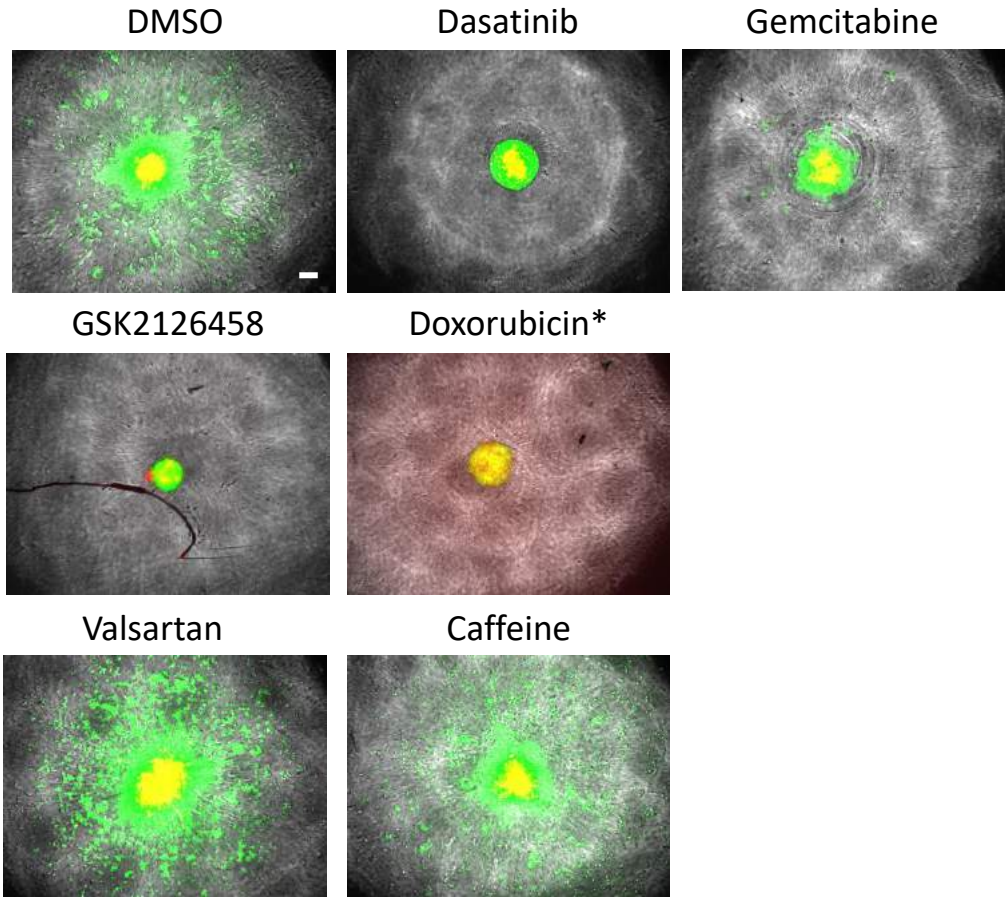

Figure 5-3: 3D spheroid invasion drug screen results.
Representative merged images of PaTu8902-GFP and PS-1-mrfpruby co-culture spheroid invasion in the presence of DMSO or 10µM drug compound treated for 96hrs. Scale bar= 100µm. *Note that Doxorubicin can be visualised in the RFP channel.

5.2.3 Drug screen results through manual scoring analysis

As the results of the drug screen were defined by the GFP signal obtained from the fluorescent images of each well, the inhibition of invasion measurement was quantified through a surrogate parameter. The area of the GFP signal determines the area of invasion indirectly, which was described in chapter 4. In order to scrutinise the use of this surrogate parameter, I have manually scored each acquired image for invasion based on a scoring system (Table 5-1). Single cell dissemination and collective cell dissemination from the spheroid would be seen as events which are highly invasive *in vitro* and *in vivo*. Both parameters are therefore multiplied by a factor of 2 to emphasise this effect over the other two parameters. Collective cell invasion describes the break-away streams or sheet like migration of collective cells from the spheroid whereas the intactness of the spheroid body describes the observation of a well-defined spheroid body border or the loss of it. Both of the latter parameters describe early stages of invasion and are therefore not multiplied. The total score is then calculated by adding up the scores of each parameter and divided by the total score of the negative control, which yields a relative invasion score. The lower the score the higher the inhibition of invasion observed and the higher the score the lower the inhibition of invasion.

The results of the manual invasion scoring demonstrated similar results as the relative invasion analysis by semi-automated quantification (Figure 5-4A). However, unlike the semi-automated analysis, the manual invasion scoring has the possibility to reach a relative invasion score of 0 when a drug demonstrates full inhibition of invasion (e.g. Dasatinib). Therefore, when a linear correlation comparison was performed, the line did not cross 0,0 (Figure 5-4B). Nevertheless, majority of the compounds which were identified as strong inhibitors of invasion by relative invasion were correlated with a relative invasive score of 0. As this was a comparison between two continuous variables, a Pearson correlation coefficient test (parametric) was performed. The Pearson coefficient demonstrated the presence of a strong correlation (between 0.5 and 1.0; Pearson r:0.72) between the scoring of both methods. Interestingly, several drug compounds demonstrated a better effect of

invasion inhibition compared to Gemcitabine on the relative invasion scale compared to the relative invasive score scale.

Table 5-1: Scoring parameters used for manual scoring of invasion

Single cell dissemination *(Score multiplicity of 2)*

Score	***Description***
0	*no dissemination*
1	*very little dissemination <15 cells*
2	*little dissemination (within 2x spheroid diameter)*
3	*moderate dissemination (within 2.5x spheroid diameter)*
4	*high dissemination (>2.50x spheroid diameter)*

Spheroid body intact *(Score multiplicity of 1)*

Score	**Description**
0	no spheroid border visible
1	partially border visible
2	intact (visible border and centre0

Collective cell dissemination from spheroid *(Score multiplicity of 2)*

Score	**Description**
0	no collective dissemination
1	little dissemination
2	moderate dissemination (invasion into more than 1 direction)
3	majority collective invasion

Collective cell invasion *(Score multiplicity of 1)*

Score	**Description**
0	no collective invasion
1	presence of collective group invasion (attached to the spheroid)
2	half of population is collective group invasion
3	majority collective group invasion

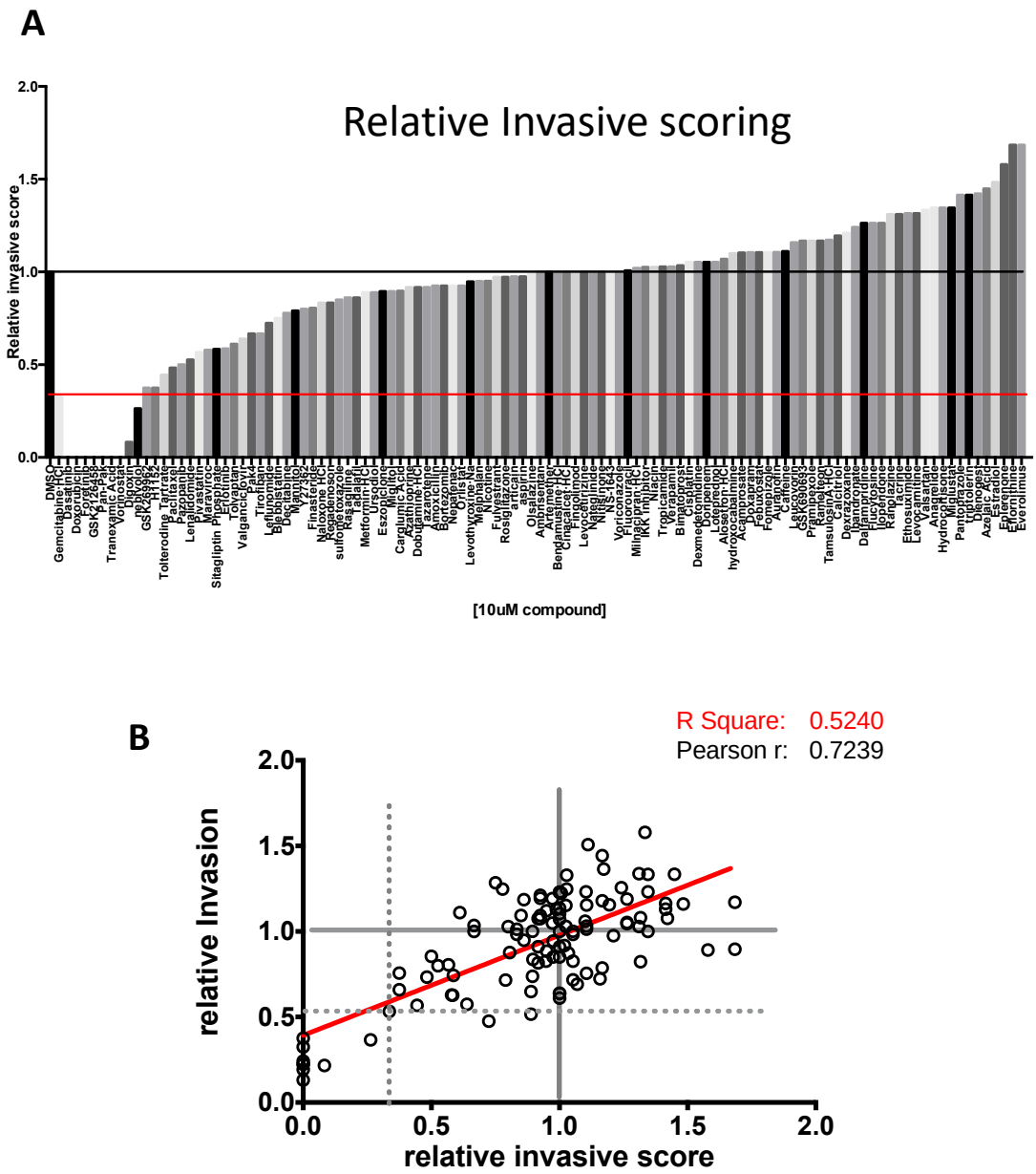

Figure 5-4. Drug screen results of invasion inhibition by manual scoring.
A) Graph of ranked results of drug screen compounds based on relative invasive scoring. Black line indicates relative invasion of 1 and red line indicates relative invasion of Gemcitabine. Data shown of average relative invasive scoring triplicates. B) Correlation graph between relative invasion and relative invasive score. Each dot represents a compound. Red line indicates the linear relationship expressed through R squared. Grey solid lines indicate the DMSO values on both axis, whereas the grey dotted line indicate the Gemcitabine values on both axis. Pearson correlation coefficient statistical analysis was performed.

5.2.4 Top hits identification and comparison

The drug screen and the follow up scoring has indicated several promising inhibitors of invasion (Figure 5-2 and 5-4). The top 12 compounds which demonstrated stronger inhibition of invasion than Gemcitabine were compared, as Gemcitabine was ranked #12 in the semi-automated analysis method. Similar drug compounds are found within the top 11 hits identified from both analysis methods (Figure 5-5 and Table 5-2). 10 identical compounds were identified as top hits from both methods, including controls Dasatinib and Gemcitabine. Only Ursodiol and Leflunomide were identified through the semi-automated analysis, whereas ROCK inhibitors GSK269962a and H1152 were picked up from the manual invasive scoring method. Only two of the common hits identified by both methods, GSK2126458 and Foretinib, are kinase inhibitors. This result demonstrates that there are several compounds which are non-kinase inhibitors that elicit strong inhibition of invasion in the drug screen.

In order to select drug compounds for follow up validation, the non FDA approved in-house drug compounds were excluded as they would potentially take longer to reach clinic and patients. These include in-house drug compounds GSK2126458, Doxorubicin and Foretinib, and will be investigated in future experiments separately. The remaining FDA approved drug compounds were filtered based on whether they are or have been tested before in clinical trials against pancreatic cancer. Vorinostat, a histone deacetylase (HDAC) inhibitor, has been found in clinical trials against pancreatic cancer. A couple of clinical trials for Vorinostat have been terminated due to lack of patient sample size, while several other phase I studies have been actively recruiting, or have been completed, but without results yet (https://clinicaltrials.gov/; NCT00831493, NCT00983268, NCT02349867, NCT00948688). Vorinostat is therefore excluded. The remaining compounds; Digoxin, Tranexamic acid, Nebivolol, Leflunomide and Ursodiol have not been taken to clinical trials yet for pancreatic cancer.

Nebivolol, Tranexamic acid and Digoxin treated spheroids demonstrated comparable inhibition of dissemination of cells and maintained a similar size of spheroid compared to Dasatinib (Figure 5-6). However, spheroids treated with Nebivolol and Tranexamic acid demonstrated a more irregular border shape, with cells trying to

invade and disseminate, whereas Digoxin treated spheroid had a well-defined border and did not show any sign of invasion. Leflunomide and Ursodiol were not able to block invasion to the extent of Nebivolol, Tranexamic acid and Digoxin (Figure 5-6). Nevertheless, both compounds demonstrated similar inhibition of invasion as Gemcitabine, reducing the amount of disseminated cells, but had minimal effects on spheroid body expansion or collective invasion. Further investigation is needed to validate these observations and define the mechanism of the drugs in the inhibition of cellular dissemination or viability. These compounds were therefore taken forward as the top 5 compounds for further validation, as all the compounds demonstrated stronger inhibition of invasion compared to Gemcitabine. The in-house drug compounds GSK269962a and H1152 are ROCK inhibitors and will be discussed later in Chapter 5.2.6.

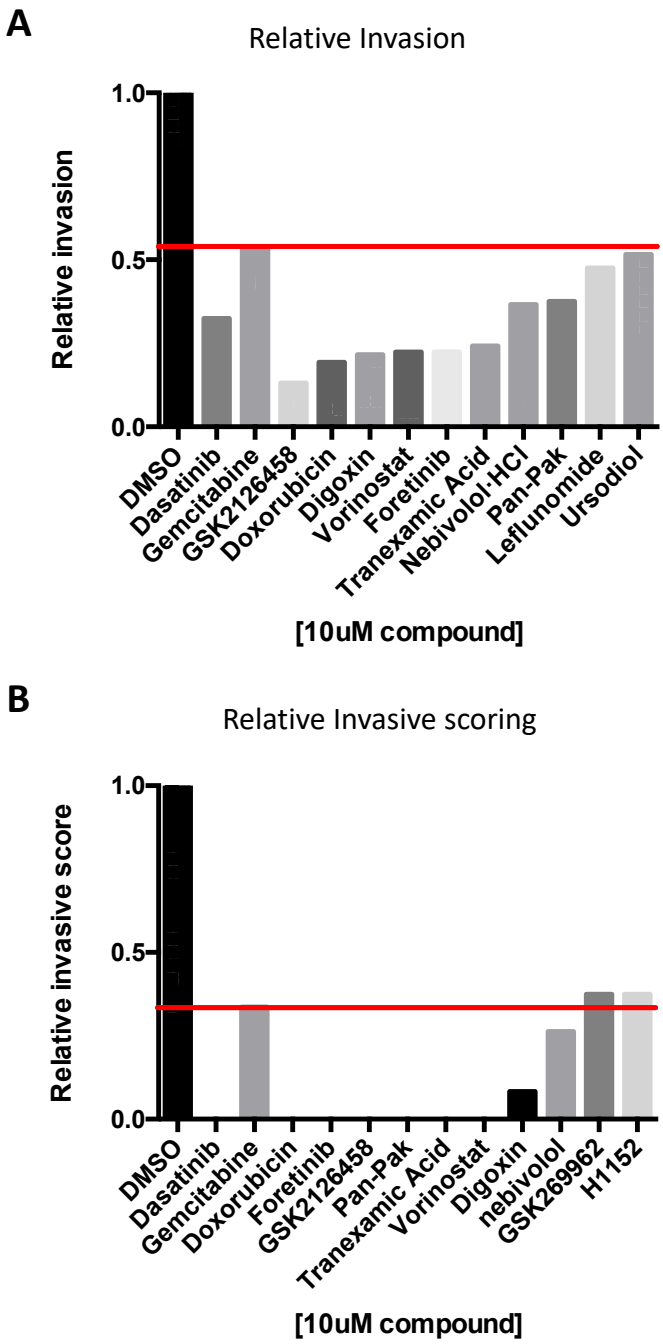

Figure 5-5. Top hits of drug screen by semi-automated analysis and manual invasive scoring.

A) Top 13 hits from drug screen based on relative invasion and B) relative invasive scoring. Red line indicates relative levels of Gemcitabine.

Table 5-2: Ranking of top 13 drugs by either relative invasive or relative invasive score.

Rank by: #	Invasion	Invasive Scoring
1	*GSK2126458*	**Dasatinib**
2	*Doxorubicin*	*Doxorubicin*
3	Digoxin	*Foretinib*
4	Vorinostat	*GSK2126458*
5	*Foretinib*	Tranexamic Acid
6	Tranexamic Acid	Vorinostat
7	**Dasatinib**	Digoxin
8	Nebivolol	Nebivolol
9	Leflunomide	**Gemcitabine**
10	Ursodiol	*GSK269962*
11	**Gemcitabine**	*H1152*

Positive control Dasatinib and Gemcitabine are highlighted in **bold**. In-house drug compounds are highlighted in *cursive*. FDA-approved compounds found in clinical trials against pancreatic cancer are underlined.

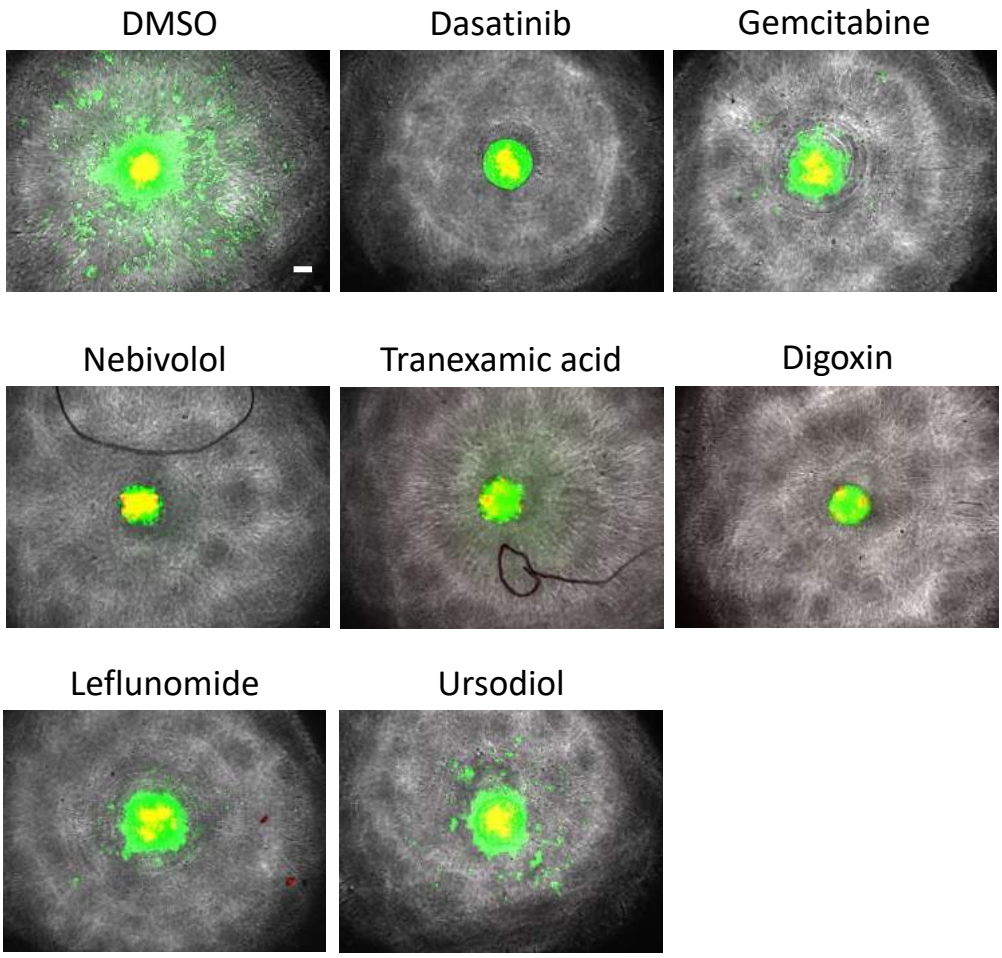

Figure 5-6: 3D Spheroid invasion drug screen top 5 results.
Representative merged images of PaTu8902-GFP and PS-1-mrfpruby co-culture spheroid invasion in the presence of DMSO or 10µM drug compound treated for 96hrs. Scale bar= 100µm.

5.2.5 Viability effect of top 5 promising hits

In order to investigate whether the top 5 drug compounds selected from the drug screen would have an effect on cell viability in addition to or instead of invasion, the compounds were tested in a viability assay. While performing the viability assay in the 3D spheroid invasion assay would be ideal, more experiments and optimisation is needed to obtain robust and accurate results from this set-up due to the challenges of homogenous penetration of the reagents all the way deep into the spheroid core. By taking a step backwards and performing the viability assay on cells grown in the 2.5D collagen I assay rather than 2D plastic, I hope to gain a better insight into the viability effects of these compounds in 3D.

PaTu8902 cells were grown on the 2.5D collagen I matrix and drugs were administered at different concentrations (Figure 5-7). Viability was measured 72 hrs post-treatment as viability effects were observed in cells treated with Gemcitabine (Figure 5-5 A&B). 72hrs treatment with 20 µM Gemcitabine demonstrated round up and detached cells from the collagen (Figure 5-7 A). Similar observations were made with Nebivolol. Majority of the cells treated with 20 µM Digoxin or Leflunomide detached from the collagen matrix and remained floating in the medium. Cells treated with 20 µM Tranexamic acid or Ursodiol did not demonstrate differences in morphology and confluency compared to DMSO. Indeed, both Tranexamic acid and Ursodiol did not affect viability even at 20 µM (Figure 5-7 B). While Nebivolol and Digoxin demonstrated strong impairment of viability, Leflunomide demonstrated partial viability inhibition at 20 µM. At the screening concentration of 10 µM in 3D, drug compounds Nebivolol, Tranexamic acid, Ursodiol and Leflunomide did not demonstrate effects on cell viability. Only Digoxin demonstrated strong effects on cellular viability even at lower concentrations up to 500nM. These results suggest that several drug compounds inhibited invasion without affecting viability and drug compounds like Digoxin which inhibited invasion and affected viability. Whether the viability reduction partially or fully contributed to the invasion inhibition is unclear. Future experiments are needed to further validate these compounds abilities to inhibit invasion in 3D and *in vivo*.

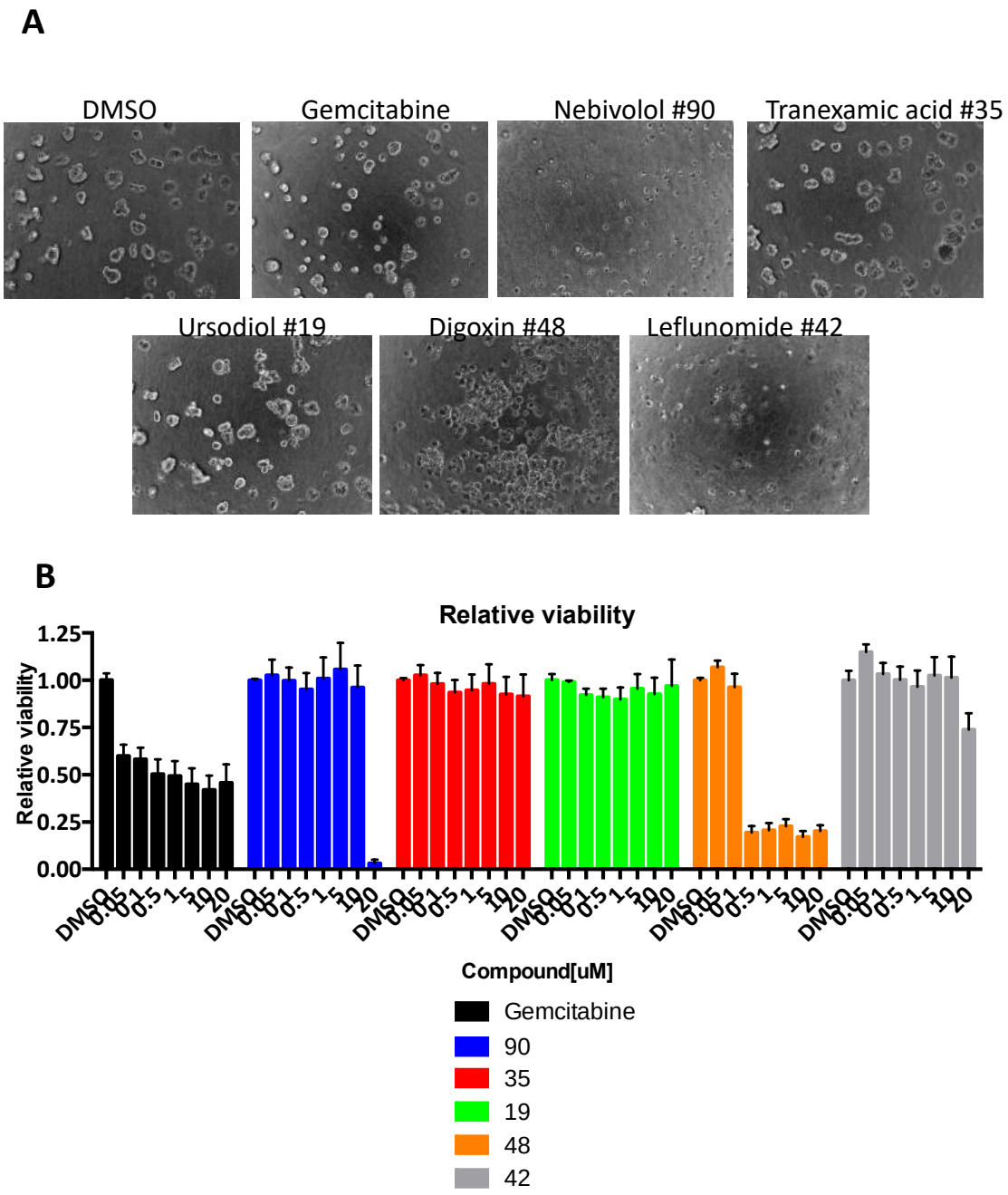

Figure 5-7. Viability validation of top hits from drug screen.
A) Representative phase contrast images of PaTu8902 cells on 2.5D collagen I matrix treated with DMSO or 20µM drug compound at 72hrs. B) Graph of relative viability of PaTu8902 cells on 2.5D collagen I matrix treated with drug compounds at different concentrations for 72hrs compared to DMSO. A final concentration of 44 uM Alamar Blue was added to the cells at the end of 72hrs to measure viability.

5.2.6 ROCK inhibitors partially inhibit invasion in 3D spheroid invasion assay

In the third chapter, it was discussed that contractility played an important role in the formation and behaviour of these pancreatic cancer cells. PaTu8902 and PaTu8988T both demonstrated presence of contractility. It was therefore of interest to observe whether ROCK inhibitors would perform well in the drug screen by reducing the contractility in the cells thus reducing their invasiveness. Indeed, drug screen results and follow up results demonstrated that PaTu8902 spheroids treated with 10µM GSK269962a or H1152 demonstrated reduced invasion and were placed in the top 12 drug compounds hits by manual scoring (Figure 5-8 & Table 5-2). A strong reduction was found in the cell dissemination events, yet the spheroid demonstrated expansion, indicating a lack of inhibition of proliferation, collective invasion or expansion of cell area/size due to loss of contractility. This therefore explains the lower ranks for both compounds analysed through the semi-automated method, which quantifies the GFP area. Further validation is prompted in different cell lines such as the PaTu8988T and to investigate the effects of these ROCK inhibitors on cell viability.

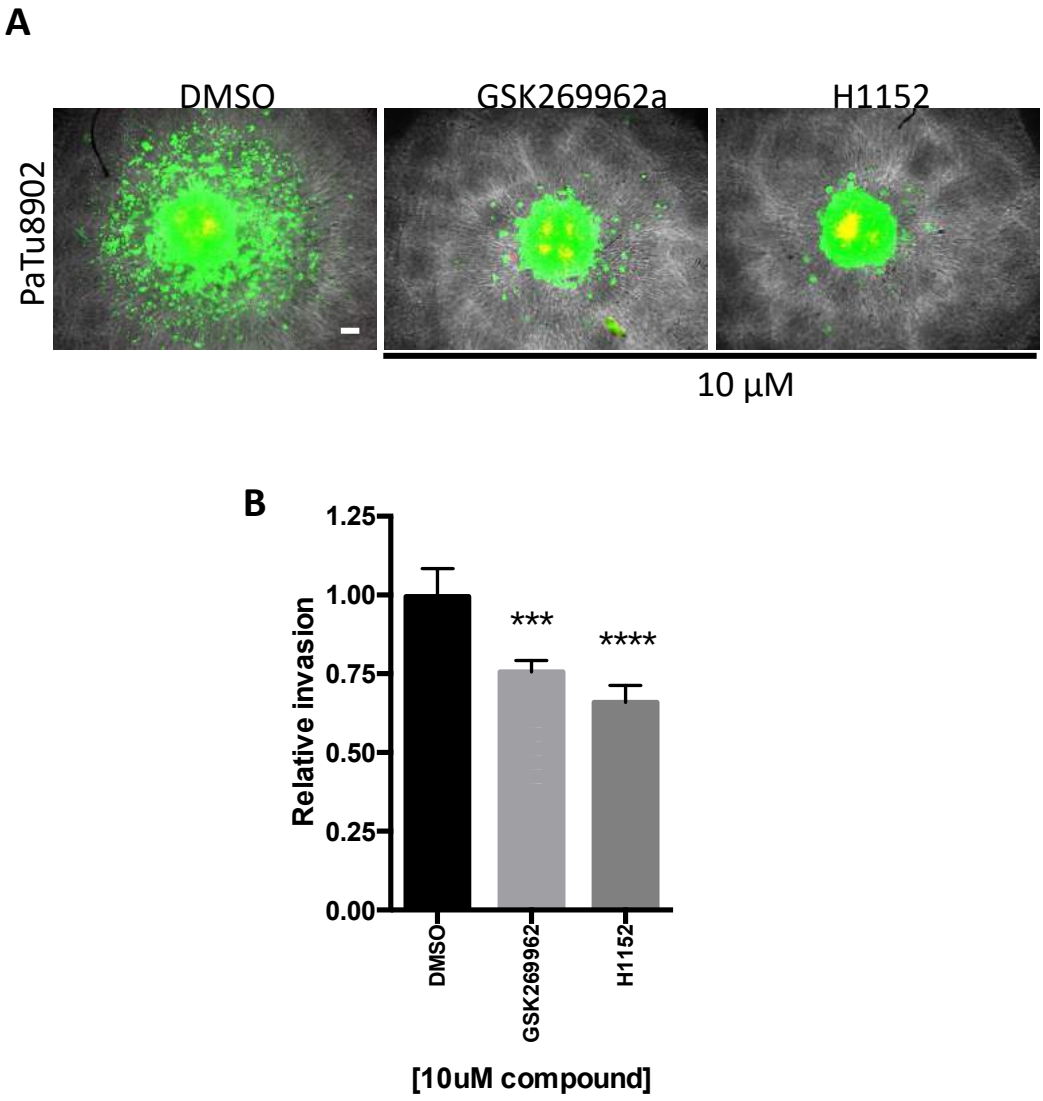

Figure 5-8. Rock inhibitors inhibiting invasion in PaTu8902 + PS-1 co-culture spheroids.
A) Representative merged images of PaTu8902-GFP and PS-1 mrfpruby co-culture spheroid invasion in the presence of 10µM GSK269962a or H1152 treated for 96hrs. Scale bar= 100µm. B) Relative invasion quantified for spheroids treated with DMSO, 10µM GSK269962a or H1152. ±SEM, n=3. One-way ANOVA with Tukey's multiple comparisons test. ****, P<0.001.

5.3 Discussion

The aim of this chapter was to perform a semi-high throughput drug screen with the assembled FDA approved drug library in the previously developed 3D spheroid invasion assay. As mentioned previously, very little work has been invested in the search for compounds blocking invasion in pancreatic cancer. Here, I have identified top 5 drug candidates which elicited stronger inhibition of invasion compared to Gemcitabine through the semi-automated analysis method.

In chapter 4 I discussed how this method would be able to pick up strong inhibition of invasion, but would not be sensitive enough to distinguish invasion inducing drug compounds with confidence. Nevertheless, Caffeine and Valsartan were initially identified as invasion inducers in this screening setting. Conversely, Caffeine has been reported to reduce migration and invasion in glioblastoma (251, 252). Interestingly, Caffeine has also been reported to upregulate pMLC through ROCK activity (251). Furthermore, Valsartan has also been shown to inhibit proliferation and invasion in nasopharyngeal carcinoma (253). Yet, these studies pre-treated their cells before assessing their invasive abilities. More work is needed to determine the effects of Caffeine and Valsartan on PaTu8902 3D spheroid invasion and validate whether this effect is cell or cancer type specific. Moreover, investigating the increase of invasion by drug treatment can be done by pre-treatment and looking at earlier time points. Drugs that increase invasion could uncover new insights into how cancer cells become invasive or become more invasive, so that therapies can be developed to target these mechanisms.

The top 5 identified drug candidates demonstrated promising results. Digoxin, a natural cardiac glycoside extracted from foxglove, is known to inhibit NA^+/K^+ atpase pumps and is used in the clinic to treat heart failure or atrial arrhythmia. Furthermore, it has been reported to induce caspase-dependent apoptosis in pancreatic cancer cells and inhibit primary tumor growth and metastasis in an orthotopical mouse model for breast cancer (254, 255). However, concentrations used in the drug screen are almost 5 times higher than the reported toxicity concentration of over 2µM (256). Therefore, future experiments are needed to determine the lowest concentration possible with observed inhibition of invasion and without toxicity effects on the heart.

Nebivolol emerged from the drug screen as one of the potent inhibitors of invasion. Nebivolol is a third generation selective β1 adrenoceptor blocker used in the clinic to treat hypertension. Several studies have suggested the implications of β-blockers as cancer therapy (257-259). Nebivolol has been demonstrated to potentiate drugs that block proliferation in neuroblastoma tumours in mice (260, 261). This was irrespective of the selectivity of the β-blockers for adrenergic receptors, suggesting that it may act through another mechanism to elicit these properties. In the viability assay (Figure 5-7), Nebivolol did not demonstrate anti proliferative effects up to 10µM, but has shown strong impact on cell viability at 20µM. Other β-blockers have been shown to potentiate the anti-proliferative effects of gemcitabine in pancreatic cancer (262). Future combination studies could validate the potentiation of anti-proliferative effects of Gemcitabine in pancreatic cancer with lower concentrations of Nebivolol. Another study has shown that Nebivolol was able to suppress NOX activity, which are mediators of ROS, cell signalling and inflammation. NOX activation has been described in various cancer and is related to cancer progression, invasion and invadopodia formation (263-266). Similarly, Nebivolol demonstrated strong inhibition of invasion with almost no dissemination of cells in the drug screen. These findings suggest that Nebivolol could be a potential pancreatic cancer therapy and should be further investigated as a therapy against invadopodia invasion(265).

Another promising drug compound that emerged from the drug screen is Tranexamic acid. Tranexamic acid is an anti-fibrinolytic and has been widely used in the clinic to stop excessive bleeding during surgery by competitively inhibiting the activation of plasminogen to plasmin, which normally prevents clotting by degrading fibrin (267). It is a well-tolerated drug with various administration routs; systemically, intravenously or orally (268). The general used dose is 10mg/kg, yet doses of 10x higher has also been reported for the management of post-surgical bleeding (269). The concentration used in the drug screen for Tranexamic acid falls into the range of the clinical concentrations and could be a potential therapy for blocking pancreatic cancer invasion.

Excitingly, Tranexamic acid has been reported to inhibit invasion but not cell viability in tongue squamous cell carcinoma *in vitro* (270). This result was also observed in the

drug screen (Figure 5-6) and the viability validation (Figure 5-7). Previously, it has been shown that treatment with Tranexamic acid decreased lung carcinoma xenograft metastasis, and administration with urokinase increased metastasis (271). This was thought to be due to the formation of fibrinogen around the tumour cells trapping cancer cells and prevent them from metastasising (272). However, later it has been discovered that Tranexamic acid is able to bind to the 5 lysine binding sites on plasminogen, preventing its activation by urokinase type or (uPA) tissue type plasminogen activator (tPA) enzymes into plasmin (273, 274). Plasmin has been reported to activate pro-matrix metalloproteinases (MMPs), and increased activity in the plasminogen activation cascade has been associated with fibrosis, cancer progression and poorer prognosis (275-278). In line with these reported results, the metastatic cell line Patu8902 used in the drug screen has been known to express and secrete high levels of urokinase, which might explain the effective inhibition of invasion by Tranexamic acid. Moreover, it has been reported that the urokinase receptor; urokinase plasminogen activator receptor (uPAR), was overexpressed in neoplastic cells in majority of the patients and was correlated with a poor survival (279, 280). These findings suggest that further studies should be done on the potential of Tranexamic acid as a potential therapeutic to be used in combination with a cytostatic drug such as gemcitabine. In addition, urokinase and its receptor uPAR could be a potential target against pancreatic cancer invasion.

The other two compounds of the top 5 drug candidates, Ursodiol and Leflunomide demonstrated higher invasive score than Gemcitabine. This is most probably due to the fact that certain drugs reduce invasion, resulting in a smaller “GFP area”. However, they may still present moderate single cell dissemination, which leads to a higher invasive scoring by the manual scoring method. Ursodiol is a synthetic secondary bile acid used for treating cholestatic liver diseases (281). Inconsistent outcomes have been reported regarding the role of Ursodiol in decreasing or increasing colorectal cancer (282). However, a recent abstract publication has reported that Ursodiol suppressed intracellular levels of ROS, decreased expression of EMT markers and stem cell formation in pancreatic cancer cells *in vitro*. As not

much has been reported regarding Ursodiol and pancreatic cancer, further investigation is needed to determine its mechanism and effect on cancer progression.

Leflunomide is an antagonist of dihydroorotate dehydrogenase, which has been associated with mitochondrial electron transport and is required for de novo pyrimidine synthesis (283). It has been used for treating rheumatoid arthritis. Although viability was not affected by lefluonomide, the drug has been reported to inhibit the growth of human prostate cancer *in vitro* and *in vivo (284, 285)*. However, another study demonstrated that leflunomide did not inhibit invasion in breast cancer (286). No studies have been conducted of leflunomide in pancreatic cancer and future experiments could further validate and determine the potentials of leflunomide as an inhibitor of pancreatic cancer invasion.

Overall, this chapter has demonstrated the limitations and potentials of the 3D spheroid invasion assay as a drug screening platform. Several promising drugs hits have emerged with the ability of affecting cell viability of the highly invasive cell line Patu8902 and also drugs with strong inhibition of invasion without affecting cell viability. These drug candidates should ultimately be further validated and perhaps tested in combination with Gemcitabine and other drugs. Moreover, the drug screen was also able to validate compounds which were hypothesised to do well against pancreatic cancer, such as the ROCK inhibitors GSK269962a and H1152. Future automation and optimisation could potentially accelerate the discovery and development of novel therapeutics against pancreatic cancer.

5.4 Future work

It is of importance to validate the screen hits further based on invasion effects and viability effects. The 3D spheroid invasion screen was able to provide insights on the effects of the drug compounds on a 3D cell structure confined in a 3D matrix, bringing in the aspect of barrier and internal concentration gradients. By utilising other forms of assays, such as the organotypic assay or 3D transwell invasion assay, the drug compounds can be further validated in 3D for invasion effects. This should also be done on other cell lines to see whether certain drugs elicit effects specific for the PaTu8902 cells, but might not have an identical impact on other cell lines with different genetic backgrounds. Nevertheless, this assay could be used to screen drugs that could work for a specific type of cancer with a specific genetic signature or background, making this assay an attractive tool for working towards personalised medicine. The only requirement is that cell lines or primary cells should be able to form consistent spheroids to yield meaningful and comparable results.

An IC_{50} value should be determined from the invasion and the viability studies in order to compare the potential dose with the toxicity dose reported for these drugs. Furthermore, the mechanism of action should be confirmed whether it is acting through the documented selective target or whether the drug is eliciting inhibition of invasion through other targets. Once the drug has been confirmed to be acting on other targets than its indicated target, mechanistic studies should be conducted. This could include but not limited to: microarray, phosphoproteomics and metabolomics to pinpoint the target and the affected signalling pathway or pathways.

Further validation of these hits should be done *in vivo* either in a xenograft model as demonstrated previously in chapter 4, which worked with success. An alternative is to have either a genetic engineered mouse model or an orthotopic xenograft model to validate the drugs further.

6. Concluding remarks

With limited amount of therapies available for pancreatic cancer, more focus is needed on the discovery of novel therapeutics against this malignant disease. Recent findings have demonstrated a crucial role for the tumour microenvironment in pancreatic cancer growth, invasion and survival (150). However, the lack of pancreatic cancer models *in vitro* that recapitulate *in vivo* behaviour, which are also suitable for drug screening against pancreatic cancer invasion remained a key hurdle. Previously, several efforts have tried to overcome this challenge by developing an organotypic assay for pancreatic cancer (203). Nevertheless, drug screening in organotypic assays are not cost effective despite their unique resemblance with desmoplasia *in vivo*. More recent work done on organoids provides researchers a tool to investigate key genetic drivers and the development of pancreatic cancer (204-206). Yet, these organoid assays are not cost effective and do not allow for drug screening against pancreatic cancer cell invasion. Since pancreatic cancer is a highly metastatic disease, this study aimed to develop a novel *in vitro* pancreatic cancer model suitable for drug screening against invasion, which accounts for components found in the tumour microenvironment such as extra cellular matrix and pancreatic stellate cells.

First, a suitable cell line model for the drug screen assay was identified from several pancreatic cancer cell lines through the characterisation of the morphology and the phenotypical behaviour of pancreatic cancer. Similar to several highly invasive cancers such as melanoma and hepatocellular carcinoma, I have demonstrated that individual pancreatic cancer cells are able to adopt the highly invasive amoeboid morphology rather than only the suggested mesenchymal morphology (113, 183, 287). This type of cellular behaviour was linked with the more invasive QM subtype as demonstrated by the increased levels of the contractility marker pMLC2, bleb or protrusion formation, and the enrichment of contractile genes. Furthermore, cells of QM subtype have a better spheroid formation ability, reflecting their *in vivo* tumour formation ability. Moreover, QM cells were more likely to adapt the individual cell phenotype on 2.5D collagen I matrix, and invade in an individual manner. The QM cell line PaTu8902 demonstrated all aforementioned phenotypical traits, had a

robust spheroid formation ability and as the most invasive cell line, it was thus chosen as the representative cell line model. During the *in vivo* validation, it was shown that injected Patu8902 cells were able to form tumours *in vivo* and disseminate from the tumour body in single cells with round and elongated morphologies (Figure 4-9), recapitulating the observations made *in vitro* (Figure 3-8, 3-10, 3-11 & 4-4). These findings demonstrate for the first time that pancreatic cancer cells have the ability to adapt an amoeboid phenotype during invasion *in vitro* and *in vivo*.

Secondly, the initial 3D co-culture spheroid invasion assay was further developed in this study and adapted for drug screening purposes. This assay demonstrated robust formation and invasion of co-culture spheroids consisting of Patu8902 cancer cells and PS-1 stromal cells, each tagged with LifeAct-GFP and LifeAct-mrfpruby respectively allowing semi-automated analysis of each compartment. No co-culture spheroids have been designed previously for pancreatic cancer with pancreatic cancer specific stromal cells; the pancreatic stellate cells. Only one study reported the use of MRC5 lung fibroblasts or pancreatic mesenchymal cell line LT2 to form co-culture spheroids with pancreatic cancer cells (215). Although, several spheroid invasion assays have recently been developed for other cancers such as breast cancer and prostate cancer, no spheroid assays have been developed to conduct drug screening against pancreatic cancer invasion (212, 288). The observations made *in vitro* from the 3D spheroid invasion assay has been validated and recapitulate *in vivo* findings in the xenograft mouse model. This means that potential drugs from the drug screen can be validated in the *in vivo* xenograft model. Furthermore, the screen allows for semi-automated analysis and can be further optimised for full automated high throughput drug screening.

The drug screening platform demonstrated robust results with Dasatinib and Gemcitabine as positive controls and DMSO as negative control. Dasatinib demonstrated strong inhibition of invasion as reported previously *in vitro* and *in vivo*, but did not inhibit cell viability in the assay nor improve patient overall survival in pancreatic cancer during clinical trials as reported previously (122, 237). However, in this study, results were obtained from effects on invasion but not viability. Viability

and proliferation could affect invasion of cells through the generation of chemogradient by nutrition competition (289). Furthermore, proliferation, survival and motility pathways overlaps and secreted growth factors are able to act on both, thus cell growth would affect cell motility (290). It is therefore crucial to be able to test viability and proliferation in the treated spheroids along with invasion. However, just like other 3D models, validation of viability of cells in 3D in matrix deemed a significant challenge to achieve robust results. Future efforts focussed on tackling viability and proliferation read out of 3D tumour spheroids in 3D matrix *in vitro* or *in vivo* will be extremely beneficial to this assay.

Another limitation of the drug screen assay design is that it is not applicable for RNAi screening or validation experiments. Cells have to form relatable spheroids and therefore caution is needed when proceeding with experiments involving knock out or RNAi silencing methods to compare against the mock cells, as this can affect spheroid formation ability. Information regarding spheroid formation can be obtained in this method, yet if spheroids are not comparable at the start of the invasion assay, it will be difficult to make sense of the results at the end of the invasion. Furthermore, as the drug screen assay was optimised to pick up drug compounds that inhibit invasion, the drug screen is therefore less sensitive and robust for uncovering drugs which increase invasion. Adjustments could be made regarding the duration of the invasion part and a positive control increasing invasion is needed. Overall, the drug screen was designed to identify drugs against pancreatic cancer and more specifically pancreatic cancer invasion. This also implicates that if isolated primary cells are able to form a spheroid, personalised drug screening can be conducted.

Lastly, after developing and optimising the drug screening platform for drug screening against pancreatic cancer, an FDA approved drug library was assembled and drugs were screened in the 3D spheroid invasion assay platform. The drug screen demonstrated robustness over the drug screen and the results yielded a range of effects on invasion, with 5 unique hits that have unknown anti-neoplastic effects and are currently or have not been in clinical trials previously. Follow up validation demonstrated that one of the 5 hits, Digoxin, demonstrated strong inhibition of

invasion and coupled with effects on viability. The other 4 hits, Tranexamic acid, Nebivolol, Ursodiol and Leflunomide demonstrated no effect on viability at screen concentration, but showed good inhibition of invasion. These results indicate that the drug screen was able to identify compounds which are able to target and affect the viability of these highly invasive and drug resistant cells. Furthermore, the drug screen also identified compounds which solely act on cell extrinsic effects, hence not affecting cellular viability but rather hinder the cells from invading into the surroundings through inhibiting secreted ECM modulating factors such as MMPs. Alternatively, these compounds demonstrate a difference in therapeutic window for effects on invasion and for viability. Together, these findings demonstrated a robust and effective drug screen assay platform, yielding several promising compounds for further validation. Future drug combination studies could also be conducted to mimic treatment in the clinic more closely.

In this study, the 2.5D collagen I matrix assay was applied to characterise pancreatic cancer cell lines and demonstrated synergies between observations made in 3D *in vitro* and *in vivo*. This suggests that the 2.5D collagen I matrix assay could be adopted for characterisation and optimisation studies prior to moving onto 3D *in vitro* or *in vivo* studies. It was demonstrated that individual QM pancreatic cancer cells adopted an amoeboid phenotype, elicit increased contractility and demonstrated high invasiveness in 3D *in vitro* and *in vivo*. These results suggested that the ROCK pathway, which modulates cellular contractility, could be a potential therapeutic target against pancreatic cancer invasion. Results of the ROCK inhibitors GSK269692a and H1152 from the drug screen and follow up studies demonstrated significant inhibition of invasion, indicating that ROCK inhibitors could be a promising treatment for pancreatic cancer. Recent studies in mouse models demonstrated that ROCK activation and increased pMLC2 levels increased extracellular modelling and increased growth and invasion of pancreatic cancer (184, 235). Another study has shown that treatment with the ROCK inhibitor Fasudil resulted in the remodelling of the extracellular matrix and enhanced the response of the pancreatic cancers to standard of care therapies (234). These studies emphasised ROCK inhibition as a promising therapeutic against pancreatic cancer. However, these studies suggest a

role of ROCK on extracellular matrix remodelling whereas results from this work suggests that ROCK inhibitors could also directly act on the pancreatic cancer cells and inhibit them from increasing contractility and adopting the invasive amoeboid phenotype. Further validation studies of inhibition of invasion in different cell line models, in vivo and effects on viability are needed to determine the potentials of ROCK inhibitors in pancreatic cancer. Furthermore, it will be of interest to demonstrate whether ROCK inhibitors are able to reduce the numbers of amoeboid and mesenchymal invading cells in the 3D spheroid invasion assay and the in vivo mouse model studies.

Overall, this study has laid the basis of the existence of the amoeboid phenotype in pancreatic cancer, which could serve as a potential target by inhibiting ROCK and actomyosin contractility pathways. Furthermore, the study has developed a 3D co-culture spheroid invasion assay and protocols for a semi-automated quantification method that was optimised for drug screening. This drug screen tool proved to recapitulate *in vivo* findings and was successful in identifying novel promising hits against pancreatic cancer and pancreatic cancer invasion. With further improvements, this cost-effective drug screen tool could accelerate the process towards personalised medicine drug discovery in pancreatic cancer.

7. Reference:

1. American-Cancer-Society. Cancer Facts & Figures 2017. 2017.

2. Shih HP, Wang A, Sander M. Pancreas organogenesis: from lineage determination to morphogenesis. Annual review of cell and developmental biology. 2013;29:81-105.

3. Leung P. Physiology of the Pancreas. The Renin-Angiotensin System: Current Research Progress in The Pancreas. Advances in Experimental Medicine and Biology. 690: Springer Netherlands; 2010. p. 13-27.

4. Maitra A, Fukushima N, Takaori K, Hruban RH. Precursors to invasive pancreatic cancer. Advances in anatomic pathology. 2005;12(2):81-91.

5. Hruban RH, Takaori K, Klimstra DS, Adsay NV, Albores-Saavedra J, Biankin AV, et al. An illustrated consensus on the classification of pancreatic intraepithelial neoplasia and intraductal papillary mucinous neoplasms. The American journal of surgical pathology. 2004;28(8):977-87.

6. Guerra C, Schuhmacher AJ, Canamero M, Grippo PJ, Verdaguer L, Perez-Gallego L, et al. Chronic pancreatitis is essential for induction of pancreatic ductal adenocarcinoma by K-Ras oncogenes in adult mice. Cancer Cell. 2007;11(3):291-302.

7. Morris JPt, Cano DA, Sekine S, Wang SC, Hebrok M. Beta-catenin blocks Kras-dependent reprogramming of acini into pancreatic cancer precursor lesions in mice. J Clin Invest. 2010;120(2):508-20.

8. Kopp JL, von Figura G, Mayes E, Liu FF, Dubois CL, Morris JPt, et al. Identification of Sox9-dependent acinar-to-ductal reprogramming as the principal mechanism for initiation of pancreatic ductal adenocarcinoma. Cancer Cell. 2012;22(6):737-50.

9. Delgiorno KE, Hall JC, Takeuchi KK, Pan FC, Halbrook CJ, Washington MK, et al. Identification and manipulation of biliary metaplasia in pancreatic tumors. Gastroenterology. 2014;146(1):233-44 e5.

10. Bailey JM, Alsina J, Rasheed ZA, McAllister FM, Fu YY, Plentz R, et al. DCLK1 marks a morphologically distinct subpopulation of cells with stem cell properties in preinvasive pancreatic cancer. Gastroenterology. 2014;146(1):245-56.

11. Ray KC, Bell KM, Yan J, Gu G, Chung CH, Washington MK, et al. Epithelial tissues have varying degrees of susceptibility to Kras(G12D)-initiated tumorigenesis in a mouse model. PLoS ONE. 2011;6(2):e16786.

12. Pylayeva-Gupta Y, Lee KE, Hajdu CH, Miller G, Bar-Sagi D. Oncogenic Kras-induced GM-CSF production promotes the development of pancreatic neoplasia. Cancer Cell. 2012;21(6):836-47.

13. von Figura G, Fukuda A, Roy N, Liku ME, Morris Iv JP, Kim GE, et al. The chromatin regulator Brg1 suppresses formation of intraductal papillary mucinous neoplasm and pancreatic ductal adenocarcinoma. Nat Cell Biol. 2014;16(3):255-67.

14. Boj SF, Hwang CI, Baker LA, Chio, II, Engle DD, Corbo V, et al. Organoid models of human and mouse ductal pancreatic cancer. Cell. 2015;160(1-2):324-38.

15. Ghaneh P, Costello E, Neoptolemos JP. Biology and management of pancreatic cancer. Gut. 2007;56(8):1134-52.

16. Borad MJ, Saadati H, Lakshmipathy A, Campbell E, Hopper P, Jameson G, et al. Skeletal metastases in pancreatic cancer: a retrospective study and review of the literature. Yale J Biol Med. 2009;82(1):1-6.

17. Cancer-Research-UK. Pancreatic cancer statistics 2014. 2014.

18. Yachida S, Iacobuzio-Donahue CA. The pathology and genetics of metastatic pancreatic cancer. Archives of pathology & laboratory medicine. 2009;133(3):413-22.

19. Howlader N NA, Krapcho M, Miller D, Bishop K, Kosary CL, Yu M, Ruhl J, Tatalovich Z, Mariotto A, Lewis DR, Chen HS, Feuer EJ, Cronin KA (eds). SEER Cancer Statistics Review 1975-2014 National Cancer Institute2017 [Available from: https://seer.cancer.gov/statfacts/html/pancreas.html.

20. American-Cancer-Society. pancreatic cancer 2017 [Available from: https://www.cancer.org/cancer/pancreatic-cancer/detection-diagnosis-staging/staging.html.

21. UK CR. Pancreatic cancer incidence statistics 2018 [Available from: http://www.cancerresearchuk.org/health-professional/cancer-statistics/statistics-by-cancer-type/pancreatic-cancer/incidence - heading-Zero.

22. Bardeesy N, DePinho RA. Pancreatic cancer biology and genetics. Nat Rev Cancer. 2002;2(12):897-909.

23. Iodice S, Gandini S, Maisonneuve P, Lowenfels AB. Tobacco and the risk of pancreatic cancer: a review and meta-analysis. Langenbecks Arch Surg. 2008;393(4):535-45.

24. Vincent A, Herman J, Schulick R, Hruban RH, Goggins M. Pancreatic cancer. Lancet. 2011;378(9791):607-20.

25. Hidalgo M. Pancreatic cancer. The New England journal of medicine. 2010;362(17):1605-17.

26. Bryant KL, Mancias JD, Kimmelman AC, Der CJ. KRAS: feeding pancreatic cancer proliferation. Trends Biochem Sci. 2014;39(2):91-100.

27. Hingorani SR, Petricoin EF, Maitra A, Rajapakse V, King C, Jacobetz MA, et al. Preinvasive and invasive ductal pancreatic cancer and its early detection in the mouse. Cancer Cell. 2003;4(6):437-50.

28. Aguirre AJ, Bardeesy N, Sinha M, Lopez L, Tuveson DA, Horner J, et al. Activated Kras and Ink4a/Arf deficiency cooperate to produce metastatic pancreatic ductal adenocarcinoma. Genes & development. 2003;17(24):3112-26.

29. Hingorani SR, Wang L, Multani AS, Combs C, Deramaudt TB, Hruban RH, et al. Trp53R172H and KrasG12D cooperate to promote chromosomal instability and widely metastatic pancreatic ductal adenocarcinoma in mice. Cancer Cell. 2005;7(5):469-83.

30. Bardeesy N, Aguirre AJ, Chu GC, Cheng KH, Lopez LV, Hezel AF, et al. Both p16(Ink4a) and the p19(Arf)-p53 pathway constrain progression of pancreatic adenocarcinoma in the mouse. Proceedings of the National Academy of Sciences of the United States of America. 2006;103(15):5947-52.

31. Bardeesy N, Cheng KH, Berger JH, Chu GC, Pahler J, Olson P, et al. Smad4 is dispensable for normal pancreas development yet critical in progression and tumor biology of pancreas cancer. Genes & development. 2006;20(22):3130-46.

32. van Heek NT, Meeker AK, Kern SE, Yeo CJ, Lillemoe KD, Cameron JL, et al. Telomere shortening is nearly universal in pancreatic intraepithelial neoplasia. Am J Pathol. 2002;161(5):1541-7.

33. Gisselsson D, Jonson T, Petersen A, Strombeck B, Dal Cin P, Hoglund M, et al. Telomere dysfunction triggers extensive DNA fragmentation and evolution of complex chromosome abnormalities in human malignant tumors. Proceedings of the National Academy of Sciences of the United States of America. 2001;98(22):12683-8.

34. Rowley M, Ohashi A, Mondal G, Mills L, Yang L, Zhang L, et al. Inactivation of Brca2 promotes Trp53-associated but inhibits KrasG12D-dependent pancreatic cancer development in mice. Gastroenterology. 2011;140(4):1303-13 e1-3.

35. Morton JP, Steele CW, Sansom OJ. Timing is everything: Brca2 and p53 mutations in pancreatic cancer. Gastroenterology. 2011;140(4):1143-6.

36. Eser S, Schnieke A, Schneider G, Saur D. Oncogenic KRAS signalling in pancreatic cancer. Br J Cancer. 2014.

37. Bailey P, Chang DK, Nones K, Johns AL, Patch AM, Gingras MC, et al. Genomic analyses identify molecular subtypes of pancreatic cancer. Nature. 2016;531(7592):47-52.

38. Campbell PJ, Yachida S, Mudie LJ, Stephens PJ, Pleasance ED, Stebbings LA, et al. The patterns and dynamics of genomic instability in metastatic pancreatic cancer. Nature. 2010;467(7319):1109-13.

39. Yachida S, Jones S, Bozic I, Antal T, Leary R, Fu B, et al. Distant metastasis occurs late during the genetic evolution of pancreatic cancer. Nature. 2010;467(7319):1114-7.

40. Morris JPt, Wang SC, Hebrok M. KRAS, Hedgehog, Wnt and the twisted developmental biology of pancreatic ductal adenocarcinoma. Nat Rev Cancer. 2010;10(10):683-95.

41. Schubbert S, Shannon K, Bollag G. Hyperactive Ras in developmental disorders and cancer. Nat Rev Cancer. 2007;7(4):295-308.

42. Pylayeva-Gupta Y, Grabocka E, Bar-Sagi D. RAS oncogenes: weaving a tumorigenic web. Nat Rev Cancer. 2011;11(11):761-74.

43. Castellano E, Downward J. RAS Interaction with PI3K: More Than Just Another Effector Pathway. Genes & cancer. 2011;2(3):261-74.

44. Ying H, Kimmelman AC, Lyssiotis CA, Hua S, Chu GC, Fletcher-Sananikone E, et al. Oncogenic Kras maintains pancreatic tumors through regulation of anabolic glucose metabolism. Cell. 2012;149(3):656-70.

45. Eser S, Reiff N, Messer M, Seidler B, Gottschalk K, Dobler M, et al. Selective requirement of PI3K/PDK1 signaling for Kras oncogene-driven pancreatic cell plasticity and cancer. Cancer Cell. 2013;23(3):406-20.

46. Collisson EA, Trejo CL, Silva JM, Gu S, Korkola JE, Heiser LM, et al. A central role for RAF-->MEK-->ERK signaling in the genesis of pancreatic ductal adenocarcinoma. Cancer Discov. 2012;2(8):685-93.

47. Ostrem JM, Peters U, Sos ML, Wells JA, Shokat KM. K-Ras(G12C) inhibitors allosterically control GTP affinity and effector interactions. Nature. 2013;503(7477):548-51.

48. Hamidi H, Lu M, Chau K, Anderson L, Fejzo M, Ginther C, et al. KRAS mutational subtype and copy number predict in vitro response of human pancreatic cancer cell lines to MEK inhibition. Br J Cancer. 2014;111(9):1788-801.

49. Torti D, Trusolino L. Oncogene addiction as a foundational rationale for targeted anti-cancer therapy: promises and perils. EMBO Mol Med. 2011;3(11):623-36.

50. Kapoor A, Yao W, Ying H, Hua S, Liewen A, Wang Q, et al. Yap1 activation enables bypass of oncogenic kras addiction in pancreatic cancer. Cell. 2014;158(1):185-97.

51. Shao DD, Xue W, Krall EB, Bhutkar A, Piccioni F, Wang X, et al. KRAS and YAP1 Converge to Regulate EMT and Tumor Survival. Cell. 2014;158(1):171-84.

52. Singh A, Greninger P, Rhodes D, Koopman L, Violette S, Bardeesy N, et al. A gene expression signature associated with "K-Ras addiction" reveals regulators of EMT and tumor cell survival. Cancer Cell. 2009;15(6):489-500.

53. Collisson EA, Sadanandam A, Olson P, Gibb WJ, Truitt M, Gu S, et al. Subtypes of pancreatic ductal adenocarcinoma and their differing responses to therapy. Nat Med. 2011;17(4):500-3.

54. Rhim AD, Stanger BZ. Molecular biology of pancreatic ductal adenocarcinoma progression: aberrant activation of developmental pathways. Progress in molecular biology and translational science. 2010;97:41-78.

55. Schneider G, Hamacher R, Eser S, Friess H, Schmid RM, Saur D. Molecular biology of pancreatic cancer--new aspects and targets. Anticancer research. 2008;28(3A):1541-50.

56. Abramson MA, Jazag A, van der Zee JA, Whang EE. The molecular biology of pancreatic cancer. Gastrointestinal cancer research : GCR. 2007;1(4 Suppl 2):S7-S12.

57. Biankin AV, Waddell N, Kassahn KS, Gingras MC, Muthuswamy LB, Johns AL, et al. Pancreatic cancer genomes reveal aberrations in axon guidance pathway genes. Nature. 2012;491(7424):399-405.

58. Waddell N, Pajic M, Patch AM, Chang DK, Kassahn KS, Bailey P, et al. Whole genomes redefine the mutational landscape of pancreatic cancer. Nature. 2015;518(7540):495-501.

59. Moffitt RA, Marayati R, Flate EL, Volmar KE, Loeza SG, Hoadley KA, et al. Virtual microdissection identifies distinct tumor- and stroma-specific subtypes of pancreatic ductal adenocarcinoma. Nat Genet. 2015;47(10):1168-78.

60. Lynch TJ, Bell DW, Sordella R, Gurubhagavatula S, Okimoto RA, Brannigan BW, et al. Activating mutations in the epidermal growth factor receptor underlying responsiveness of non-small-cell lung cancer to gefitinib. The New England journal of medicine. 2004;350(21):2129-39.

61. Slamon DJ, Leyland-Jones B, Shak S, Fuchs H, Paton V, Bajamonde A, et al. Use of chemotherapy plus a monoclonal antibody against HER2 for metastatic breast cancer that overexpresses HER2. The New England journal of medicine. 2001;344(11):783-92.

62. Conroy T, Desseigne F, Ychou M, Bouche O, Guimbaud R, Becouarn Y, et al. FOLFIRINOX versus gemcitabine for metastatic pancreatic cancer. The New England journal of medicine. 2011;364(19):1817-25.

63. Von Hoff DD, Ervin T, Arena FP, Chiorean EG, Infante J, Moore M, et al. Increased survival in pancreatic cancer with nab-paclitaxel plus gemcitabine. The New England journal of medicine. 2013;369(18):1691-703.

64. de Sousa Cavalcante L, Monteiro G. Gemcitabine: metabolism and molecular mechanisms of action, sensitivity and chemoresistance in pancreatic cancer. Eur J Pharmacol. 2014;741:8-16.

65. Yardley DA. nab-Paclitaxel mechanisms of action and delivery. J Control Release. 2013;170(3):365-72.

66. Smith DB, Neoptolemos JP. Capecitabine: an evidence-based review of its effectiveness in the treatment of carcinoma of the pancreas. Core Evid. 2007;2(2):111-9.

67. Longley DB, Harkin DP, Johnston PG. 5-fluorouracil: mechanisms of action and clinical strategies. Nat Rev Cancer. 2003;3(5):330-8.

68. Peters GJ, Backus HH, Freemantle S, van Triest B, Codacci-Pisanelli G, van der Wilt CL, et al. Induction of thymidylate synthase as a 5-fluorouracil resistance mechanism. Biochimica et biophysica acta. 2002;1587(2-3):194-205.

69. Moore MJ, Goldstein D, Hamm J, Figer A, Hecht JR, Gallinger S, et al. Erlotinib plus gemcitabine compared with gemcitabine alone in patients with advanced pancreatic cancer: a phase III trial of the National Cancer Institute of Canada Clinical Trials Group. J Clin Oncol. 2007;25(15):1960-6.

70. Xiong HQ, Rosenberg A, LoBuglio A, Schmidt W, Wolff RA, Deutsch J, et al. Cetuximab, a monoclonal antibody targeting the epidermal growth factor receptor, in combination with gemcitabine for advanced pancreatic cancer: a multicenter phase II Trial. J Clin Oncol. 2004;22(13):2610-6.

71. Kleger A, Perkhofer L, Seufferlein T. Smarter drugs emerging in pancreatic cancer therapy. Ann Oncol. 2014;25(7):1260-70.

72. Amakye D, Jagani Z, Dorsch M. Unraveling the therapeutic potential of the Hedgehog pathway in cancer. Nat Med. 2013;19(11):1410-22.

73. Kindler HL, Niedzwiecki D, Hollis D, Sutherland S, Schrag D, Hurwitz H, et al. Gemcitabine plus bevacizumab compared with gemcitabine plus placebo in patients with advanced pancreatic cancer: phase III trial of the Cancer and Leukemia Group B (CALGB 80303). J Clin Oncol. 2010;28(22):3617-22.

74. Brahmer JR, Tykodi SS, Chow LQ, Hwu WJ, Topalian SL, Hwu P, et al. Safety and activity of anti-PD-L1 antibody in patients with advanced cancer. The New England journal of medicine. 2012;366(26):2455-65.

75. Royal RE, Levy C, Turner K, Mathur A, Hughes M, Kammula US, et al. Phase 2 trial of single agent Ipilimumab (anti-CTLA-4) for locally advanced or metastatic pancreatic adenocarcinoma. J Immunother. 2010;33(8):828-33.

76. Rizvi NA, Hellmann MD, Snyder A, Kvistborg P, Makarov V, Havel JJ, et al. Cancer immunology. Mutational landscape determines sensitivity to PD-1 blockade in non-small cell lung cancer. Science. 2015;348(6230):124-8.

77. Snyder A, Makarov V, Merghoub T, Yuan J, Zaretsky JM, Desrichard A, et al. Genetic basis for clinical response to CTLA-4 blockade in melanoma. The New England journal of medicine. 2014;371(23):2189-99.

78. Cunningham D, Chau I, Stocken DD, Valle JW, Smith D, Steward W, et al. Phase III randomized comparison of gemcitabine versus gemcitabine plus capecitabine in patients with advanced pancreatic cancer. J Clin Oncol. 2009;27(33):5513-8.

79. Rucki AA, Zheng L. Pancreatic cancer stroma: understanding biology leads to new therapeutic strategies. World J Gastroenterol. 2014;20(9):2237-46.

80. Stromnes IM, DelGiorno KE, Greenberg PD, Hingorani SR. Stromal reengineering to treat pancreas cancer. Carcinogenesis. 2014;35(7):1451-60.

81. Wormann SM, Diakopoulos KN, Lesina M, Algul H. The immune network in pancreatic cancer development and progression. Oncogene. 2014;33(23):2956-67.

82. Mahadevan D, Von Hoff DD. Tumor-stroma interactions in pancreatic ductal adenocarcinoma. Mol Cancer Ther. 2007;6(4):1186-97.

83. Tape CJ, Ling S, Dimitriadi M, McMahon KM, Worboys JD, Leong HS, et al. Oncogenic KRAS Regulates Tumor Cell Signaling via Stromal Reciprocation. Cell. 2016;165(7):1818.

84. Assifi MM, Hines OJ. Anti-angiogenic agents in pancreatic cancer: a review. Anti-cancer agents in medicinal chemistry. 2011;11(5):464-9.

85. Provenzano PP, Cuevas C, Chang AE, Goel VK, Von Hoff DD, Hingorani SR. Enzymatic targeting of the stroma ablates physical barriers to treatment of pancreatic ductal adenocarcinoma. Cancer Cell. 2012;21(3):418-29.

86. Ozdemir BC, Pentcheva-Hoang T, Carstens JL, Zheng X, Wu CC, Simpson TR, et al. Depletion of carcinoma-associated fibroblasts and fibrosis induces

immunosuppression and accelerates pancreas cancer with reduced survival. Cancer Cell. 2014;25(6):719-34.

87. Rhim AD, Oberstein PE, Thomas DH, Mirek ET, Palermo CF, Sastra SA, et al. Stromal elements act to restrain, rather than support, pancreatic ductal adenocarcinoma. Cancer Cell. 2014;25(6):735-47.

88. Miller BW, Morton JP, Pinese M, Saturno G, Jamieson NB, McGhee E, et al. Targeting the LOX/hypoxia axis reverses many of the features that make pancreatic cancer deadly: inhibition of LOX abrogates metastasis and enhances drug efficacy. EMBO Mol Med. 2015;7(8):1063-76.

89. Hingorani SR, Zheng L, Bullock AJ, Seery TE, Harris WP, Sigal DS, et al. HALO 202: Randomized Phase II Study of PEGPH20 Plus Nab-Paclitaxel/Gemcitabine Versus Nab-Paclitaxel/Gemcitabine in Patients With Untreated, Metastatic Pancreatic Ductal Adenocarcinoma. J Clin Oncol. 2018;36(4):359-66.

90. Lunardi S, Muschel RJ, Brunner TB. The stromal compartments in pancreatic cancer: are there any therapeutic targets? Cancer Lett. 2014;343(2):147-55.

91. Wilson JS, Pirola RC, Apte MV. Stars and stripes in pancreatic cancer: role of stellate cells and stroma in cancer progression. Front Physiol. 2014;5:52.

92. Bachem MG, Schunemann M, Ramadani M, Siech M, Beger H, Buck A, et al. Pancreatic carcinoma cells induce fibrosis by stimulating proliferation and matrix synthesis of stellate cells. Gastroenterology. 2005;128(4):907-21.

93. Apte MV, Wilson JS, Lugea A, Pandol SJ. A starring role for stellate cells in the pancreatic cancer microenvironment. Gastroenterology. 2013;144(6):1210-9.

94. Tape CJ, Ling S, Dimitriadi M, McMahon KM, Worboys JD, Leong HS, et al. Oncogenic KRAS Regulates Tumor Cell Signaling via Stromal Reciprocation. Cell. 2016;165(4):910-20.

95. Fujita H, Ohuchida K, Mizumoto K, Egami T, Miyoshi K, Moriyama T, et al. Tumor-stromal interactions with direct cell contacts enhance proliferation of human pancreatic carcinoma cells. Cancer Sci. 2009;100(12):2309-17.

96. Hamada S, Masamune A, Takikawa T, Suzuki N, Kikuta K, Hirota M, et al. Pancreatic stellate cells enhance stem cell-like phenotypes in pancreatic cancer cells. Biochem Biophys Res Commun. 2012;421(2):349-54.

97. Al-Assar O, Demiciorglu F, Lunardi S, Gaspar-Carvalho MM, McKenna WG, Muschel RM, et al. Contextual regulation of pancreatic cancer stem cell phenotype and radioresistance by pancreatic stellate cells. Radiotherapy and oncology : journal of the European Society for Therapeutic Radiology and Oncology. 2014;111(2):243-51.

98. Hwang RF, Moore T, Arumugam T, Ramachandran V, Amos KD, Rivera A, et al. Cancer-associated stromal fibroblasts promote pancreatic tumor progression. Cancer Res. 2008;68(3):918-26.

99. Vonlaufen A, Joshi S, Qu C, Phillips PA, Xu Z, Parker NR, et al. Pancreatic stellate cells: partners in crime with pancreatic cancer cells. Cancer Res. 2008;68(7):2085-93.

100. Xu Z, Vonlaufen A, Phillips PA, Fiala-Beer E, Zhang X, Yang L, et al. Role of pancreatic stellate cells in pancreatic cancer metastasis. Am J Pathol. 2010;177(5):2585-96.

101. Lee JJ, Perera RM, Wang H, Wu DC, Liu XS, Han S, et al. Stromal response to Hedgehog signaling restrains pancreatic cancer progression. Proceedings of the National Academy of Sciences of the United States of America. 2014;111(30):E3091-100.

102. Ohlund D, Handly-Santana A, Biffi G, Elyada E, Almeida AS, Ponz-Sarvise M, et al. Distinct populations of inflammatory fibroblasts and myofibroblasts in pancreatic cancer. J Exp Med. 2017;214(3):579-96.

103. Loberg RD, Bradley DA, Tomlins SA, Chinnaiyan AM, Pienta KJ. The lethal phenotype of cancer: the molecular basis of death due to malignancy. CA: a cancer journal for clinicians. 2007;57(4):225-41.

104. Fidler IJ. The pathogenesis of cancer metastasis: the 'seed and soil' hypothesis revisited. Nat Rev Cancer. 2003;3(6):453-8.

105. Friedl P, Alexander S. Cancer invasion and the microenvironment: plasticity and reciprocity. Cell. 2011;147(5):992-1009.

106. Mueller BK, Mack H, Teusch N. Rho kinase, a promising drug target for neurological disorders. Nat Rev Drug Discov. 2005;4(5):387-98.

107. Riento K, Ridley AJ. Rocks: multifunctional kinases in cell behaviour. Nature reviews Molecular cell biology. 2003;4(6):446-56.

108. Sadok A, McCarthy A, Caldwell J, Collins I, Garrett MD, Yeo M, et al. Rho kinase inhibitors block melanoma cell migration and inhibit metastasis. Cancer Res. 2015;75(11):2272-84.

109. Ito M, Nakano T, Erdodi F, Hartshorne DJ. Myosin phosphatase: structure, regulation and function. Molecular and cellular biochemistry. 2004;259(1-2):197-209.

110. Madsen CD, Hooper S, Tozluoglu M, Bruckbauer A, Fletcher G, Erler JT, et al. STRIPAK components determine mode of cancer cell migration and metastasis. Nat Cell Biol. 2015;17(1):68-80.

111. Sahai E, Marshall CJ. Differing modes of tumour cell invasion have distinct requirements for Rho/ROCK signalling and extracellular proteolysis. Nat Cell Biol. 2003;5(8):711-9.

112. Sanz-Moreno V, Gaggioli C, Yeo M, Albrengues J, Wallberg F, Viros A, et al. ROCK and JAK1 signaling cooperate to control actomyosin contractility in tumor cells and stroma. Cancer Cell. 2011;20(2):229-45.

113. Sanz-Moreno V, Gadea G, Ahn J, Paterson H, Marra P, Pinner S, et al. Rac activation and inactivation control plasticity of tumor cell movement. Cell. 2008;135(3):510-23.

114. Paluch EK, Raz E. The role and regulation of blebs in cell migration. Curr Opin Cell Biol. 2013;25(5):582-90.

115. Orgaz JL, Pandya P, Dalmeida R, Karagiannis P, Sanchez-Laorden B, Viros A, et al. Diverse matrix metalloproteinase functions regulate cancer amoeboid migration. Nature communications. 2014;5:4255.

116. Kikuta K, Masamune A, Watanabe T, Ariga H, Itoh H, Hamada S, et al. Pancreatic stellate cells promote epithelial-mesenchymal transition in pancreatic cancer cells. Biochem Biophys Res Commun. 2010;403(3-4):380-4.

117. Mizuuchi Y, Aishima S, Ohuchida K, Shindo K, Fujino M, Hattori M, et al. Anterior gradient 2 downregulation in a subset of pancreatic ductal adenocarcinoma is a prognostic factor indicative of epithelial-mesenchymal transition. Laboratory investigation; a journal of technical methods and pathology. 2015;95(2):193-206.

118. Timpson P, McGhee EJ, Morton JP, von Kriegsheim A, Schwarz JP, Karim SA, et al. Spatial regulation of RhoA activity during pancreatic cancer cell invasion driven by mutant p53. Cancer Res. 2011;71(3):747-57.

119. Nobis M, Herrmann D, Warren SC, Kadir S, Leung W, Killen M, et al. A RhoA-FRET Biosensor Mouse for Intravital Imaging in Normal Tissue Homeostasis and Disease Contexts. Cell Rep. 2017;21(1):274-88.

120. Zimmerman NP, Roy I, Hauser AD, Wilson JM, Williams CL, Dwinell MB. Cyclic AMP regulates the migration and invasion potential of human pancreatic cancer cells. Mol Carcinog. 2015;54(3):203-15.

121. Canel M, Serrels A, Miller D, Timpson P, Serrels B, Frame MC, et al. Quantitative in vivo imaging of the effects of inhibiting integrin signaling via Src and FAK on cancer cell movement: effects on E-cadherin dynamics. Cancer Res. 2010;70(22):9413-22.

122. Morton JP, Karim SA, Graham K, Timpson P, Jamieson N, Athineos D, et al. Dasatinib inhibits the development of metastases in a mouse model of pancreatic ductal adenocarcinoma. Gastroenterology. 2010;139(1):292-303.

123. Kalluri R, Weinberg RA. The basics of epithelial-mesenchymal transition. J Clin Invest. 2009;119(6):1420-8.

124. Arumugam T, Ramachandran V, Fournier KF, Wang H, Marquis L, Abbruzzese JL, et al. Epithelial to mesenchymal transition contributes to drug resistance in pancreatic cancer. Cancer Res. 2009;69(14):5820-8.

125. Jiang JH, Liu C, Cheng H, Lu Y, Qin Y, Xu YF, et al. Epithelial-mesenchymal transition in pancreatic cancer: Is it a clinically significant factor? Biochimica et biophysica acta. 2015;1855(1):43-9.

126. Sarkar FH, Li Y, Wang Z, Kong D. Pancreatic cancer stem cells and EMT in drug resistance and metastasis. Minerva chirurgica. 2009;64(5):489-500.

127. Maier HJ, Wirth T, Beug H. Epithelial-mesenchymal transition in pancreatic carcinoma. Cancers. 2010;2(4):2058-83.

128. Nakajima S, Doi R, Toyoda E, Tsuji S, Wada M, Koizumi M, et al. N-cadherin expression and epithelial-mesenchymal transition in pancreatic carcinoma. Clin Cancer Res. 2004;10(12 Pt 1):4125-33.

129. Krebs AM, Mitschke J, Lasierra Losada M, Schmalhofer O, Boerries M, Busch H, et al. The EMT-activator Zeb1 is a key factor for cell plasticity and promotes metastasis in pancreatic cancer. Nat Cell Biol. 2017;19(5):518-29.

130. Rhim AD, Mirek ET, Aiello NM, Maitra A, Bailey JM, McAllister F, et al. EMT and dissemination precede pancreatic tumor formation. Cell. 2012;148(1-2):349-61.

131. Li A, Morton JP, Ma Y, Karim SA, Zhou Y, Faller WJ, et al. Fascin is regulated by slug, promotes progression of pancreatic cancer in mice, and is associated with patient outcomes. Gastroenterology. 2014;146(5):1386-96 e1-17.

132. Friedl P, Locker J, Sahai E, Segall JE. Classifying collective cancer cell invasion. Nat Cell Biol. 2012;14(8):777-83.

133. Meng W, Takeichi M. Adherens junction: molecular architecture and regulation. Cold Spring Harbor perspectives in biology. 2009;1(6):a002899.

134. Hegerfeldt Y, Tusch M, Brocker EB, Friedl P. Collective cell movement in primary melanoma explants: plasticity of cell-cell interaction, beta1-integrin function, and migration strategies. Cancer Res. 2002;62(7):2125-30.

135. Hidalgo-Carcedo C, Hooper S, Chaudhry SI, Williamson P, Harrington K, Leitinger B, et al. Collective cell migration requires suppression of actomyosin at cell-cell contacts mediated by DDR1 and the cell polarity regulators Par3 and Par6. Nat Cell Biol. 2011;13(1):49-58.

136. Ewald AJ, Brenot A, Duong M, Chan BS, Werb Z. Collective epithelial migration and cell rearrangements drive mammary branching morphogenesis. Developmental cell. 2008;14(4):570-81.

137. Terry SJ, Elbediwy A, Zihni C, Harris AR, Bailly M, Charras GT, et al. Stimulation of cortical myosin phosphorylation by p114RhoGEF drives cell migration and tumor cell invasion. PLoS ONE. 2012;7(11):e50188.

138. Friedl P, Gilmour D. Collective cell migration in morphogenesis, regeneration and cancer. Nature reviews Molecular cell biology. 2009;10(7):445-57.

139. Peglion F, Llense F, Etienne-Manneville S. Adherens junction treadmilling during collective migration. Nat Cell Biol. 2014;16(7):639-51.

140. Reffay M, Parrini MC, Cochet-Escartin O, Ladoux B, Buguin A, Coscoy S, et al. Interplay of RhoA and mechanical forces in collective cell migration driven by leader cells. Nat Cell Biol. 2014;16(3):217-23.

141. Coleman SJ, Chioni AM, Ghallab M, Anderson RK, Lemoine NR, Kocher HM, et al. Nuclear translocation of FGFR1 and FGF2 in pancreatic stellate cells facilitates pancreatic cancer cell invasion. EMBO Mol Med. 2014;6(4):467-81.

142. Froeling FE, Mirza TA, Feakins RM, Seedhar A, Elia G, Hart IR, et al. Organotypic culture model of pancreatic cancer demonstrates that stromal cells modulate E-cadherin, beta-catenin, and Ezrin expression in tumor cells. Am J Pathol. 2009;175(2):636-48.

143. Scales TM, Jayo A, Obara B, Holt MR, Hotchin NA, Berditchevski F, et al. alpha3beta1 integrins regulate CD151 complex assembly and membrane dynamics in carcinoma cells within 3D environments. Oncogene. 2013;32(34):3965-79.

144. Wyckoff JB, Pinner SE, Gschmeissner S, Condeelis JS, Sahai E. ROCK- and myosin-dependent matrix deformation enables protease-independent tumor-cell invasion in vivo. Curr Biol. 2006;16(15):1515-23.

145. Balaban EP, Mangu PB, Khorana AA, Shah MA, Mukherjee S, Crane CH, et al. Locally Advanced, Unresectable Pancreatic Cancer: American Society of Clinical Oncology Clinical Practice Guideline. J Clin Oncol. 2016;34(22):2654-68.

146. Hanahan D, Weinberg RA. Hallmarks of cancer: the next generation. Cell. 2011;144(5):646-74.

147. Clark AG, Vignjevic DM. Modes of cancer cell invasion and the role of the microenvironment. Curr Opin Cell Biol. 2015;36:13-22.

148. Thiery JP, Chopin D. Epithelial cell plasticity in development and tumor progression. Cancer metastasis reviews. 1999;18(1):31-42.

149. Merrell AJ, Stanger BZ. Adult cell plasticity in vivo: de-differentiation and transdifferentiation are back in style. Nature reviews Molecular cell biology. 2016;17(7):413-25.

150. Carr RM, Fernandez-Zapico ME. Pancreatic cancer microenvironment, to target or not to target? EMBO Mol Med. 2016;8(2):80-2.

151. Karnevi E, Rosendahl AH, Hilmersson KS, Saleem MA, Andersson R. Impact by pancreatic stellate cells on epithelial-mesenchymal transition and pancreatic cancer cell invasion: Adding a third dimension in vitro. Exp Cell Res. 2016;346(2):206-15.

152. Cai D, Chen SC, Prasad M, He L, Wang X, Choesmel-Cadamuro V, et al. Mechanical feedback through E-cadherin promotes direction sensing during collective cell migration. Cell. 2014;157(5):1146-59.

153. Sanz-Moreno V, Marshall CJ. The plasticity of cytoskeletal dynamics underlying neoplastic cell migration. Curr Opin Cell Biol. 2010;22(5):690-6.

154. Deer EL, Gonzalez-Hernandez J, Coursen JD, Shea JE, Ngatia J, Scaife CL, et al. Phenotype and genotype of pancreatic cancer cell lines. Pancreas. 2010;39(4):425-35.

155. Wang Y, Gangeswaran R, Zhao X, Wang P, Tysome J, Bhakta V, et al. CEACAM6 attenuates adenovirus infection by antagonizing viral trafficking in cancer cells. J Clin Invest. 2009;119(6):1604-15.

156. Kocher HM, Sandle J, Mirza TA, Li NF, Hart IR. Ezrin interacts with cortactin to form podosomal rosettes in pancreatic cancer cells. Gut. 2009;58(2):271-84.

157. Vezeridis MP, Tzanakakis GN, Meitner PA, Doremus CM, Tibbetts LM, Calabresi P. In vivo selection of a highly metastatic cell line from a human pancreatic carcinoma in the nude mouse. Cancer. 1992;69(8):2060-3.

158. Fofaria NM, Srivastava SK. STAT3 induces anoikis resistance, promotes cell invasion and metastatic potential in pancreatic cancer cells. Carcinogenesis. 2015;36(1):142-50.

159. Elsasser HP, Lehr U, Agricola B, Kern HF. Structural analysis of a new highly metastatic cell line PaTu 8902 from a primary human pancreatic adenocarcinoma. Virchows Arch B Cell Pathol Incl Mol Pathol. 1993;64(4):201-7.

160. Moore PS, Sipos B, Orlandini S, Sorio C, Real FX, Lemoine NR, et al. Genetic profile of 22 pancreatic carcinoma cell lines. Analysis of K-ras, p53, p16 and DPC4/Smad4. Virchows Archiv : an international journal of pathology. 2001;439(6):798-802.

161. Marques IJ, Weiss FU, Vlecken DH, Nitsche C, Bakkers J, Lagendijk AK, et al. Metastatic behaviour of primary human tumours in a zebrafish xenotransplantation model. BMC Cancer. 2009;9:128.

162. Schumacher G, Kataoka M, Roth JA, Mukhopadhyay T. Potent antitumor activity of 2-methoxyestradiol in human pancreatic cancer cell lines. Clin Cancer Res. 1999;5(3):493-9.

163. Kyriazis AP, McCombs WB, 3rd, Sandberg AA, Kyriazis AA, Sloane NH, Lepera R. Establishment and characterization of human pancreatic adenocarcinoma cell line SW-1990 in tissue culture and the nude mouse. Cancer Res. 1983;43(9):4393-401.

164. Yonezawa S, Byrd JC, Dahiya R, Ho JJ, Gum JR, Griffiths B, et al. Differential mucin gene expression in human pancreatic and colon cancer cells. Biochem J. 1991;276 (Pt 3):599-605.

165. Nagaraj NS, Smith JJ, Revetta F, Washington MK, Merchant NB. Targeted inhibition of SRC kinase signaling attenuates pancreatic tumorigenesis. Mol Cancer Ther. 2010;9(8):2322-32.

166. McCloy RA, Rogers S, Caldon CE, Lorca T, Castro A, Burgess A. Partial inhibition of Cdk1 in G 2 phase overrides the SAC and decouples mitotic events. Cell Cycle. 2014;13(9):1400-12.

167. Coleman SJ, Watt J, Arumugam P, Solaini L, Carapuca E, Ghallab M, et al. Pancreatic cancer organotypics: High throughput, preclinical models for pharmacological agent evaluation. World J Gastroenterol. 2014;20(26):8471-81.

168. Janky R, Binda MM, Allemeersch J, Van den Broeck A, Govaere O, Swinnen JV, et al. Prognostic relevance of molecular subtypes and master regulators in pancreatic ductal adenocarcinoma. BMC Cancer. 2016;16:632.

169. Daemen A, Peterson D, Sahu N, McCord R, Du X, Liu B, et al. Metabolite profiling stratifies pancreatic ductal adenocarcinomas into subtypes with distinct sensitivities to metabolic inhibitors. Proceedings of the National Academy of Sciences of the United States of America. 2015;112(32):E4410-7.

170. Choi W, Porten S, Kim S, Willis D, Plimack ER, Hoffman-Censits J, et al. Identification of distinct basal and luminal subtypes of muscle-invasive bladder cancer with different sensitivities to frontline chemotherapy. Cancer Cell. 2014;25(2):152-65.

171. Neve RM, Chin K, Fridlyand J, Yeh J, Baehner FL, Fevr T, et al. A collection of breast cancer cell lines for the study of functionally distinct cancer subtypes. Cancer Cell. 2006;10(6):515-27.

172. Gradiz R, Silva HC, Carvalho L, Botelho MF, Mota-Pinto A. MIA PaCa-2 and PANC-1 - pancreas ductal adenocarcinoma cell lines with neuroendocrine differentiation and somatostatin receptors. Sci Rep. 2016;6:21648.

173. Aghdassi A, Sendler M, Guenther A, Mayerle J, Behn CO, Heidecke CD, et al. Recruitment of histone deacetylases HDAC1 and HDAC2 by the transcriptional repressor ZEB1 downregulates E-cadherin expression in pancreatic cancer. Gut. 2012;61(3):439-48.

174. Genovese G, Carugo A, Tepper J, Robinson FS, Li L, Svelto M, et al. Synthetic vulnerabilities of mesenchymal subpopulations in pancreatic cancer. Nature. 2017;542(7641):362-6.

175. Ye X, Weinberg RA. Epithelial-Mesenchymal Plasticity: A Central Regulator of Cancer Progression. Trends in cell biology. 2015;25(11):675-86.

176. Pandya P, Orgaz JL, Sanz-Moreno V. Modes of invasion during tumour dissemination. Mol Oncol. 2017;11(1):5-27.

177. Wu PH, Phillip JM, Khatau SB, Chen WC, Stirman J, Rosseel S, et al. Evolution of cellular morpho-phenotypes in cancer metastasis. Sci Rep. 2015;5:18437.

178. Lammermann T, Sixt M. Mechanical modes of 'amoeboid' cell migration. Curr Opin Cell Biol. 2009;21(5):636-44.

179. Friedl P, Wolf K. Plasticity of cell migration: a multiscale tuning model. The Journal of cell biology. 2010;188(1):11-9.

180. Herraiz C, Calvo F, Pandya P, Cantelli G, Rodriguez-Hernandez I, Orgaz JL, et al. Reactivation of p53 by a Cytoskeletal Sensor to Control the Balance Between DNA Damage and Tumor Dissemination. J Natl Cancer Inst. 2016;108(1).

181. Giampieri S, Manning C, Hooper S, Jones L, Hill CS, Sahai E. Localized and reversible TGFbeta signalling switches breast cancer cells from cohesive to single cell motility. Nat Cell Biol. 2009;11(11):1287-96.

182. Cantelli G, Orgaz JL, Rodriguez-Hernandez I, Karagiannis P, Maiques O, Matias-Guiu X, et al. TGF-beta-Induced Transcription Sustains Amoeboid Melanoma Migration and Dissemination. Curr Biol. 2015;25(22):2899-914.

183. Beerling E, Oosterom I, Voest E, Lolkema M, van Rheenen J. Intravital characterization of tumor cell migration in pancreatic cancer. Intravital. 2016;5(3):e1261773.

184. Laklai H, Miroshnikova YA, Pickup MW, Collisson EA, Kim GE, Barrett AS, et al. Genotype tunes pancreatic ductal adenocarcinoma tissue tension to induce matricellular fibrosis and tumor progression. Nat Med. 2016;22(5):497-505.

185. Napolitano AP, Chai P, Dean DM, Morgan JR. Dynamics of the self-assembly of complex cellular aggregates on micromolded nonadhesive hydrogels. Tissue Eng. 2007;13(8):2087-94.

186. Tzanakakis ES, Hansen LK, Hu WS. The role of actin filaments and microtubules in hepatocyte spheroid self-assembly. Cell Motil Cytoskeleton. 2001;48(3):175-89.

187. Sodek KL, Ringuette MJ, Brown TJ. Compact spheroid formation by ovarian cancer cells is associated with contractile behavior and an invasive phenotype. Int J Cancer. 2009;124(9):2060-70.

188. Ohata H, Ishiguro T, Aihara Y, Sato A, Sakai H, Sekine S, et al. Induction of the stem-like cell regulator CD44 by Rho kinase inhibition contributes to the maintenance of colon cancer-initiating cells. Cancer Res. 2012;72(19):5101-10.

189. Ishiguro T, Sato A, Ohata H, Ikarashi Y, Takahashi RU, Ochiya T, et al. Establishment and Characterization of an In Vitro Model of Ovarian Cancer Stem-like Cells with an Enhanced Proliferative Capacity. Cancer Res. 2016;76(1):150-60.

190. Tilson SG, Haley EM, Triantafillu UL, Dozier DA, Langford CP, Gillespie GY, et al. ROCK Inhibition Facilitates In Vitro Expansion of Glioblastoma Stem-Like Cells. PLoS ONE. 2015;10(7):e0132823.

191. Kumper S, Mardakheh FK, McCarthy A, Yeo M, Stamp GW, Paul A, et al. Rho-associated kinase (ROCK) function is essential for cell cycle progression, senescence and tumorigenesis. Elife. 2016;5:e12994.

192. Koga T, Koga T, Awai M, Tsutsui J, Yue BY, Tanihara H. Rho-associated protein kinase inhibitor, Y-27632, induces alterations in adhesion, contraction and motility in cultured human trabecular meshwork cells. Exp Eye Res. 2006;82(3):362-70.

193. King H, Thillai K, Whale A, Arumugam P, Eldaly H, Kocher HM, et al. PAK4 interacts with p85 alpha: implications for pancreatic cancer cell migration. Sci Rep. 2017;7:42575.

194. Gandalovicova A, Rosel D, Fernandes M, Vesely P, Heneberg P, Cermak V, et al. Migrastatics-Anti-metastatic and Anti-invasion Drugs: Promises and Challenges. Trends Cancer. 2017;3(6):391-406.

195. Hu M, Polyak K. Microenvironmental regulation of cancer development. Curr Opin Genet Dev. 2008;18(1):27-34.

196. Quail DF, Joyce JA. Microenvironmental regulation of tumor progression and metastasis. Nat Med. 2013;19(11):1423-37.

197. Qian LW, Mizumoto K, Maehara N, Ohuchida K, Inadome N, Saimura M, et al. Co-cultivation of pancreatic cancer cells with orthotopic tumor-derived fibroblasts: fibroblasts stimulate tumor cell invasion via HGF secretion whereas cancer cells exert a minor regulative effect on fibroblasts HGF production. Cancer Lett. 2003;190(1):105-12.

198. Apte MV, Park S, Phillips PA, Santucci N, Goldstein D, Kumar RK, et al. Desmoplastic reaction in pancreatic cancer: role of pancreatic stellate cells. Pancreas. 2004;29(3):179-87.

199. Cody NA, Zietarska M, Filali-Mouhim A, Provencher DM, Mes-Masson AM, Tonin PN. Influence of monolayer, spheroid, and tumor growth conditions on

chromosome 3 gene expression in tumorigenic epithelial ovarian cancer cell lines. BMC Med Genomics. 2008;1:34.

200. Chang TT, Hughes-Fulford M. Monolayer and spheroid culture of human liver hepatocellular carcinoma cell line cells demonstrate distinct global gene expression patterns and functional phenotypes. Tissue Eng Part A. 2009;15(3):559-67.

201. Francia G, Man S, Teicher B, Grasso L, Kerbel RS. Gene expression analysis of tumor spheroids reveals a role for suppressed DNA mismatch repair in multicellular resistance to alkylating agents. Mol Cell Biol. 2004;24(15):6837-49.

202. Yeon SE, No da Y, Lee SH, Nam SW, Oh IH, Lee J, et al. Application of concave microwells to pancreatic tumor spheroids enabling anticancer drug evaluation in a clinically relevant drug resistance model. PLoS ONE. 2013;8(9):e73345.

203. Froeling FE, Marshall JF, Kocher HM. Pancreatic cancer organotypic cultures. J Biotechnol. 2010;148(1):16-23.

204. Baker LA, Tiriac H, Clevers H, Tuveson DA. Modeling pancreatic cancer with organoids. Trends Cancer. 2016;2(4):176-90.

205. Boj SF, Hwang CI, Baker LA, Engle DD, Tuveson DA, Clevers H. Model organoids provide new research opportunities for ductal pancreatic cancer. Mol Cell Oncol. 2016;3(1):e1014757.

206. Huang L, Holtzinger A, Jagan I, BeGora M, Lohse I, Ngai N, et al. Ductal pancreatic cancer modeling and drug screening using human pluripotent stem cell- and patient-derived tumor organoids. Nat Med. 2015;21(11):1364-71.

207. Herreros-Villanueva M, Hijona E, Cosme A, Bujanda L. Mouse models of pancreatic cancer. World J Gastroenterol. 2012;18(12):1286-94.

208. Aparicio S, Hidalgo M, Kung AL. Examining the utility of patient-derived xenograft mouse models. Nat Rev Cancer. 2015;15(5):311-6.

209. Hidalgo M, Amant F, Biankin AV, Budinska E, Byrne AT, Caldas C, et al. Patient-derived xenograft models: an emerging platform for translational cancer research. Cancer Discov. 2014;4(9):998-1013.

210. Dolznig H, Walzl A, Kramer N, Rosner M, Garin-Chesa P, Hengstschläger M. Organotypic spheroid cultures to study tumor–stroma interaction during cancer development. Drug Discovery Today: Disease Models. 2011;8(2):113-9.

211. Katt ME, Placone AL, Wong AD, Xu ZS, Searson PC. In Vitro Tumor Models: Advantages, Disadvantages, Variables, and Selecting the Right Platform. Front Bioeng Biotechnol. 2016;4:12.

212. Vinci M, Box C, Eccles SA. Three-dimensional (3D) tumor spheroid invasion assay. J Vis Exp. 2015(99):e52686.

213. Longati P, Jia X, Eimer J, Wagman A, Witt MR, Rehnmark S, et al. 3D pancreatic carcinoma spheroids induce a matrix-rich, chemoresistant phenotype offering a better model for drug testing. BMC Cancer. 2013;13:95.

214. Ham SL, Joshi R, Thakuri PS, Tavana H. Liquid-based three-dimensional tumor models for cancer research and drug discovery. Exp Biol Med (Maywood). 2016;241(9):939-54.

215. Majety M, Pradel LP, Gies M, Ries CH. Fibroblasts Influence Survival and Therapeutic Response in a 3D Co-Culture Model. PLoS ONE. 2015;10(6):e0127948.

216. Sousa CM, Biancur DE, Wang X, Halbrook CJ, Sherman MH, Zhang L, et al. Pancreatic stellate cells support tumour metabolism through autophagic alanine secretion. Nature. 2016;536(7617):479-83.

217. McCarroll JA, Naim S, Sharbeen G, Russia N, Lee J, Kavallaris M, et al. Role of pancreatic stellate cells in chemoresistance in pancreatic cancer. Front Physiol. 2014;5:141.

218. Witkiewicz AK, Balaji U, Eslinger C, McMillan E, Conway W, Posner B, et al. Integrated Patient-Derived Models Delineate Individualized Therapeutic Vulnerabilities of Pancreatic Cancer. Cell Rep. 2016;16(7):2017-31.

219. Knudsen ES, Balaji U, Mannakee B, Vail P, Eslinger C, Moxom C, et al. Pancreatic cancer cell lines as patient-derived avatars: genetic characterisation and functional utility. Gut. 2017.

220. Mollenhauer J, Roether I, Kern HF. Distribution of extracellular matrix proteins in pancreatic ductal adenocarcinoma and its influence on tumor cell proliferation in vitro. Pancreas. 1987;2(1):14-24.

221. Kleinman HK, Martin GR. Matrigel: basement membrane matrix with biological activity. Semin Cancer Biol. 2005;15(5):378-86.

222. Sawai H, Okada Y, Funahashi H, Takahashi H, Matsuo Y, Yasuda A, et al. Basement membrane proteins play an important role in the invasive processes of human pancreatic cancer cells. J Surg Res. 2008;144(1):117-23.

223. Walenta S, Doetsch J, Mueller-Klieser W, Kunz-Schughart LA. Metabolic imaging in multicellular spheroids of oncogene-transfected fibroblasts. J Histochem Cytochem. 2000;48(4):509-22.

224. Zanoni M, Piccinini F, Arienti C, Zamagni A, Santi S, Polico R, et al. 3D tumor spheroid models for in vitro therapeutic screening: a systematic approach to enhance the biological relevance of data obtained. Sci Rep. 2016;6:19103.

225. Hongisto V, Jernstrom S, Fey V, Mpindi JP, Kleivi Sahlberg K, Kallioniemi O, et al. High-throughput 3D screening reveals differences in drug sensitivities between culture models of JIMT1 breast cancer cells. PLoS ONE. 2013;8(10):e77232.

226. Wen Z, Liao Q, Hu Y, You L, Zhou L, Zhao Y. A spheroid-based 3-D culture model for pancreatic cancer drug testing, using the acid phosphatase assay. Braz J Med Biol Res. 2013;46(7):634-42.

227. Labernadie A, Kato T, Brugues A, Serra-Picamal X, Derzsi S, Arwert E, et al. A mechanically active heterotypic E-cadherin/N-cadherin adhesion enables fibroblasts to drive cancer cell invasion. Nat Cell Biol. 2017;19(3):224-37.

228. Osterholm C, Lu N, Liden A, Karlsen TV, Gullberg D, Reed RK, et al. Fibroblast EXT1-levels influence tumor cell proliferation and migration in composite spheroids. PLoS ONE. 2012;7(7):e41334.

229. Cheung KJ, Gabrielson E, Werb Z, Ewald AJ. Collective invasion in breast cancer requires a conserved basal epithelial program. Cell. 2013;155(7):1639-51.

230. Nguyen-Ngoc KV, Cheung KJ, Brenot A, Shamir ER, Gray RS, Hines WC, et al. ECM microenvironment regulates collective migration and local dissemination in normal and malignant mammary epithelium. Proceedings of the National Academy of Sciences of the United States of America. 2012;109(39):E2595-604.

231. Cavo M, Fato M, Penuela L, Beltrame F, Raiteri R, Scaglione S. Microenvironment complexity and matrix stiffness regulate breast cancer cell activity in a 3D in vitro model. Sci Rep. 2016;6:35367.

232. Zaman MH, Trapani LM, Sieminski AL, Mackellar D, Gong H, Kamm RD, et al. Migration of tumor cells in 3D matrices is governed by matrix stiffness along with cell-matrix adhesion and proteolysis. Proceedings of the National Academy of Sciences of the United States of America. 2006;103(29):10889-94.

233. Jesse S, Koenig A, Ellenrieder V, Menke A. Lef-1 isoforms regulate different target genes and reduce cellular adhesion. Int J Cancer. 2010;126(5):1109-20.

234. Vennin C, Chin VT, Warren SC, Lucas MC, Herrmann D, Magenau A, et al. Transient tissue priming via ROCK inhibition uncouples pancreatic cancer progression, sensitivity to chemotherapy, and metastasis. Sci Transl Med. 2017;9(384).

235. Rath N, Kalna G, Clark W, Olson MF. ROCK signalling induced gene expression changes in mouse pancreatic ductal adenocarcinoma cells. Sci Data. 2016;3:160101.

236. Shields MA, Dangi-Garimella S, Krantz SB, Bentrem DJ, Munshi HG. Pancreatic cancer cells respond to type I collagen by inducing snail expression to promote membrane type 1 matrix metalloproteinase-dependent collagen invasion. J Biol Chem. 2011;286(12):10495-504.

237. Evans TRJ, Van Cutsem E, Moore MJ, Bazin IS, Rosemurgy A, Bodoky G, et al. Phase 2 placebo-controlled, double-blind trial of dasatinib added to gemcitabine for patients with locally-advanced pancreatic cancer. Ann Oncol. 2017;28(2):354-61.

238. Chee CE, Krishnamurthi S, Nock CJ, Meropol NJ, Gibbons J, Fu P, et al. Phase II study of dasatinib (BMS-354825) in patients with metastatic adenocarcinoma of the pancreas. Oncologist. 2013;18(10):1091-2.

239. Sato N, Kohi S, Hirata K, Goggins M. Role of hyaluronan in pancreatic cancer biology and therapy: Once again in the spotlight. Cancer Sci. 2016;107(5):569-75.

240. Ohlund D, Franklin O, Lundberg E, Lundin C, Sund M. Type IV collagen stimulates pancreatic cancer cell proliferation, migration, and inhibits apoptosis through an autocrine loop. BMC Cancer. 2013;13:154.

241. Wurth R, Thellung S, Bajetto A, Mazzanti M, Florio T, Barbieri F. Drug-repositioning opportunities for cancer therapy: novel molecular targets for known compounds. Drug Discov Today. 2016;21(1):190-9.

242. Ashburn TT, Thor KB. Drug repositioning: identifying and developing new uses for existing drugs. Nat Rev Drug Discov. 2004;3(8):673-83.

243. Gupta SC, Sung B, Prasad S, Webb LJ, Aggarwal BB. Cancer drug discovery by repurposing: teaching new tricks to old dogs. Trends Pharmacol Sci. 2013;34(9):508-17.

244. Singhal S, Mehta J, Desikan R, Ayers D, Roberson P, Eddlemon P, et al. Antitumor activity of thalidomide in refractory multiple myeloma. The New England journal of medicine. 1999;341(21):1565-71.

245. Steinbach G, Lynch PM, Phillips RK, Wallace MH, Hawk E, Gordon GB, et al. The effect of celecoxib, a cyclooxygenase-2 inhibitor, in familial adenomatous polyposis. The New England journal of medicine. 2000;342(26):1946-52.

246. Vortherms AR, Dang HN, Doyle RP. Anticancer conjugates and cocktails based on methotrexate and nucleoside synergism. Clin Med Oncol. 2009;3:19-26.

247. Sleire L, Forde HE, Netland IA, Leiss L, Skeie BS, Enger PO. Drug repurposing in cancer. Pharmacol Res. 2017;124:74-91.

248. Belz GG, Breithaupt-Grogler K, Osowski U. Treatment of congestive heart failure--current status of use of digitoxin. Eur J Clin Invest. 2001;31 Suppl 2:10-7.

249. Addison CL, Simos D, Wang Z, Pond G, Smith S, Robertson S, et al. A phase 2 trial exploring the clinical and correlative effects of combining doxycycline with bone-targeted therapy in patients with metastatic breast cancer. J Bone Oncol. 2016;5(4):173-9.

250. Zhang JH, Chung TD, Oldenburg KR. A Simple Statistical Parameter for Use in Evaluation and Validation of High Throughput Screening Assays. J Biomol Screen. 1999;4(2):67-73.

251. Chen Y, Chou WC, Ding YM, Wu YC. Caffeine inhibits migration in glioma cells through the ROCK-FAK pathway. Cell Physiol Biochem. 2014;33(6):1888-98.

252. Kang SS, Han KS, Ku BM, Lee YK, Hong J, Shin HY, et al. Caffeine-mediated inhibition of calcium release channel inositol 1,4,5-trisphosphate receptor subtype 3 blocks glioblastoma invasion and extends survival. Cancer Res. 2010;70(3):1173-83.

253. Wang Q, Zhao W, Wu G. Valsartan inhibits NPC cell line CNE-2 proliferation and invasion and promotes its sensitivity to radiation. Eur J Cancer Prev. 2009;18(6):510-7.

254. Prassas I, Karagiannis GS, Batruch I, Dimitromanolakis A, Datti A, Diamandis EP. Digitoxin-induced cytotoxicity in cancer cells is mediated through distinct kinase and interferon signaling networks. Mol Cancer Ther. 2011;10(11):2083-93.

255. Zhang H, Wong CC, Wei H, Gilkes DM, Korangath P, Chaturvedi P, et al. HIF-1-dependent expression of angiopoietin-like 4 and L1CAM mediates vascular metastasis of hypoxic breast cancer cells to the lungs. Oncogene. 2012;31(14):1757-70.

256. Goldberger ZD, Goldberger AL. Therapeutic ranges of serum digoxin concentrations in patients with heart failure. Am J Cardiol. 2012;109(12):1818-21.

257. Kozanoglu I, Yandim MK, Cincin ZB, Ozdogu H, Cakmakoglu B, Baran Y. New indication for therapeutic potential of an old well-known drug (propranolol) for multiple myeloma. J Cancer Res Clin Oncol. 2013;139(2):327-35.

258. Liao X, Che X, Zhao W, Zhang D, Bi T, Wang G. The beta-adrenoceptor antagonist, propranolol, induces human gastric cancer cell apoptosis and cell cycle arrest via inhibiting nuclear factor kappaB signaling. Oncol Rep. 2010;24(6):1669-76.

259. Stanojkovic TP, Zizak Z, Mihailovic-Stanojevic N, Petrovic T, Juranic Z. Inhibition of proliferation on some neoplastic cell lines-act of carvedilol and captopril. J Exp Clin Cancer Res. 2005;24(3):387-95.

260. Pasquier E, Street J, Pouchy C, Carre M, Gifford AJ, Murray J, et al. beta-blockers increase response to chemotherapy via direct antitumour and anti-angiogenic mechanisms in neuroblastoma. Br J Cancer. 2013;108(12):2485-94.

261. Pasquier E, Andre N, Trahair T, Kavallaris M. Reply: Comment on 'Beta-blockers increase response to chemotherapy via direct anti-tumour and anti-angiogenic mechanisms in neuroblastoma'--beta-blockers are potent anti-angiogenic and chemo-sensitising agents, rather than cytotoxic drugs. Br J Cancer. 2013;109(7):2024-5.

262. Shan T, Ma Q, Zhang D, Guo K, Liu H, Wang F, et al. beta2-adrenoceptor blocker synergizes with gemcitabine to inhibit the proliferation of pancreatic cancer cells via apoptosis induction. Eur J Pharmacol. 2011;665(1-3):1-7.

263. Quoc Lu'o'ng KV, Nguyen LT. The roles of beta-adrenergic receptors in tumorigenesis and the possible use of beta-adrenergic blockers for cancer treatment: possible genetic and cell-signaling mechanisms. Cancer Manag Res. 2012;4:431-45.

264. Han M, Zhang T, Yang L, Wang Z, Ruan J, Chang X. Association between NADPH oxidase (NOX) and lung cancer: a systematic review and meta-analysis. J Thorac Dis. 2016;8(7):1704-11.

265. Choi JA, Jung YS, Kim JY, Kim HM, Lim IK. Inhibition of breast cancer invasion by TIS21/BTG2/Pc3-Akt1-Sp1-Nox4 pathway targeting actin nucleators, mDia genes. Oncogene. 2016;35(1):83-93.

266. Weaver AM. Regulation of cancer invasion by reactive oxygen species and Tks family scaffold proteins. Sci Signal. 2009;2(88):pe56.

267. Dean A, Tuffin P. Fibrinolytic inhibitors for cancer-associated bleeding problems. J Pain Symptom Manage. 1997;13(1):20-4.

268. Dowd NP, Karski JM, Cheng DC, Carroll JA, Lin Y, James RL, et al. Pharmacokinetics of tranexamic acid during cardiopulmonary bypass. Anesthesiology. 2002;97(2):390-9.

269. Karski JM, Teasdale SJ, Norman P, Carroll J, VanKessel K, Wong P, et al. Prevention of bleeding after cardiopulmonary bypass with high-dose tranexamic acid. Double-blind, randomized clinical trial. J Thorac Cardiovasc Surg. 1995;110(3):835-42.

270. Suojanen J, Sorsa T, Salo T. Tranexamic acid can inhibit tongue squamous cell carcinoma invasion in vitro. Oral Dis. 2009;15(2):170-5.

271. Tanaka N, Ogawa H, Tanaka K, Kinjo M, Kohga S. Effects of tranexamic acid and urokinase on hematogenous metastases of Lewis lung carcinoma in mice. Invasion Metastasis. 1981;1(3):149-57.

272. Tanaka N, Ogawa H, Kinjo M, Kohga S, Tanaka K. Ultrastructural study of the effects of tranexamic acid and urokinase on metastasis of Lewis lung carcinoma. Br J Cancer. 1982;46(3):428-35.

273. Andreasen PA, Kjoller L, Christensen L, Duffy MJ. The urokinase-type plasminogen activator system in cancer metastasis: a review. Int J Cancer. 1997;72(1):1-22.

274. Hijazi N, Abu Fanne R, Abramovitch R, Yarovoi S, Higazi M, Abdeen S, et al. Endogenous plasminogen activators mediate progressive intracerebral hemorrhage after traumatic brain injury in mice. Blood. 2015;125(16):2558-67.

275. Carmeliet P, Moons L, Lijnen R, Baes M, Lemaitre V, Tipping P, et al. Urokinase-generated plasmin activates matrix metalloproteinases during aneurysm formation. Nat Genet. 1997;17(4):439-44.

276. Werb Z. ECM and cell surface proteolysis: regulating cellular ecology. Cell. 1997;91(4):439-42.

277. Murthi P, Barker G, Nowell CJ, Rice GE, Baker MS, Kalionis B, et al. Plasminogen fragmentation and increased production of extracellular matrix-degrading proteinases are associated with serous epithelial ovarian cancer progression. Gynecol Oncol. 2004;92(1):80-8.

278. Look MP, van Putten WL, Duffy MJ, Harbeck N, Christensen IJ, Thomssen C, et al. Pooled analysis of prognostic impact of urokinase-type plasminogen activator and its inhibitor PAI-1 in 8377 breast cancer patients. J Natl Cancer Inst. 2002;94(2):116-28.

279. de Geus SW, Baart VM, Boonstra MC, Kuppen PJ, Prevoo HA, Mazar AP, et al. Prognostic Impact of Urokinase Plasminogen Activator Receptor Expression in Pancreatic Cancer: Malignant Versus Stromal Cells. Biomark Insights. 2017;12:1177271917715443.

280. Cantero D, Friess H, Deflorin J, Zimmermann A, Brundler MA, Riesle E, et al. Enhanced expression of urokinase plasminogen activator and its receptor in pancreatic carcinoma. Br J Cancer. 1997;75(3):388-95.

281. Paumgartner G, Beuers U. Ursodeoxycholic acid in cholestatic liver disease: mechanisms of action and therapeutic use revisited. Hepatology. 2002;36(3):525-31.

282. Hansen JD, Kumar S, Lo WK, Poulsen DM, Halai UA, Tater KC. Ursodiol and colorectal cancer or dysplasia risk in primary sclerosing cholangitis and inflammatory bowel disease: a meta-analysis. Dig Dis Sci. 2013;58(11):3079-87.

283. Evans DR, Guy HI. Mammalian pyrimidine biosynthesis: fresh insights into an ancient pathway. J Biol Chem. 2004;279(32):33035-8.

284. Shawver LK, Schwartz DP, Mann E, Chen H, Tsai J, Chu L, et al. Inhibition of platelet-derived growth factor-mediated signal transduction and tumor growth by N-

[4-(trifluoromethyl)-phenyl]5-methylisoxazole-4-carboxamide. Clin Cancer Res. 1997;3(7):1167-77.

285. Hail N, Jr., Chen P, Bushman LR. Teriflunomide (leflunomide) promotes cytostatic, antioxidant, and apoptotic effects in transformed prostate epithelial cells: evidence supporting a role for teriflunomide in prostate cancer chemoprevention. Neoplasia. 2010;12(6):464-75.

286. Jin UH, Kim SB, Safe S. Omeprazole Inhibits Pancreatic Cancer Cell Invasion through a Nongenomic Aryl Hydrocarbon Receptor Pathway. Chem Res Toxicol. 2015;28(5):907-18.

287. Crosas-Molist E, Bertran E, Rodriguez-Hernandez I, Herraiz C, Cantelli G, Fabra A, et al. The NADPH oxidase NOX4 represses epithelial to amoeboid transition and efficient tumour dissemination. Oncogene. 2017;36(21):3002-14.

288. Evensen NA, Li J, Yang J, Yu X, Sampson NS, Zucker S, et al. Development of a high-throughput three-dimensional invasion assay for anti-cancer drug discovery. PLoS ONE. 2013;8(12):e82811.

289. Griffith LG, Swartz MA. Capturing complex 3D tissue physiology in vitro. Nature reviews Molecular cell biology. 2006;7(3):211-24.

290. Alexander S, Friedl P. Cancer invasion and resistance: interconnected processes of disease progression and therapy failure. Trends Mol Med. 2012;18(1):13-26.

8. Appendix: List of drugs

Rank	*Name*	*Drug class*
1	GSK2126458	PI3K (p110) and mTOR inhibitor
2	Doxorubicin	Topo isomerase 2 inhibitor
3	Digoxin	Sodium potassium adenosine triphosphatase inhibitor
4	Vorinostat	HDAC inhibitor
5	Foretinib	c-MET and VEGFR inhibitor
6	Tranexamic Acid	Plasminogen/plasmin inhibitor
7	Dasatinib	Src and BCR/ABL inhibitor
8	Nebivolol·HCl	β1 receptor inhibitor
9	Leflunomide	Dihydroorotate dehydrogenase inhibitor
10	Gemcitabine·HCl	Deoxycytidine analog
11	Ursodiol	Bile; reduces cholersterol absorption
12	Tolterodine Tartrate	Antagonist M2 and M3 muscarinic receptor
13	Valganciclovir·HCl	Inhibitor of deoxyguanosine triphosphate
14	Cinacalcet·HCl	Calcimimetic
15	Sitagliptin Phosphate	Dipeptidyl-peptidase inhibitor
16	Maraviroc	CCR5 antagonist
17	Ambrisentan	Endothelin receptor antagonist
18	Artemether	Inhibition of PfATP6 and anti-oxidant enzymes
19	Metformin·HCl	Enhance release of glucagon-like peptide 1
20	H1152	Rock inhibitor
21	Alosetron·HCl	5-HT_3 antagonist
22	Mannitol	Osmotic diuretic, Sweetener
23	Doripenem	Inhibitor of penicillin-binding proteins
24	Leucovorin Calcium Pentahydrate	Folic acid
25	Paclitaxel (Taxol)	Arrests cells in G2/M phase of cell cycle
26	Miglitol	Inhibition of membrane bound intestinal a-glucoside hydrolase enzymes
27	Erlotinib	EGFR inhibitor
28	Febuxostat	Inhibitor of xanthine oxidase
29	GSK269962	Rock inhibitor
30	Ramelteon	MT1 and MT2 agonist
31	Lenalidomide	Upregulation of p21, T-cell activation, reduce VEGF, TNF-a and IL-6
32	Pitavastatin Calcium	HMG-CoA reductase inhibitor
33	Tazarotene	Agonist of retinoic acid receptor

34	Levocarnitine	Carrier molecule in the transport of long-chain fatty acids
35	Levothyroxine·Na	Agonist for thyroid hormone receptor alpha and beta
36	Loteprednol Etabonate	Inhibitor of Type II glucocorticoid receptor
37	Carglumic Acid	Allosteric activator of CPS1
38	articaine	Antagonist of voltage gated sodium channels
39	Levocetirizine Dihydrochloride	Inhibitor of H1 receptors
40	Pazopanib·HCl	RTK inhibitor of VEGFR1/2/3, PDGFRa/b and c-kit
41	Bimatoprost	Agonist of prostaglandin FP receptors
42	Finasteride	Inhibitor of Type II 5a reductase
43	Nicotine	Agonist of nAChRs
44	Eplerenone	Antagonist of mineralcorticoid receptor
45	Everolimus	mTOR inhibitor
46	Fingolimod	Inhibitor of sphingosine 1-phosphate receptors
47	Dobutamine·HCl	Agonist of beta-1 receptors
48	Milnacipran·HCl	Inhibitor of NET and SERT
49	aspirin	Cox inhibitor
50	Tadalafil	Inhibitor of PDE5
51	Dexrazoxane	Free radical scavenger and Topoisomerase II inhibitor
52	Cisplatin (Cis-Diamineplatinum(Ii) Dichloride)	DNA alkylating agent
53	Naloxone HCl	Antagonist of opioid receptors
54	Hydrocortisone	Agonist of glucocorticoid receptor
55	Dexmedetomidine·HCl	Agonist of alpha-2 adrenoceptor
56	Eszopiclone	Interaction with GABAA receptors
57	Regadenoson	A2A receptor agonist
58	Fomepizole	Inhibitor of alcohol dehydrogenase
59	Y27362	Rock inhibitor
60	Ranolazine·2HCl	P-gp inhibitor
61	Niacin (Known As Vitamin B3, Nicotinic Acid And Vitamin Pp)	Binds to niacin receptor, nicotinic acid phophoribosyltransferase and Nicotinate D-ribonucleoside pyrophosphate
62	Doxapram·HCl H2O	Inhibits potassium channel K2P

63	Tirofiban·HCl	Antagonist of GP IIb/IIIa receptor
64	Iloperidone	D2 and 5HT2A receptor antagonist
65	Fulvestrant	Estrogen receptor antagonist
66	Flucytosine	Uracil analog, inhibits RNA synthesis
67	hydroxocabalamin	Vitamin B12a, cofactor of methionine synthase
68	NS-1643	Ion channel inhibitor
69	Nepafenac	COX inhibitor
70	Azathioprine	Inhibitor of hypoxanthine-guanine phosphoribosyltransferase
71	Dienogest	Progesterone receptor agonist
72	Ethosuximide	Inhibitor of T-type calcium channel subunit alpha 1G
73	amoxicillin	Inhibitor of PBP-1A
74	sulfametoxazole	Inhibitor of dihydropteroat synthase
75	Bendamustine·HCl	Alkylating agent; inhibits DNA synthesis
76	Tolvaptan	Vasopressin V1a and 2 antagonist
77	Melphalan	Alkylating agent; inhibits DNA synthesis
78	Triptorelin Acetate	Gonadotropin-releasing hormone receptor agonist
79	Olsalazine·Na	Thiopurine S-methyltransferase inhibitor
80	Nitisinone	4-hydroxyphenylpyruvate dioxygenase inhibitor
81	IKK 16	IKK inhibitor
82	Auranofin	NFKB inhibitor
83	Calcitriol	Vitamin D3 receptor antagonist
84	Estradiol	Estrogen receptor lapha agonist
85	Pantoprazole	Potassium-transporting ATPase alpha chain1 inhibitor
86	Eflornithine·HCl	Ornithine decarboxylase antagonist
87	Gsk690693	Akt1/2/3 inhibitor
88	Rasagiline Mesylate	Amine oxidase inhibitor
89	Dalfampridine (4-Aminopyridine)	Inhibitor of potassium coltage-gated channels
90	Rosiglitazone	PPAR-gamma receptor agonist
91	Orlistat (Tetrahydrolipstatin)	Inhibitor of pancreatic triacylglycerol lipase and fatty acid synthase
92	Bortezomib	Inhibitor of proteasome subunit beta
93	Fluorouracil (5-Fluorouracil)	Inhibits DNA and RNA synthesis by inhibiting thymidylate synthase

94	Nateglinide	Inhibitor of ATP-binding cassette
95	Voriconazole	Inhibitor of Lanosterol 14-alpha demethylase
96	Acamprosate	NMDA antagonist; GABA-A receptor agonist
97	Miglustat (N-Butyldeoxynojirimycin·HCl)	Ceramide glucosyltransferase inhibitor
98	Decitabine	DNA – methyltransferase 1 inhibitor
99	Verapamil·HCl	Voltage dependent L-type calcium channel inhibitor
100	Ibandronate·Na Monohydrate	Farnesyl pyrophosphate synthase inhibitor
101	Blebbistatin	Myosin inhibitors
102	Tropicamide	Muscarinic acethylcholine receptor antagonist
103	Anagrelide	Inhibitor of cGMP-inhibited 3',5'-cyclic phosphodiesterase A
104	Azelaic Acid	Inhibitor of Tyrosinase, 3-oxo-5-beta/alpha-steroid 4-dehydrogenase 2
105	Tacrine·HCl	Acetylcholinesterase inhibitor
106	Tamsulosin·HCl	Alpha-1A adrenergic receptor antagonist
107	Pramipexole Dihydrochloride Monohydrate	Dopamine 2/3/4 receptor agonist
108	Caffeine	Adenosine receptor A1/2a antagonist
109	Valsartan	Type 1 angiotensin II receptor antagonist